Dinoflagellate proxies for surface water property changes in the Miocene Atlantic Ocean

Dissertation zur Erlangung des Doktorgrades der Naturwissenschaften

im Fachbereich Geowissenschaften der Universität Bremen

vorgelegt von

Sonja Heinrich

Mai 2012

Tag des Kolloquiums:

9. Juli 2012

Gutachter:

1. Prof. Dr. Helmut Willems

2. Prof. Dr. Rüdiger Henrich

Erklärung

Hiermit versichere ich, dass ich

1. die Arbeit ohne unerlaubte fremde Hilfe

angefertigt habe,

2. keine anderen als die von mir angegebenen

Quellen und Hilfsmittel benutzt habe

und

3. die den benutzten Werken wörtlich oder

inhaltlich entnommenen Stellen als solche

kenntlich gemacht habe.

Bremen, den 9.5.2012

Contents

Acknowledgements

The projects within the Ph.D. study was carried out are financed by the German Science Foundation (DFG), as a subproject of the International Graduate College “Proxies in Earth History” (EUROPROX).

First of all, I sincerely thank Prof. Dr. Helmut Willems for giving me the opportunity for this thesis and for his trust in me to accomplish this work.

I also grateful acknowledge PD Dr. Karin Zonneveld for supervising this work, for her general support and for nice coffee meetings early in the morning.

All members of the AG Willems are thanked. Special thanks to Maria Petrogiannis for being such a nice person and for the first smiling face, when I came to ask for a “job”. Thanks also to Marion Milling-Goldbach for lots of laughter. I also would like to thank my colleges which whom I shared an office: Katarzyna Bison, Liang Chen. Special thanks hereby to Kara Bogus, - what would I have done without your English corrections; Stefanie Dekeyzer, - I enjoyed our nice coffee and chat breaks and - I managed to stop working before giving birth to my child! Ilham, you have become a true friend of mine, - thanks for your warm heart.

I also want to thank the “old” ones: Uli Holzwart, for your fantastic sense of humour and Marion Kohn, for our profound chats in the lab. Vanessa Lüer and Oliver Esper are thanked for nice sushi evenings.

A special thank also to Catalina Gonzales for being a super EUROPROX Postdoc and much more.

During this project, I was given the opportunity for an internship at Maersk Oil. In this connection thanks to Henrik Sulsbrück for establishing the contact. Thanks also to the people of the Halfdan Center and at Baltikavej for a nice working atmosphere. Special thanks are given to Mads Willumsen, Henriette Steinhardt, Stephen Crittenden and Morten Ahlborn for the supervision and help during my time at Maersk. Thanks also to Mette Ernstsen for taking care of my son during this time.

In the final phase of my Ph.D. I moved to Denmark. Marianne Ellegaard gave me the fantastic opportunity to get a working place in the Biological Department, where I spend three months. Thanks for this chance and also thanks to the whole group for a very nice

welcome. Special thanks hereby to Liz, for pleasant chats in the morning and for always being in a good mood. Warm thanks also to Sirje, my office maid during this time. I truly enjoyed our time together in the office, which mad it hard for me to leave after the three months.

I would like to thank all my friends beside the University for their support and for always having an "open ear" for me. Especially I would like to thank Claudia Reihert and Stefan Ochs. Without you two I would have never been managed to come to the University.

Warm thanks are given to my parents. It would not have been possible for me to do this work without all the hours of child care. Thanks to you, mom, for carrying first Thore and than Mattis hours for hours and for letting the whole house being a Pirate ship! Special thanks also to you, dad. It seems that I got some of your characteristics with the joy for learning new things and the curiosity for new challenges. I have still not met somebody else with such knowledge about almost everything, like you.

I also would like to thank my sister, for listening to my complainings and for nothing more than just being my sister!

However, my biggest and warmest thanks go to three persons.

Thore and Mattis, - my two fantastic boys. I want to thank you for "keeping my feet on earth" and for showing me the real important things in life. I hope I was not too bad in times of increasing stress, - just before conferences or submitting a paper or in the very last phase of my Ph.D. time.

Verner, I would like to thank you for being at my side and that you walked this way together with me. You always gave me the feeling that no matter if I succeed or not, I will always have a home where I can return to.

Tak for din kærlighed. Jeg håber at det kommer mange år sammen med dig!

Summary

Oceanographic and environmental changes had a strong impact on the climate progression during the middle and late Miocene (ca. 16-5.3 Ma). The climatic cooling during this time interval, involving the glaciation of Antarctica and the development of the Antarctic Circumpolar Current, influenced the initiation of oceanographic features of the South Atlantic Ocean, such as the Benguela upwelling in the eastern South Atlantic Ocean. The initiation of the Benguela upwelling, together with the associated Benguela Current, specifically had a strong impact on the global heat budget. It represented an important pathway for heat transport from the South Atlantic across the equator into the North Atlantic. This heat transport, combined with the return path via the North Atlantic Deep Water, encompasses a significant part of the thermohaline circulation. Another important development during the Miocene that affected thermohaline circulation was the closure of the Central American Seaway. However, it is still a matter of intense debate if thermohaline circulation, particularly the portion regarding equatorial heat transport via the North Brazil Current as well as the production of North Atlantic Deep Water, was possible at times of an open seaway between the Atlantic and Pacific.

Thus, the overall aim of the present Ph.D. project was to document and understand the processes that (1) led to the establishment of the Benguela upwelling regime together with (2) the heat transport into the North Atlantic by way of the North Brazil Current. Of special interest to this project was also to understand the changing pathway of the North Brazil Current in relation to the closure of the Central American Seaway, as well as its influence on regional features such as the pathway of the Amazon outflow and sedimentary load.

For this purpose a detailed palaeoceanographic reconstruction has been established based on the calcareous dinoflagellate cyst content of two sites located on the heat transport pathway namely: ODP Site 1085 (Benguela upwelling regime, eastern South Atlantic Ocean) and Site 926 (Ceara Rise, western equatorial Atlantic Ocean).

Samples from ODP Site 1085 were investigated for changes in productivity as well as water quality with data derived from calcareous dinoflagellate cyst associations. Two distinct increases in productivity and corresponding decreases in upper water temperatures reflect upwelling pulses off Namibia in relation to the Miocene cooling events, Mi-5 and Mi-6. Both cooling events are associated with the glaciation of Antarctica, which probably increased the southeasterly winds and, in turn, led to the upwelling pulses. Between the two upwelling pulses, the cyst association demonstrates enhanced transport of terrigenous material via the Orange River into the upwelling area. At about 11.1 Ma, productivity increased and the polar species *Caracomia arctica* was found for the first time. The occurrence of *C. arctica* implies a fundamental change in the water quality, which was likely related to the influence of subantarctic water and allowed upwelling to fully develop into modern conditions. *C. arctica* is constantly found in the association from about 10.4 Ma on, which indicates that the Benguela upwelling regime was firmly established from this time forward (Chapter 4).

Investigations into changes in the accumulation rates as well as in the association of calcareous dinoflagellate cysts were undertaken on samples from ODP Site 926. Better calcite preservation based on the cyst accumulation rate was reconstructed from about 12.4-11.8 Ma, as well as at about 11.5, 10.1 and 9.7 Ma, pointing to the influence of North Atlantic Deep Water, which was forced to flow into the South Atlantic after a first uplift of the Panama Sill. From about 11.2 Ma, the dinoflagellate cyst diversity increased. The first appearance and subsequent increase of the cyst species *Leonella granifera* at this time implies an influence of river discharge waters, which can be related to the developing Amazon River. Amazon River waters reached Site 926 as a result of a southward reversal of the North Brazil Current. After about 10.5 Ma, the cyst association reflects a decrease in Amazon influence, probably related to a reduction in the inflow of Pacific waters into the Atlantic and a reversal of the North Brazil Current to its modern pathway (Chapter 5).

Furthermore, samples from Site 926 were analyzed for the isotopic composition of the calcareous dinoflagellates cyst *Thoracosphaera heimii*. Stable oxygen isotope values of *T. heimii* were compared to those of the foraminifer *Globogerinoides sacculifer*. The

comparison displayed an offset, which is probably related to symbiont photosynthetic activity of *G. sacculifer*. Temperatures were calculated for the late Miocene by using the equation for inorganic calcite (Kim and O´Neill, 1997) and a new equation based specifically on *T. heimii* (Dekeyzer et al., subm.). The reconstructed temperatures show lower mean tropical temperatures for the western equatorial Atlantic in comparison to today. At about 10.9 Ma, the isotope and temperature trends reflect an influence of freshwater, derived from the developing Amazon River, and delivered by the southward-flowing North Brazil Current. At about 9.9 Ma, the isotope values show a strong decrease, which is probably related to the major sea level low stand existing at that time. The increase in isotope values afterwards could be the result of a decrease in Amazon freshwater influence. Amazon waters were, at this time, likely transported away from Site 926 by the North Brazil Current, which changed direction again to its modern flow pattern. This shift in the current direction was probably due to a decrease in Pacific inflow through the Central American Seaway. The stable oxygen isotopes, as well as reconstructed temperatures based on the calcareous dinoflagellate cyst *T. heimii*, are presented and discussed for the first time from the late Miocene (Chapter 6).

The results of this thesis reveal an interaction between the cooling that occurred in the middle to late Miocene and the initiation, and establishment, of upwelling in the eastern South Atlantic Ocean. This interaction is primarily described through the changing calcareous dinoflagellate cyst association. Furthermore, it has been shown that the heat transport into the North Atlantic, across the Equator via the North Brazil Current (western equatorial Atlantic) as a part of the thermohaline circulation, is linked to the closure of the Central American Seaway. More localized oceanographic features, such as the transport of Amazon discharge waters, were also influenced by the changing flow pattern of the North Brazil Current. This is evident through the changing calcareous dinoflagellate cyst association, as well as the variations in the stable oxygen isotopic values of *T. heimii*.

The coincident occurrence of the first registered Antarctic waters in the Benguela region (Site 1085) and the first influence of Amazon waters at Ceara Rise (Site 926) leads to the interpretation that the controlling climate features, the Antarctic glaciations and Andean

tectonism, are linked. Furthermore, another coincidence is observed between the timing of the establishment of the Benguela upwelling and the reversal of the North Brazil Current due to the temporary closure of the Central American Seaway.

Kurzfassung

Veränderungen in der Ozeanographie und Umwelt hatten im mittleren und oberen Miozän (16-5.3 Ma) einen starken Einfluss auf die Klimaentwicklung. Die Abkühlung des Klimas, die mit Vereisungen der Antarktis und der Entwicklung des Zirkumpolarstromes einherging, beeinflusste die Ozeanographie des Südatlantiks, wie z. B die Initiierung des Benguela Auftriebes im östlichen Südatlantik. Die Initiierung des Benguela Auftriebes zusammen mit dem dazugehörigen Benguelastrom üben einen großen Einfluss auf den globalen Wärmehaushalt aus. Der Benguelastrom stellt einen wichtigen Pfad für den Wärmetransport vom Südatlantik über den Äquator in den Nordatlantik dar. Dieser Wärmetransport bildet heutzutage, zusammen mit dem Rücktransport über das Nordatlantische Tiefenwasser, einen Hauptteil der thermohalinen Zirkulation. Ein anderer Prozess, der ebenso die thermohaline Zirkulation während des Miozäns beeinflusste ist die Schließung des Panamaseeweges. Es ist jedoch noch immer nicht geklärt, ob eine thermohaline Zirkulation, insbesondere der äquatoriale Wärmetransport durch den Nordbrasilstrom sowie die Produktion von Nord Atlantischem Tiefenwasser mit einem offenen Panamaseeweg zwischen dem Atlantik und Pazifik möglich war.

Das Ziel dieser Doktorarbeit war es daraufhin, die Prozesse zu verstehen und zu dokumentieren, die 1) zur Etablierung des Benguela Auftiebes im Zusammenhang mit 2) dem Wärmetransport über den Nordbrasilstrom in den Nordatlantik geführt haben. Von besonderem Interesse waren hierbei die Veränderung der Strömungsrichtung des Nordbrasilstromes im Zusammenhang mit der Schließung des Panamaseeweges sowie dessen Auswirkungen auf regionale Vorkommnisse, wie z. B. den Weg des Flusseintrages vom Amazonas.

Zu diesem Zweck wurde, basierend auf dem Vorkommen von kalkigen Dinoflagellatenzysten, eine detaillierte Rekonstruktion der Ozeanographie von zwei

Stationen erstellt, welche sich beide im Weg des Wärmetransportes befinden: ODP Site 1085 (Benguela Auftriebsgebiet, östlicher Südatlantik) und Site 926 (Ceara Rise; westlicher äquatorialer Atlantik).

Proben von ODP Site 1085 wurden auf Veränderung in der Produktivität sowie der Wasserqualität zusammen mit Daten von der Assoziation von kalkigen Dinoflagellaten Zysten untersucht. Zwei deutliche Anstiege in Produktivität zusammen mit einer Temperaturabnahme der oberen Wasserschichten reflektieren Auftriebsimpulse vor Namibia im Zusammenhang mit den Miozänen Abkühlungsereignissen Mi-5 und Mi-6. Beide Abkühlungsereignisse werden mit Vereisungen der Antarktis in Zusammenhang gebracht, welche voraussichtlich zu einer Verstärkung der Südostwinde geführt haben, die daraufhin die Auftriebsimpulse verursachten. Zwischen den beiden Auftriebsereignissen zeigt die Zystenassoziation einen verstärkten terrigenen Eintrag in das Auftriebsgebietes durch den längsten Fluss im südlichen Afrika, den Oranje. Um ca. 11.2 Ma steigt die Produktivität und die polare Art *Caracomia arctica* wurde zum ersten Mal gefunden. Das Auftreten von *C. arctica* stellt einen fundamentalen Wechsel in der Wasserqualität dar, welche voraussichtlich nun von subantarktischem Wasser beeinflusst wurde, dass zur vollständigen Entwicklung des heutigen Auftriebes führte. Von ca. 10.4 Ma an, ist *C. arctica* konstant in der Artenvergesellschaftung vertreten, was zu dem Schluss führt, dass das Benguela Auftriebsgebiet sich von dieser Zeit an etabliert hatte (Kapitel 4).

Untersuchungen zur Akkumulationsrate sowie zur Assoziation kalkiger Dinoflagellatenzysten wurden an Proben von ODP Site 926 durchgeführt. Eine verbesserte Kalkerhaltung wurde von ca. 12.4-11.8 Ma, sowie um ca. 11.5, 10.1 und 9.7 Ma rekonstruiert, basierend auf der Akkumulationsrate der Zysten. Die verbesserte Kalkerhaltung ist voraussichtlich auf den Einfluss von Nordatlantischem Tiefenwasser zurück zu führen, welches aufgrund einer Anhebung der Panama Strasse dazu geleitet wurde in den Südatlantik zu fließen. Von ca. 11.2 Ma an steigt die Diversität der Kalkzysten. Das Auftreten und steigende Vorkommen der Zystenart *Leonella granifera* impliziert Flusseintrag, welcher voraussichtlich im Zusammenhang zu dem sich entwickelnden Amazonas steht. Das Flusswasser des Amazonas wurde durch den

umgeleiteten, südwärts fließenden Nordbrasilstrom zu Site 926 transportiert. Der Einfluss des Amazonas verringert sich nach ca. 10.5 Ma, welches voraussichtlich in Relation zu einem geringeren Durchfluss von pazifischem Wasser in den Atlantik und der Umkehr des Nordbrasilstromes zu seinem heutigen Verlauf steht (Kapitel 5).

Von Site 926 wurden zusätzlich Proben auf die Isotopen Zusammensetzung der kalkigen Dinoflagellatenzyste *Thoracosphaera heimii* analysiert. Stabile Sauerstoffisotopenwerte von *T. heimii* wurden mit solchen der Foraminifere *Globogerinoides sacculifer* vergleicht. Der Vergleich zeigt eine Diskrepanz zwischen den Werten, welche voraussichtlich auf die Aktivität von Symbionten während der Photosynthese bei *Globogerinoides sacculifer* zurückzuführen ist. Für das späte Miozän wurden Temperaturen berechnet an Hand der Gleichung für inorganischen Kalzit (Kim and O´Neill, 1997) und einer neuen Gleichung, speziell entwickelt für *T. heimii* (Dekeyzer et al., subm.). Die rekonstruierten Temperaturen zeigen geringere mittlere tropische Temperaturen für den westlichen äquatorialen Atlantik im Vergleich zu heute. Um ca. 10.9 Ma zeigen die Isotopen- und Temperaturtrends einen Frischwassereintrag, kommend vom Amazonas und transportiert durch den südwärts fließenden Nordbrasilstromes. Um ca. 9.9 Ma fallen die Isotopenwerte, welches voraussichtlich auf einen starken Meeresspiegelabfall während dieser Zeit basiert. Der darauf folgende Anstieg der Isotopenwerte kann womöglich im Zusammenhang zu einer Verringerung des Frischwassereintrages vom Amazonas stehen, welche zu dieser Zeit voraussichtlich bereits vom umgeleiteten, jetzt nordwärts fließenden Nordbrasilstrom von Site 926 weg transportiert wurde. Stabile Isotopen sowie auch rekonstruierte Temperaturen basierend auf der kalkigen Dinoflagellatenzystenart *Thoracosphaera heimii* werden zum ersten Mal für das späte Miozän gezeigt und diskutiert (Kapitel 6).

Die Resultate dieser Dissertation zeigen einen Zusammenhang zwischen dem Abkühlungstrend, welcher im mittleren und späten Miozän auftrat, und der Initiierung und Etablierung des Auftriebes im östlichen Südatlantik. Dieser Zusammenhang wird hauptsächlich durch Veränderungen in der Assoziation der kalkigen Dinoflagellatenzysten beschrieben. Zusätzlich wurde gezeigt, dass der Wärmetransport in den Nordatlantik über den Äquator durch den Nordbrasilstrom (westlicher äquatorialer Atlantik) als ein Teil der thermohalinen Zirkulation, im Zusammenhang zur Schließung

des Panamaseeweges steht. Mehr lokale ozeanographische Vorkommen, wie z. B. der Transport von Amazonaswasser, wurden ebenfalls durch den Wechsel in der Fließrichtung des Nordbrasilstromes verursacht. Dieses zeigt sich in den Veränderungen der Zystenassoziation sowie in den Variationen der stabilen Sauerstoffisotopenwerte von *T. heimii*.

Die Übereinstimmung des Auftretens von antarktischem Wasser in der Benguela Region (Site 1085) und der erste Einfluss von Amazonas Wasser am Ceara Rise (Site 926) leiten zu der Interpretation, dass die antarktischen Vereisungen und die tektonischen Aktivitäten in den Anden miteinander im Zusammenhang stehen. Zusätzlich wurde eine weitere zeitliche Übereinstimmung gefunden zwischen der Etablierung des Benguela Auftriebes und der Umkehr der Fließrichtung des Nordbrasilstromes, verursacht durch die Schließung des Panamaseeweges.

Chapter 1: General introduction

1.1 Climate Change today and during the Miocene

The debate about our climate today, specifically regarding how it is changing and what consequences will result out of these changes, is often fractious and entices constant interest. Several different observations describe a warming of our climate system due to an increase in atmospheric CO_2, accompanied by a decrease in glacier extent, sea ice cover and polar ice sheets on Greenland and Antarctica (IPCC, 2007). These changing climatic features are, in turn, thought to have a strong influence on the oceanic circulation system, termed thermohaline circulation, which is driven by density differences and transports huge amounts of heat (e.g. Broecker, 1997; Clark et al., 2002; Marotzke, 2000, Rahmstorf, 2002). A significant perturbation of the oceanic circulation system could lead to enormous problems for Earth's ecosystems, and thereby human economics (e.g. fishery industry, temperate European climate). The response of the oceanic system to climate change is, however, far from being completely understood. For a better understanding of the interaction of climatic processes, it is imperative to investigate time intervals in the past that demonstrate examples of significant changes in the Earth's climate. The Miocene contains such a time interval, characterized by a cooling trend that encouraged the build-up of Arctic and Antarctic ice sheets and the evolution of the present orography (e.g. Holbourn et al., 2005, 2007; Zachos et al., 2001). The ice build-up and orographic changes, such as the opening and closing of oceanic gateways, exerted a strong influence on the progression of wind and upwelling regimes to recent conditions, and the initial development of the modern thermohaline circulation (Wefer et al., 1998; Zachos et al., 2001, 2008).

1.2 The role of the Atlantic Ocean in thermohaline circulation

The Atlantic Ocean plays a key role because of the pathway for heat transport via ocean currents from the south, across the equator, into the northern hemisphere. This surface heat transport balances the deep return flow of cold northern deep waters (North Atlantic

Deep Water) and, overall, describes an important part of the thermohaline circulation (*Fig.1.1*) (Wefer et al., 1998). This heat transfer across the Equator, in turn, is influenced by the closure of an oceanic gateway, the Central American Seaway, which connected the Atlantic and Pacific Ocean during the early Miocene. It has been shown that with an open Central American Seaway, Pacific surface waters flow into the Atlantic, and lead to a reversal in the flow direction of the North Brazil Current. As a consequence, the heat crossing the Equator decreased and, thus, the production of northern deep waters slowed (Butzin et al., 2011; Prange and Schulz, 2004). A proto-northern deep water mass probably flowed into the Pacific when there was an open Seaway. However, during the middle and late Miocene the first uplift of the Panama sill occurred and prevented the flow of Atlantic deep waters into the Pacific (at about 12.9-11.8 Ma; Duque-Caro, 1990; Nisancioglu et al., 2003) and, later, upper waters (at about 10.7 Ma; Kameo and Sato, 2000). The prevention of surface water flow into the Pacific by the uplift of the Panama sill enhanced the northward energy transfer across the equator, which increased the evaporation in the North Atlantic, and produced higher salinity waters. These waters then cooled and sank to greater depths to form the deep return flow of North Atlantic Deep Water towards the South (e.g. Kameo and Sato, 2000; Newkirk and Martin, 2009; Wefer et al., 1998). In addition to the pathway of the oceanic currents, another factor influences the thermohaline circulation. This is the strength of the ocean currents that carry the heat. One important current is the Benguela Current, which receives its heat from the Indian Ocean via the Agulhas Current (Gordon, 1985; 1986). The driving forces for the Benguela Current are the trade winds, which are responsible for the flow pathway and strength of this current. It has been assumed that wind-driven oceanic circulation was already an existing feature of the Southern Hemisphere mid-latitudes during the Cenozoic (e.g. Barker et al., 2007; Huber et al., 2003). However, the strength of the trade winds is dependent on the equator-to-pole surface temperature gradient, which was probably weaker at times of reduced Antarctic glaciations and a weaker Antarctic Circumpolar Current (e.g. Barker et al., 2007). During the middle and late Miocene, several increases in continental Antarctic ice occurred (Miller et al., 1991; Shevenell et al., 2004; Zachos et al., 2001), which led to a strengthening of the Antarctic Circumpolar Current and a northwards shift of the Polar Frontal Zone (Pagani et al., 2000; Paulsen, 2005). This probably increased the equator-to-pole temperature gradient, and caused intensification in the wind regime, which, in turn, led to a strengthening of the Benguela Current (Vincent

and Berger, 1985). The strengthening of the Benguela Current resulted in an increased heat transfer by way of the South Equatorial Current and North Brazil Current across the equator into the North Atlantic. The strengthening of the Benguela Current also resulted in the development of an eastern boundary upwelling regime, the Benguela upwelling (Berger and Wefer, 2002).

.

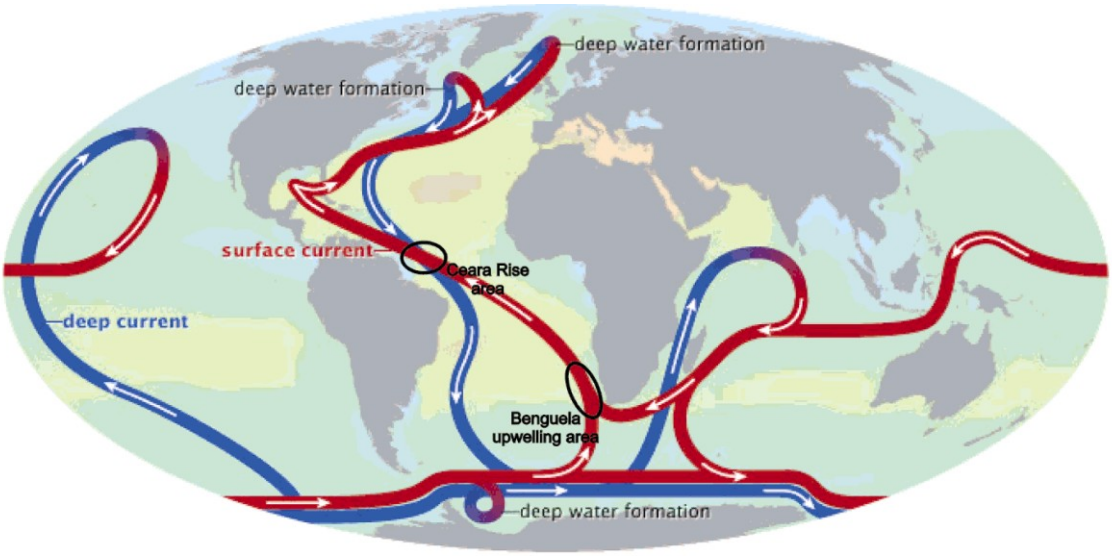

Fig. 1.1 Position of the Ceara Rise area (area of Equator passing heat transport and cold return flow) and the Benguela upwelling area within the global thermohaline circulation. (modified after: map of thermohaline circulation, source: www.earthobservatory.nasa.gov).

Within the Neogene climate cooling periods, coastal upwelling plays an important role, probably by producing a positive feedback loop where increased upwelling favors further climate cooling (Berger and Wefer, 2002). One of these feedback mechanisms is tied to the sequestration of organic carbon during the upwelling process and thus leads to a decrease in the total amount of carbon in the ocean-atmosphere system (Vincent and Berger, 1985). Another feedback mechanism is shown by the fact that upwelling is a self-stabilizing and self-reinforcing process (Berger and Wefer, 2002). Within these processes, cold waters reach the surface and stabilize offshore high pressure centers, which lead to the stabilization of eastern boundary currents, such as the Benguela Current. Extremely dry regions develop landwards of upwelling areas (e.g. Namibian desert) because the offshore high pressure centers prevent moist marine air from entering

the land areas. This hereby increases the regional albedo, which favors further cooling and acts, therefore, as a reinforcing factor for the upwelling process (Berger and Wefer, 2002).

1.3 Calcareous Dinoflagellate Cysts

Dinoflagellates form a capacious and ecologically important group of aquatic protists. They exist in virtually all aquatic environments (e.g. Arndt and Mathes, 1991; Graham et al., 2004) but are most prominent in the marine realm. They show their highest diversities in the tropics and in neritic temperate waters (e.g. Dale and Dale, 1992; Marret and Zonneveld, 2003; Stover et al., 1996). Dinoflagellates are so named due to their two flagella (one transverse and one longitudinal), which allow for vertical migration in a spiralling motion (Taylor and Pollingher, 1987). Their living position in the water column is, however, relatively stable and their migratory distances are not more than several meters (Anderson, 1985; Kamykowski et al., 1998; Zonneveld, 2004). The motile dinoflagellate cells are covered by a cellulosic theca, which is generally not fossilizable. However, some species produce preservable cysts as a part of their life cycle. These can be composed organic material, silica, or calcite, and are morphologically characteristic with regard to the original motile species. Currently about 30 species are known to incorporate calcite into their cell walls, and are thus termed calcareous dinoflagellate cysts (also referred to as calcareous dinoflagellates). As this thesis deals exclusively with calcareous dinoflagellate cysts, only those species life strategies are subsequently discussed in detail.

Two different life strategies are involved in the production of calcareous cysts: a sexual life cycle, which results in the formation of resting cysts, and an asexual life cycle with a dominant vegetative-coccoid stage (*Fig. 1.2*.) (Fensome et al., 1993; 1996; Meyer et al., 2007). In the first life cycle (sexual), the haploid phase dominates. The diploid stage, in which the cyst is formed after sexual fusion of two haploid thecae, is limited to the zygote (Meier et al., 2007; Olli and Anderson, 2005; Sgrosso et al., 2001). In the other life cycle (asexual), the dominant stage is a calcareous vegetative cell (*Fig. 1.3*.). Cells, which

hatch from the calcareous shell, divide and form aplanospores, and then start to calcify (Inouye and Pienaar, 1983; Meier et al., 2007; Tangen et al., 1982). The reproduction time for the vegetative cells is between one to two days, which is much faster than the reproduction time necessary for resting cysts (e.g. Dale, 1992b; Tangen et al., 1982).

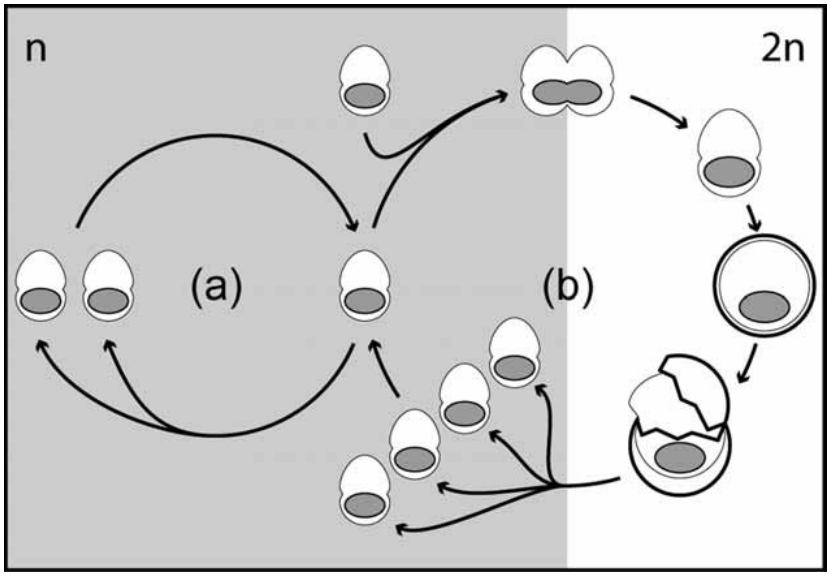

Fig.1 2. Simplified sexueal life cycle with the formation of calcareous dinoflagellate resting cysts. Within the vegetative life-cycle phase (a) the motile stages are haploid (n) and can reproduce by mitotic division. The fusion of two haploid motile cells results in the formation of a diploid (2n) planozygote that subsequently undergoes encystment (b). After excystment, four haploid daughter cells are formed by meiotic division (after Meier et al., 2007).

The first life cycle, the sexual strategy that forms resting cysts, has mainly been observed for neritic calcareous dinoflagellates, mostly of the genus *Scrippsiella* (e.g. Lewis, 1991; Olli and Anderson, 2002; Sgrosso et al., 2001), whereas the asexual life cycle was described for the first time for the oceanic species *Thoracosphaera heimii* (Tangen et al., 1982), and later for another oceanic species, *Leonella granifera* (Meier et al., 2007). Janofske and Karwath (2000) suggested that the oceanic species *Calciodinellum albatrosianum* and *Pernambugia tuberosa* also form their cysts during vegetative reproduction. However, Meier et al. (2007) more conclusively showed, based on culture experiments, that both species form resting cysts according to the sexual life

cycle. These species probably adapted to the oceanic environment through continuous cyst production and short dormancy periods, which prevented the cysts from sinking to water depths from which they cannot return (Meyer et al., 2007). Since calcareous cyst-forming dinoflagellates are autotrophic/mixotrophic, light availability is required and their living habitat is restricted to the photic zone (e.g. Tangen et al., 1982).

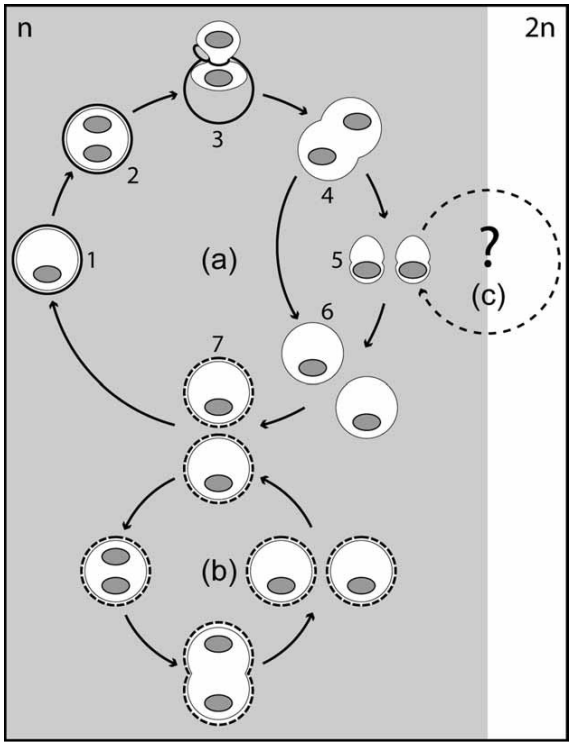

Fig. 1.3. Simplified asexual life cycle with a dominant vegetative-coccoid stage. The calcareous vegetative cells (a, 1–2) are presumably haploid (n). After a cell hatches from the calcareous shell (a, 3), it divides (a, 4) and forms aplanospores, either directly (a, 6) or via the production of planospores (a, 5). The aplanospores start to calcify (a, 7). Weakly calcified cells are capable of mitotic division (b) (after Meier et al., 2007).

The controlling factors for cyst production (encystment) are still being debated. One factor that is diversely discussed is the influence of nutrient availability (especially nitrate and phosphate) on cyst formation. Culture experiments showed that nutrient depletion can induce cyst formation (e.g. Anderson and Olli, 2002), whereas, in field studies, maximal cyst formation occurred without an observed nutrient depletion (e.g. Montresor et al., 1998) or even without any observable relation of cyst production and nutrients

(Godhe et al., 2001). Other influences on encystment might include temperature, ambient light radiation and day length. It has been shown in cultures that the highest growth rates of some cysts (*Pernambugia tuberosa*, *Calciodinellum albatrosianum*, *Leonella granifera*) were observed at almost the same temperatures as in field studies (Meier et al., 2004). However, temperature seems not to be a factor triggering cyst formation (Zonneveld et al., 2005). Sgrosso et al. (2001) tested the effect of temperature, day length and nutrient conditions on the cyst production of four dinoflagellate species (*Scrippsiella trochoidea var. aciculifera*, *Pentapharsodinium tyrrhenicum*, *Calciodinellum operosum*, *S.? rotunda*). They discovered that encystment of these species was regulated by a complex interaction of, at least, all the tested possible factors. Zonneveld et al. (2005) concluded that encystment of dinoflagellates is rather favored by optimal conditions for vegetative growth than related to different stress factors.

Encystment factors for vegetative cysts, produced asexually, have been investigated with culture experiments on *Thoracosphaera heimii* (Karwath et al., 2000a; Kohn and Zonneveld, 2010). Kohn and Zonneveld (2010) found no significant correlation between cyst concentration and temperature, salinity and chlorophyll-a concentration. They speculated that turbulence of the upper water masses is a major factor controlling cyst production with a decrease in production associated to an increasing turbulence of the water column. Field studies, however, showed that, in contrast to the culture experiments of Kohn and Zonneveld (2010), *T. heimii* cyst production was high in areas of enhanced nutrient availability (Vink, 2004; Wendler et al., 2002 a/b). After the encystment process, resting cysts remain in a dormancy period after which germination starts. The length of this period is species-specific and can last between 12 hours to 12 months (e. g. Pfiester and Anderson, 1987).

The controlling factors for excystment can also be manifold (e.g. temperature, light availability, oxygen concentration). It has been shown in cultures that an increase in temperature can increase germination, whereupon every species has a specific ideal temperature range (e.g. Kremp and Anderson, 2000). The availability of light, as well as oxygen, seems to be highly important and possibly even required for germination (e.g. Kremp and Anderson, 2000; Nuzzo and Montresor, 1999).

1.4 Use of Calcareous Dinoflagellate Cysts in Paleoclimate Reconstructions

The use of calcareous dinoflagellate cysts for (paleo)environmental studies has generated much interest in the last two decades. Their long fossil record (since the upper Triassic; Janofske, 1992) as well as their cyst-specific paleoenvironmental significance makes them extremely useful as proxies for surrounding water conditions. Numerous studies have previously shown their suitability for climate reconstructions (e.g. Bison et al., 2009; Esper et al., 2000, 2004; Meier and Willems, 2003; Richter et al., 2007; Vink, 2004; Zonneveld et al., 2000, 2005).

In addition to the use of the calcareous dinoflagellate cyst association to interpret past oceanographic conditions, another important, and relatively new, tool for deciphering paleoceanography and, thus climate, is the use of oxygen isotopes measured from their cysts (also called shells) in order to reconstruct water temperatures (Friedrich and Meier, 2003; 2006; Dekeyzer, 2012; Kohn et al., 2011; Zonneveld, 2004). For this study, stable oxygen isotopes are measured on the shells of the dinoflagellates cyst *Thoracosphaera heimii*. *T. heimii* is a species of special interest as it is thought to have some advantages for isotopic measurements (Kohn and Zonneveld, 2010; Kohn et al., 2011; Zonneveld, 2004). *T. heimii* has a broad geographic and stratigraphic distribution and, as such, occurs in a wide swath between sub-polar and tropical environments (e.g. Esper, 2000; Hildebrand-Habel and Willems, 2000; Meier and Willems, 2003; Streng et al., 2004; Vink, 2004; Wendler et al., 2002a; Zonneveld et al., 1999, 2000). Furthermore, it has been shown that *T. heimii* reproduces and calcifies throughout the year at a certain depth, which implies that temperature calculations resulting from the isotopic signal will reflect mean annual seawater conditions in or just above this depth, the deep chlorophyll maximum (DCM; Inoyer and Pienar, 1982; Kohn and Zonneveld 2010; Wendler et al. 2002a). Another reason for the suitability of *T. heimii* for isotopic measurements is that the photosynthetic species does not bear symbionts, which are known to alter the isotopic signal.

1.5 Stable Oxygen Isotopes and the Oxygen Balance

Oxygen is the one of the most important elements on earth. It occurs in heavy and light varieties, which are called isotopes. Three stable oxygen isotopes are known, which are distinguished by different amounts of neutrons in the atom and show significant differences in their natural occurrence:

$\delta^{16}O \rightarrow 99.76\ \%$

$\delta^{17}O \rightarrow 0.04\ \%$

$\delta^{18}O \rightarrow 0.20\ \%$

The isotopic composition of carbonate is generally measured by using a mass spectrometer. Measured oxygen isotope ratios ($^{18}O/^{16}O$) are then compared to a known international standard. The standard for carbonate samples is referred to VPDB (Cretaceous belemnite formation at Peedee in South Carolina, USA).

The oxygen isotope results are expressed with the standard δ notation (McKinney et al., 1950):

$$\delta^{18}O_{sample}\ (‰) = \frac{(^{18}O/^{16}O)_{sample} - (^{18}O/^{16}O)_{standard}}{(^{18}O/^{16}O)_{standard}} \times 1000$$

The two processes that have the greatest influence on the isotopic composition of seawater are evaporation and condensation. Water molecules containing lighter oxygen (^{16}O) evaporate more readily than molecules with heavier oxygen (^{18}O). Water vapor,

which evaporates from the sea surface, is therefore depleted in ^{18}O in relation to the ocean water. In contrast, the precipitation from a moist air mass is enriched in ^{18}O in relation to the cloud moisture, as the heavier isotope will condense earlier. The processes that involve the enrichment of one isotope in relation to another are called isotope fractionations. Several factors are known to have an influence on the isotope fractionation process, such as temperature, latitude, height, freshwater input, melting or freezing of sea ice, and mixing between water masses (e.g. Paul et al., 1999).

For palaeoceanographic applications, it is not possible to directly measure the isotopic composition of past seawater masses; however, an indirect measurement of the seawater signal can be performed on the calcite of marine organisms. The precipitation of calcite from water is a so-called equilibrium fractionation process, which means that the isotopic composition of the seawater is preserved in the calcareous shells of organisms (e.g. foraminifera, coccolithophorids and dinoflagellate cysts). The fractionation factor is, thereby, temperature dependent and can be used for the calculation of the water temperature in which the precipitation occurred.

The commonly used equation for the calculation of temperature from the oxygen isotopic composition of calcareous organisms is expressed as:

$$T\ (°C) = a + b\ (\delta^{18}O_{calcite} - \delta^{18}O_{water}) + c\ (\delta^{18}O_{calcite} - \delta^{18}O_{water})^{2}$$

a = temperature when $(\delta^{18}O_{calcite} - \delta^{18}O_{water}) = 0$

b = slope

c = second order term for curvature

An overview of other commonly used temperature equations is beyond the scope of this thesis but can be found in Bemis et al. (1998).

Several factors are known to have an enormous influence on the isotopic composition as well as on the resulting temperature calculations, such as global ice volume, seawater

salinity, ecology and physiology of individual species (Bice et al., 2000, Bickert, 2000; Mulitza et al., 2003; Spero and Lea, 1993, 1996, Zachos et al., 1994). This issue will be discussed in detail in Chapter 6.

1.6 Objectives

The main objectives of this study are to cast more light on (1) the processes that triggered the onset of the upwelling off Namibia, (2) to trace the pathway of the thermohaline circulation in relation to the closure of the Central American Seaway, and (3) to measure, for the first time, stable oxygen isotopes on Miocene-aged dinoflagellate cysts and evaluate environmental factors that may influence it. The development of local features, such as the Amazon and the Orange Rivers, and its effect on the oceanography during that time interval (middle to late Miocene) will be addressed as well. An additional and concluding question of this thesis is, if there exist a connection between the different climatic processes, which is reflected by the calcareous dinoflagellate proxies.

The following chapters of the thesis are organized as follows: Chapters 2 and 3 provide specific information regarding the oceanographic setting of the study area, both Modern and in the Miocene, and a detailed discussion of the methods employed in this thesis, respectively. The main results of this thesis are summarized in three first-author manuscripts, which are presented in Chapters 4, 5 and 6. One of the manuscripts (Chapter 4) has been peer-reviewed and published in Paleoceanography. The manuscripts are:

Chapter 4

The Benguela upwelling related to the Miocene cooling events and the development of the Antarctic Circumpolar Current: Evidence from calcareous dinoflagellate cysts

Heinrich, S., Zonneveld, K.A.F., Bickert, T., Willems, H.

(Paleoceanography, 26, PA3209, doi:10.1029/2010PA002065, 2011)

Chapter 5

Western equatorial Atlantic (Ceara Rise) changes in surface and deep ocean circulation related to the middle/late Miocene closure of the Central American Seaway based on calcareous dinoflagellate cysts

Heinrich, S., Bickert, T., Zonneveld, K.A.F., Willems, H.

((In preparation for Palaeogeography, Palaeoclimatology, Palaeoecology)

Chapter 6

Late Miocene stable oxygen isotopes of Thoracosphaera heimii from the western equatorial Atlantic Ocean (Ceara Rise)

Heinrich, S. and Zonneveld K. A.F.

(In preparation for Micropalaeontology)

Finally, concluding remarks as well as future suggestions for further research are discussed in Chapter 7.

Chapter 2: Study area

2.1 Ocean Circulation in the modern Equatorial and South Atlantic

The study area in this project covers the equatorial and southern Atlantic Ocean (*Fig 2.1.*). Two ODP Sites (Site 1085 - Benguela upwelling regime; Site 926 - Ceara Rise) have been chosen due to their locations near important ocean currents, which allows for the tracing of the developing oceanic current during the middle and upper Miocene.

Atmospheric circulation affects the surface currents of the equatorial and South Atlantic and is strongly influenced by the Coriolis Effect. The Coriolis Effect (the curl of wind stress) leads to a deflection of the winds, and produces the northeast trade winds in the Northern Hemisphere and the southeast trade winds in the Southern Hemisphere. The trade winds converge along a belt of low pressure, called the Intertropical Convergence Zone (ITCZ), where the highest sea surface temperatures of the Atlantic occur (e.g. Höflich, 1974; Grodsky and Carton, 2002). The latitudinal position of the ITCZ varies from 15 °N, due to strong southeast trade winds in Boreal summer and autumn, to 1 °N, due to weaker northeast trade winds in Boreal winter and spring.

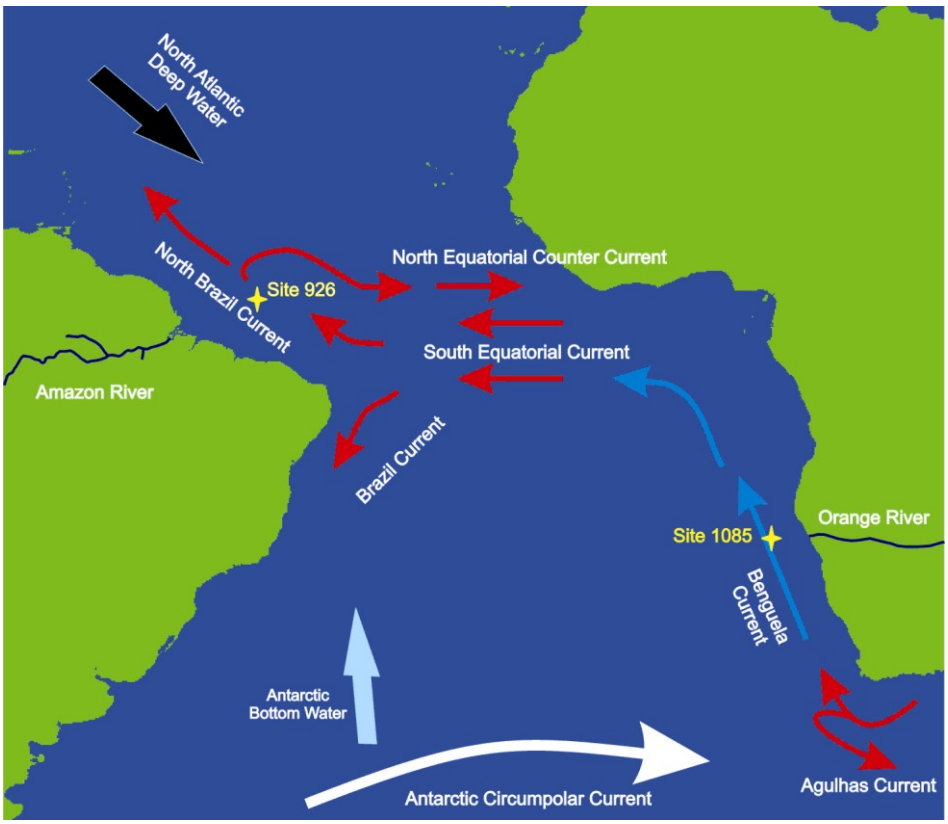

Fig. 2.1. Research areas (Site 926, Site 1085) and major sea surface and deep water currents of the recent equatorial and South Atlantic Ocean (after Peterson and Stramma, 1991; Philander, 2001).

In the South Atlantic, the southeast trade winds control the strength of the South Atlantic Gyre. The southern branch of the South Atlantic Gyre, known as the South Atlantic Current, transports temperate nutrient-poor thermocline waters eastward (Stramma and England, 1999). South of the South Atlantic Current is the location of the Subtropical Front, which separates the South Atlantic Current from the Antarctic Circumpolar Current (Peterson and Stramma, 1991). The Antarctic Circumpolar Current is banded into different fronts extending from the sea surface to the seafloor, and characterizes the boundaries between zones with different physical, chemical and ecological properties (Rintoul, 2009). The strong westerlies, which occur at mid and high latitudes where the isobars are nearly zonal and air-sea exchange of buoyancy, are the driving force for the Antarctic Circumpolar Current (Rintoul, 2009). The Antarctic Circumpolar Current and the South Atlantic Current converge south of the African continent with the Agulhas Current, which originates in the Indian Ocean. At this convergence zone, a retroflection area develops where a part of the Agulhas Current is

redirected towards the south and east, creating the Agulhas Return Current (Lutjeharms, 2001; Lutjeharms and de Ruijter, 1996). The other part of the Agulhas Current forms eddies at the retroflection area where a leakage of warm and saline Indian Ocean waters flow into the South Atlantic (Gordon, 1986, Peterson and Stramma, 1991). A direct inter-ocean transfer of Agulhas waters into the South Atlantic occurs occasionally via filaments (Lutjeharms and Cooper, 1996). The Agulhas Current and South Atlantic Current waters comprise the main source of the Benguela Current. The Benguela Current flows along the west coast of South Africa, adjacent to the Namibian desert. The largest and only perennial river in South Africa is the Orange River, which is located at about 28.5 °S (Dingle and Hendry, 1984; Nelson and Hutchings, 1983). Its freshwater input, however, only weakly influences the salinity of the Benguela Current (Nelson and Hutchings, 1983). The southern boundary of the Benguela Current is mainly located between 36 - 38 °S (Nelson and Hutchings, 1983; Shannon, 1985). The Benguela Current can be divided into the strong Benguela Coastal Current, which flows north towards the equator parallel to the African coast, and the weaker Benguela Oceanic Current. The Benguela Oceanic Current veers northwest at about 28 °S.

Eckman pumping leads to the development of coastal upwelling in this region. About eight permanent upwelling cells related to the Benguela Current can be observed where cold thermocline water comes to the surface (Lutjeharms and Meeuwis, 1987; Shannon et al., 2001). Surface water filaments transport these cold and nutrient rich waters offshore. To the north, the Benguela Current is bounded by the poleward flowing Angola Current, generating the Angola-Benguela Front. The Angola-Benguela Front is marked by a sharp horizontal temperature gradient, and is situated throughout the year between 14 °S and 17 °S (Meeuwis and Lutjeharms, 1990; Shannon, 1985; Shannon et al., 2001).

Towards the west, the Benguela Currrent feeds into the broad South Equatorial Current, which flows towards the eastern promontory of South America. There it bifurcates into the stronger northward flowing North Brazil Current, and the weaker southwards flowing Brazil Current (Peterson and Stramma, 1991). The strong trade winds, as well as the fast northward shift of the Inter Tropical Convergence Zone (ITCZ) during boreal summer, leads to a strong positive curl of the wind stress at about 8 °N and 51 °W. Most of the

North Brazil Current generates a series of unstable anticyclonic eddies, which contribute to the development of the eastwards flowing North Equatorial Counter Current (Muller-Karger et al., 1988, Philander and Pacanowski, 1986 a; Richardsen and Mc Kee, 1984). On the northern flanks of these eddies upwelling, and thus nutrient enrichment, can occur (Longhurst, 1993). The unretroflected water of the North Brazil Current continues to the northwest into the northern hemisphere as the Guyana Current and the Caribbean Current to form the basis of the Gulf Stream. The Guyana and Caribbean Currents are additionally fed by waters from the North Equatorial Current that flows at about 15° N, transporting relatively cold saline waters from the Canary Current westwards into the tropics. When the southeast trade winds are weaker, as during boreal winter, the North Equatorial Counter Current and the North Brazil Current retroflection area diminishes or even vanishes. The North Brazil Current and associated retroflection area is also important for the freshwater input from the Amazon River that enters into the tropical Atlantic. At about 70% of the Amazon discharge water flows around the retroflection area into the North Equatorial Counter Current (Muller-Karger et al., 1995), which translates into a freshwater contribution to the tropical Atlantic of about 6 x 1012 m^3 (Gibbs, 1970).

Beneath the equatorial surface currents, but within the thermocline layer, water is transported eastwards by the Equatorial Undercurrent (Philander, 2001). Most of this water mass originates from the South Atlantic by way of the North Brazil Current (Metcalf and Stalcup, 1967).

At intermediate depths in the equatorial and southern Atlantic, northwards flowing Antarctic Intermediate Water is present (Shannon and Nelson, 1996; Shannon et al., 2001). Below the intermediate waters, the North Atlantic Deep Water flows southwards, forming the bottom waters in the equatorial and northern South Atlantic. In the southern part of the South Atlantic, bottom waters are formed by northwards flowing Antarctic Bottom Waters (Peterson and Stramma, 1991; Shannon et al., 2001). Compared to the North Atlantic Deep Water, the Antarctic Bottom Water is relatively corrosive with respect to carbonate dissolution.

2.2 Reconstructed Oceanography of the Miocene Equatorial and South Atlantic Ocean

The South Atlantic Ocean during the Miocene was strongly influenced by the initiation and development of the Antarctic Circumpolar Current. During the early Miocene, at about 20.3-19.5 Ma, the Drake Passage opened to deep water flow and initiated hereby the Antarctic Circumpolar Current (Pagani et al., 2000). The formation of cold/nutrient rich Antarctic Intermediate Waters occurred, which were important for the progress of an upper water temperature gradient (e.g. thermocline) that, in turn, is needed for the formation of high-productivity areas, such as the Benguela upwelling region. A strengthening of the Antarctic Circumpolar Current, however, is not thought to have occurred before 14 Ma (Shevenell et al., 2004). The Benguela Current system during the middle Miocene was located further to the south than it is today because of weaker trade winds and a weaker Benguela Current. From about 14 Ma on, the Benguela Current system strengthened and shifted northwards, due to a strengthening of the subtropical anticyclone in relation to the enhanced Antarctic glaciations (Diester-Haass et al., 1992; Van Zinderen Bakker, 1984). The stronger winds present during cool periods also influenced the continental climate and led to a dryer climate over South Africa (Gingele, 1996), along with the development of the Namibian desert (Berger and Wefer, 2002).

The equatorial Atlantic during the middle and late Miocene was mainly influenced by the closure of the Central American Seaway. Before about 13 Ma, it is thought that an open Central American Seaway made an unrestricted exchange of water masses between the Pacific and Atlantic Oceans possible with an inflow of cool upper Pacific waters (Butzin et al., 2011, Chiasson and D'Hondt, 2000; Kameo and Sato, 2000; Maier-Reimer et al., 1990; Newkirk and Martin, 2009; Nisancioglu et al., 2003; Prange and Schulz, 2004). The volume flux from the Pacific into the Atlantic was balanced by a southward transport of warm waters, which is thought to have caused a reversal of the North Brazil Current in comparison to today (Butzin et al., 2011; Prange and Schulz, 2004). The inflow of upper Pacific waters into the Atlantic reduced zonal temperature and pressure gradients, which led to a weakening of the northern salt and heat transport (part of the thermohaline circulation) and thereby decreased North Atlantic Deep Water production

(Maier-Reimer et al., 1990; Prange and Schulz 2004). The initial North Atlantic Deep Water probably flowed into the Pacific through the open Central American Seaway until the first rapid uplift of the Panama Sill at about 12.9 - 11.8 Ma (Duque-Caro, 1990) forced the North Atlantic Deep Water to change direction and flow as a western boundary current into the South Atlantic (Nisancioglu et al., 2003). With a further uplift of the Panama Sill, the circumtropical circulation disappeared. The North Brazil Current reversed to its modern flow path into the North Atlantic, which provided for a strengthening the Gulf Stream and consequently directed the heat transport towards higher latitudes.

Chapter 3: Methods

3.1 Changes in Calcareous Dinoflagellate Cyst Assemblages

In order to investigate changes in calcareous dinoflagellate cyst assemblages, 53 samples were chosen from ODP Site 1085 (Benguela upwelling regime) and 43 samples from ODP Site 926 (Ceara Rise) were analyzed. These samples spanned the time interval of the middle to upper Miocene.

From each sample 1 ml was taken and dried at 60 °C (24 h). About 0.25 g of the dried material was dispersed in tap water. The solution was sieved through 63 µm and 20 µm sieves, transferred to a test tube and centrifuged at 3200 rpm for 6 min. The fractions coarser 63 µm and smaller 20 µm were not analyzed, as they contained no dinoflagellate cysts. The overlying water of the centrifuged material was removed and the material was transferred to an Eppendorf cup. Then, the volume was standardized to 1 ml. A certain amount of material was placed onto a microscopic slide, mounted in glycerine jelly and sealed airtight using paraffin wax. Whole calcareous dinoflagellate cysts were counted by using a light microscope (Zeiss Axioplan) with polarised light (Janofske, 1996). At least one slide per sample was counted. If a slide contained less than 150 specimens, additional slides were counted entirely. Relative cyst abundances as well as cyst accumulation rates (cysts cm^{-2} ky^{-1}) were calculated for all samples.

3.2 Separation of *Thoracosphaera heimii* for Isotopic Measurements

For the isotopic measurements, 78 samples were taken from ODP Site 926 (Ceara Rise), covering the time interval of the middle and upper Miocene.

In order to separate the calcareous dinoflagellate cyst species *Thorscosphaera heimii* from the sediment matrix, the density/size separation method described by Zonneveld (2004) was used. The method is a combination of sieving, settling and decanting steps that removes calcareous material other than *T. heimii* from the sediment. The different steps are rerun until ≥ 85% of the calcareous particles remaining are *T. heimii*. This is done because it has been shown that more than 15% of other calcareous material will alter the isotopic signal (Zonneveld, 2004).

From the 78 samples treated with the density/size separation method, 57 samples were used for further isotopic measurements. In 15 samples no or too few cysts of *T. heimii* were found, and 6 samples were too contaminated from a high amount of calcareous debris to achieve the 85% purity.

The measurements of the stable isotopes were performed at the Center for Marine Environmental Sciences (MARUM), University of Bremen, Bremen, Germany. A Finnigan MAT 251 mass spectrometer was used with an automatic preparation line (KIEL II carbonate device). Analytical precision of the N18O analysis was 0.07‰. Stable isotope values are given in δ-notation versus Vienna Pee Dee Belemnite (VDPD).

Paper I

Chapter 4: Paper I

The Benguela upwelling related to the Miocene cooling events and the development of the Antarctic Circumpolar Current: Evidence from calcareous dinoflagellate cysts

Heinrich, S.[1], Zonneveld, K.A.F.[1], Bickert, T.[2] , Willems, H.[1]

[1]*Department of Geosciences, University of Bremen, P.O. Box 330 440, D-28334 Bremen, Germany*

[2] *Marum-Center for Marine Environmental Sciences, P.O. Box 330 440, D-28334 Bremen, Germany*

(Paleoceanography 2011)

Abstract

Sediment samples from ODP Site 1085 were investigated in order to obtain more information on the initiation and development of the Benguela upwelling system during the middle and upper Miocene. In particular, our intent was to establish the causes of the upwelling as well as the response of the upwelling regime to the development of the Antarctic Circumpolar Current. Based on changes in the calcareous dinoflagellate cyst association, we found an initial increase of the dinoflagellate cyst productivity, probably related to the initiation of upwelling about 11.8 Ma ago. Two distinct increases in cyst productivity in conjunction with temperature decreases of the upper water masses reflect upwelling pulses off Namibia and occur at the end of the Miocene cooling events Mi5 (about 11.5 Ma) and Mi6 (about 10.5 Ma). Both cooling events are associated with an ice volume increase in Antarctica and are thought to have led to an increase in southeasterly winds, possibly causing these two upwelling pulses. We demonstrate a decrease in dinoflagellate cyst productivity and enhanced terrigenous input via the Orange River after the Mi5 event. At about 11.1 Ma, the dinoflagellate cyst productivity increases again. The polar cyst species *Caracomia arctica* occurs here for the first time. This implies an influence of subantarctic mode water and therefore a change in the quality of the upwelling water which allowed the Benguela upwelling to develop into modern conditions. From about 10.4 Ma, *C. arctica* forms a permanent part of the association, pointing to an establishment of the upwelling regime.

4.1 Introduction

The middle- to late Miocene epoch is characterized by major climatic shifts to colder global temperatures. These periods of cooling (Mi events) have been obtained from oxygen isotopic shifts that have been related to stepwise increases of the Antarctic ice-sheet (e.g. Miller et al., 1991). To date there exist many hypotheses about the causes of the Antarctic ice build-up that are currently debated (DeConto and Pollard, 2000; Holbourn et al., 2005; Holbourn et al., 2007; Pagani et al., 2005). Two climatic features are considered to have a major influence on the cooling of the climate: 1) the decrease in atmospheric CO2, and 2) the isolation from heat by oceanic currents (Ruddiman, 2008). A major factor that is considered to have had an important impact on both features is the intensification of the Antarctic Circumpolar Current, which has induced an increasing temperature gradient between the poles and the equator, favouring the development of zonal winds. In turn, enhanced zonal winds provoke the development of coastal upwelling along eastern boundary currents, such as the Benguela Current and its associated Benguela upwelling (Vincent and Berger, 1985).

Today the Benguela Upwelling system is one of the four major eastern boundary upwelling regions of the world ocean, driven by the south easterly trades. It can be divided in a coastal upwelling, where the south easterly trades drive an offshore surface drift causing upwelling over most of the continental shelf and an oceanic upwelling. The oceanic upwelling develops, where the seaward extension of the coastal upwelling forms a thermal front. This front follows the shelf break. Both upwelling features result in zones of enhanced productivity. Studies of the Benguela upwelling have shown a first initiation of high productivity in relation to upwelling during the Miocene at about 10 Ma on Walvis Ridge (DSDP 362, 532; Diester-Haass et al., 1990; 1992; Siesser, 1980). More recent studies closer to the southwest African coast (ODP 1085, 1086, 1087) provide strong indications that the occurrence of a first initiation takes place earlier, about 12-11.5 Ma (Diester-Haass et al., 2004; Paulsen, 2005). These studies document an increase in mass accumulation rates of organic carbon and benthic foraminifera accumulation rates, which indicates an increase in productivity at that time (Diester-Haass et al., 2004). These

changes in productivity coincide with changes in the regional climate. Based on sedimentological analyzes, Diester-Haass et al. (2004) observed enhanced input of terrigenous material in the marine realm originating from the Orange River as well as a high content of shelf derived particles. They suggest that a major regression occurred, causing enhanced erosion of the shelf. This is supported by a study of Haq et al. (1987) who documented a regression in the global sea-level curve at this time interval. The reconstructed time interval for the upwelling initiation also coincides with the Mi 5 event, which has been observed in an increase of $\delta^{18}O$ values at Site 1085 between 11.9-11.5 Ma (Westerhold et al., 2005). Westerhold (2003) and Westerhold et al. (2005) suggest a strong relation between the increases in $\delta^{18}O$ during the Mi events with enhanced down slope transport of terrigenous matter and a sea-level low stand in periods of extended ice-sheets on Antarctica. A relation between the initiation of the upwelling and the ice build-up on Antarctica seems therefore to be reasonable. This is in line with the observed relationship between global cooling and coastal upwelling in the form of a positive feedback mechanism (Berger and Wefer, 2002). However, it remains an open question why the initiation of upwelling was not recorded earlier during or just after the Middle Miocene Climate Transition? During this transition at about 14.8-12.5 Ma strong evidence is present that a major growth of the East Antarctic ice sheet with an associated global cooling took place (Billups and Schrag, 2002; Flower and Kennett, 1994). For this time interval it is documented that the atmospheric and oceanic circumpolar circulation intensified (Shevenell et al., 2004), resulting in an increased meridional temperature gradient and strengthened zonal winds, which could have initiated the Benguela upwelling. However, there is yet no explanation why there is a time lag of the initiation of the Benguela upwelling and the middle Miocene climate. A possible explanation might be a change in the nutrient availability of the upwelled water. Sarmiento et al. (2004) showed that, beside the intensity of south east trade winds, nutrient advection from the subantarctic region is also an important factor promoting the productivity in the upwelling area. They demonstrated that nowadays subantarctic mode water, which originates in the winter time mixed layers around the Southern Ocean and spreads throughout the entire Southern Hemisphere and North Atlantic Ocean, is the main source of nutrients for the thermocline. When more nutrient rich waters such as subantarctic mode waters became the main source of the upwelled waters only some time after the initiation of the upwelling, this could explain the delayed start of the enhanced

productivity which in turn could be an explanation why indications for an established upwelling were registered at such a late time. First indications for this scenario are already given by Paulsen (2005) who observed a first influence of southern water masses from 11.1 Ma on based on the occurrence of the polar foraminifer species *N. pachyderma (s)*.

Here, we want to contribute to this discussion by providing information about both the initiation of productivity as well as the source of the upwelled waters for the interval just after the Middle Miocene Transition. For this we establish a detailed reconstruction of past oceanographic conditions at Site 1085 located off the coast of Namibia using calcareous dinoflagellate cysts. Dinoflagellates represent one of the major phytoplankton groups and are abundant in all oceanic environments (Dale and Dale, 1992; Marret and Zonneveld, 2003). Calcareous-cyst-forming dinoflagellates are phototrophic/mixotrophic and live in the photic zone. The cysts are species-specific, and the fossilized assemblages in ocean sediments reflect the environmental conditions of the surface water masses at times of their production (Vink, 2004; Zonneveld et al., 2000). Numerous studies have shown their suitability for palaeoclimate reconstructions (Bison et al., 2009; Esper et al., 2000; Esper et al., 2004; Meier and Willems, 2003; Richter et al., 2007; Vink, 2004; Zonneveld et al., 2005; Zonneveld et al., 2000).

Today there is a clear differentiation in dinoflagellates association between regions of the Antarctic Circumpolar Current, the upwelling regions and the central South Atlantic Ocean. We document a first initiation of productivity at 11.5 Ma. At 11.1 Ma species typical for Antarctic Circumpolar regions appear for the first time in the Benguela upwelling. This species forms a permanent member of the association after 10.5 Ma indicating a pronounced shift in the nutrient availability in the Benguela upwelling area at that time.

4.2 Study area

4.2.1 Climate and hydrography

Today the south African climate is controlled by the two subtropical anticyclones, the South Atlantic High and the Indian Ocean High and a continental pressure field above South Africa (Shannon, 1985). The pressure difference between the South Atlantic High and the continental pressure field results in alongshore winds (trade winds). These trade winds are the prevailing winds offshore western South Africa today. The strength and position of the anticyclones and the resulting winds control the dry climate of western South Africa, the Namibian Desert (Gasse, 2000). The only perennial River in South Africa is the Orange River with the river mouth located at 28.5° S (Nelson and Hutchings, 1983). The Orange River is with a length of 2160 km and a catchment area of 973000 km2 the largest River in South Africa, and it delivers a big amount of freshwater and terrigenous material towards the Ocean (Dingle and Hendey, 1984).

The anticyclonic motion of winds around the South Atlantic High is reflected in the flow of one of the main currents of the South Atlantic, the South Atlantic Gyre. Its southern branch, the South Atlantic Current transports temperate, nutrient-poor thermocline waters eastwards (Stramma and England, 1999). South of the South Atlantic Current is the location of the Subtropical Front, which separates the South Atlantic Current from the Antarctic Circumpolar Current (Peterson and Stramma, 1991). The Antarctic Circumpolar Current is banded into different fronts, extending from the sea surface to the sea floor and marking the boundaries between zones with different physical, chemical and ecological properties (Rintoul et al., 2009). The driving force for the Antarctic Circumpolar Current are the strong westerlies as well as air-sea exchange of buoyancy (Rintoul et al., 2009).

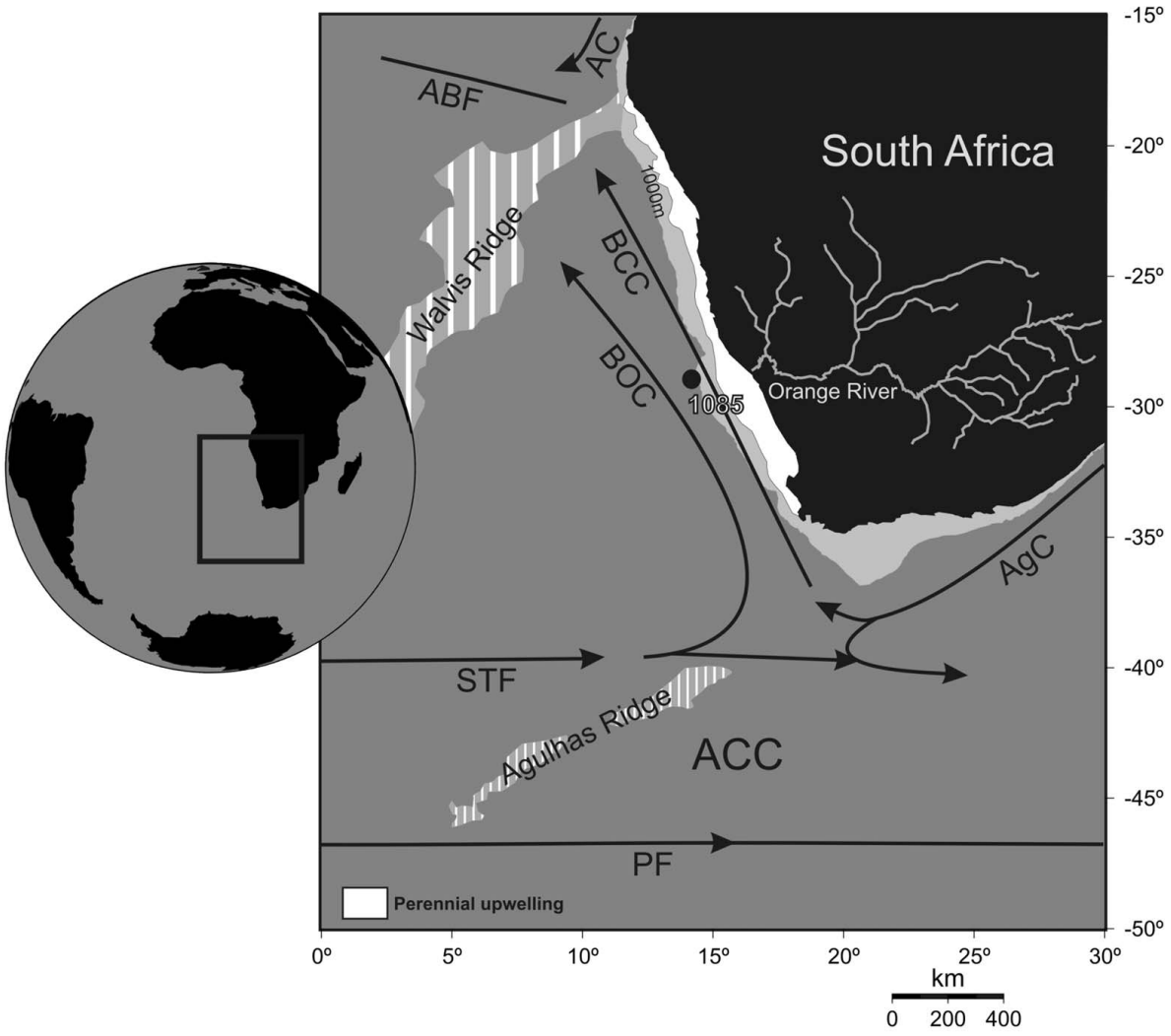

Figure 4.1. Map of the research area depicting the core site ODP 1085 and major oceanic surface currents. Surface currents after Peterson and Stramma (1991). AC, Angola Current; ABF, Angola - Benguela Front; BCC, Benguela Coastal Current; BOC, Benguela Oceanic Current; AgC, Agulhas Current; STF, Subtropical Front; ACC, Antarctic Circumpolar Current; PF, Polar Front.

The South Atlantic Current and the Antarctic Circumpolar Current meet south of Africa the Agulhas Current which comes from the Indian Ocean (*Fig. 4.1.*). Here, in the so called retroflection area, a part of the Agulhas Current becomes redirected towards the south and east, creating the Agulhas Return Current (Lutjeharms and de Ruijter, 1996; Lutjeharms et al., 2001). The other part of the Agulhas Current form eddies which are shed at the retroflection area (Gordon, 1986) and transport warm and saline water into the South Atlantic. Occasionally a direct transfer of Agulhas waters into the South Atlantic occur via filaments (Lutjeharms and Cooper, 1996). The Agulhas waters and the South

Atlantic Current form the main source for the Benguela Current. The Benguela Current is driven by the alongshore trade winds and can be divided into an equator ward fast flowing Benguela Coastal Current and a weaker Benguela Oceanic Current which turns northwest at about 28° S (*Fig. 4.1.*). Eckman pumping leads to the development of coastal upwelling. Today about eight permanent upwelling cells can be observed off the South western African coast. In these cells cold thermocline water well up to the surface (Lutjeharms and Meeuwis, 1987; Shannon et al., 2001). Surface water filaments transport these cold and nutrient-rich waters offshore. The most intense upwelling can be observed near Lüderitz (27° S) where the upwelled water is coldest and the offshore extension of the filaments is largest (Nelson and Hutchings, 1983). The strength of the upwelling cells shows a decreasing trend towards the north and south. In the North the Benguela Current is bound by the pole ward flowing Angola Current hereby generating the Angola-Benguela Front. The Angola-Benguela Front is a permanent feature, marked by a sharp horizontal temperature gradient and is situated throughout the year between 14° S-17° S (Meeuwis and Lutjeharms, 1990; Shannon, 1985; Shannon et al., 2001). The southern boundary of the Benguela Current varies considerably, but is mainly located between 36° S-38° S (Nelson and Hutchings, 1983; Shannon, 1985)

Below the Benguela Current, equator ward flowing Antarctic Intermediate Water is present between 500 to 1200 m (Shannon and Nelson, 1996; Shannon et al., 2001). At depths between 1000 and 3500 m well oxygenated North Atlantic Deep Water flows pole ward (Shannon et al., 2001). The deepest water mass of the Cape Basin is formed by the clockwise circulating Antarctic Bottom Water at depths below 4000 m. The Antarctic Bottom Water is restricted in its northward extension by the Walvis Ridge.

4.2.2 Miocene Oceanography

During the Middle Miocene the Benguela Current system was located more to the south than today, because of weaker trade winds as well as a weaker Benguela Current. At that time the Benguela current was flowing in the Cape Basin off the southwest African coast and turning west within the Cape Basin, not reaching Walvis Ridge (Diester-Haass et al.,

1992). During Antarctic glacial periods in the late Miocene the subtropical anticyclone strengthened and the Benguela system shifted northwards. The Benguela Current turned west and reached Walvis Ridge (Diester-Haass et al., 1992; Van Zinderen Bakker, 1984). The strengthening of the subtropical anticyclone and the Benguela Current with the development of upwelling was responsible for the beginning aridification of the Namibian desert (Van Zinderen Bakker, 1984; Van Zinderen Bakker and Mercer, 1986).

The formation of the Antarctic Circumpolar Current occurred already during the early Miocene due to the opening of the Drake Passage to deep-water flow at about 20.3-19.5 Ma Pagani et al., 2000). At this time it is considered that the formation of a cold and nutrient rich proto Antarctic Intermediate Water occurred (Pagani et al., 2000) which was important for the development of an upper water temperature gradient (e.g. thermocline), which in turn is necessary for the formation of high productivity areas, such as the Benguela upwelling. However, a strengthening of the Circumpolar Current is not documented prior to 14 Ma ago (Shevenell et al., 2004).

4.3 Material and Methods

4.3.1 Site description and stratigraphic framework

ODP Hole 1085 A (29°22.47`S; 13°59.41`E) was drilled during Leg 175 in a water depth of 1713 m on the continental slope of Southwest Africa in the southern Cape Basin along the western margin of the present-day Benguela upwelling region (Wefer et al., 1998). It is located 250 km east of the Orange River mouth, and the sediments mainly consist of greenish-gray nannofossil-foraminifer ooze diluted by variable amounts of terrigenous silt and clay (Wefer et al., 1998). 53 Samples were used for dinoflagellate studies from cores 48 X to 61 X at depths of 440-574 mbsf. Sample spacing ranges between 10 and 100 cm and at depths of 488-536 mbsf between 5 and 20 cm with a higher resolution (5-20 cm) at depths of 488-536 mbsf (*Fig. 4.2*.).

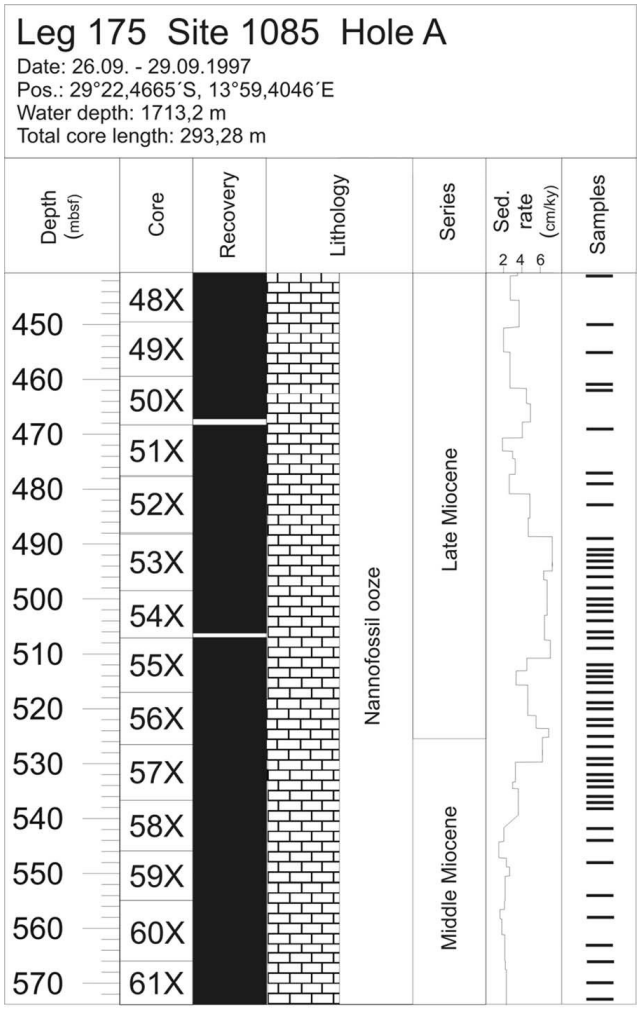

Figure 4.2. Lithologic column of the ODP core 1085 depicting the sample position of the calcareous dinoflagellates cyst analysis after Wefer et al. (1998). Sedimentation rates based on the age model by Westerhold et al. (2005).

The stratigraphic framework is based on the data of Westerhold et al. (2005), generated by orbital tuning of an XRF-Fe intensity record to an Eccentricity-Tilt-Precession (ETP) target curve. The sedimentation rates vary between 1.0 and 7.3 cm/ky (Westerhold et al., 2005). The 53 samples span the time interval of the middle to upper Miocene (12.4-9.2 Ma), which correspond to time intervals of 10-200 kyrs. During this time period three Miocene cooling events have been observed (Mi 5, Mi 6, Mi 7; Miller et al., 1991; Westerhold et al., 2005).

4.3.2 Sample procedure

From each sample 1 cm 3 sediment was dried at 60 ° C. About 0.25 g of the dried material was dispersed in tap water and sieved through 63 µm and 20 µm sieves. The fractions coarser 63 µm and smaller 20 µm contained no dinocysts and have not been analysed. The fractions between 20-63 µm were transferred to a test tube and centrifuged at 3200 rpm for 6 min. The overlaying water was decanted using a pipette, and the material was transferred to an Eppendorf cup where the volume was standardized to 1 ml. A fixed amount of material was placed upon a microscopic slide, mounted in glycerine jelly and sealed by air using paraffin wax. Calcareous-walled dinoflagellate cysts were counted using a light microscope with polarised light (Janofske, 1996). At least one slide per sample was counted. If a slide contained less than 150 specimens, additional slides were analysed. We calculated relative cyst abundances as well as cyst accumulation rates (cysts cm $^{-2}$ ky $^{-1}$) for all samples.

Based on the ecological characteristics of species in modern environments three different environmental indicators were distinguished.

Warm-water indicator

Calciodinellum albatrosianum is in modern sediments adapted to temperate to tropical conditions. It forms an increasing part of the association with increasing surface water temperatures (Esper et al., 2000; Vink, 2004; Wendler et al., 2002a).

Cold-water indicators

Calciodinellum levantinum and *Caracomia arctica* are restricted to colder water conditions (Vink, 2004). *Calciodinellum levantinum* has preference for relatively cool environments in a temperature range of 13-20 ° C (Vink, 2004). *Caracomia arctica* is today limited to polar regions south of the subpolar front at temperatures ≤ 10 °C (Streng et al., 2002; Vink, 2004).

Nutrient indicators

Leonella granifera, *Thoracosphaera heimii*, *Caracomia arctica* and *Calciodinellum levantinum*: These species have high abundances in areas characterized by enhanced nutrient availability in the surface waters, such as e.g. upwelling areas, river plumes etc. Of these species *Leonella granifera* is exclusively found in areas characterized by terrestrial input, mainly of fluvial origin (Richter et al., 2007; Vink, 2004; Wendler et al., 2002a).

Others

Scrippsiella regalis, *Pernambugia tuberosa*, *Pirumella parva* and one unidentified species: These species just occurred in low numbers or their ecological significance is not known. Therefore they are successively grouped as " others ".

4.3.3 Statistical analysis

The Modern Analogue Technique (C2 data analysis; Juggins, S. 2007) was chosen in order to highlight the relationship between dinocyst species distribution and environmental parameters. We compared our Miocene dinocyst distribution with a data set of recent dinocysts and environmental parameters, such as temperature and phosphate in the surface waters of the South Atlantic (Vink 2004).

4.4 Results

From the beginning of the dinocyst record at 12.4 Ma until about 11.9 Ma the sedimentation rates as well as the accumulation rates of all cyst species have low values. Nutrient indicators are present throughout this time in low absolute abundances. *Leonella granifera* that is characteristic for terrestrial input in the marine realm is present in low concentrations. The reconstructed phosphate concentrations of the surface waters show low values as well. The warm-water indicator forms the most dominant group of the

dinoflagellate cyst association at that time with high relative abundances. Sea surface temperatures increase at the beginning of the record and remain at relatively high temperatures. With the exception of a few recordings of *C. levantinum* between 12.3-12.2 Ma, the cold-water indicator as well as the polar species are absent (*Fig. 4.3*.).

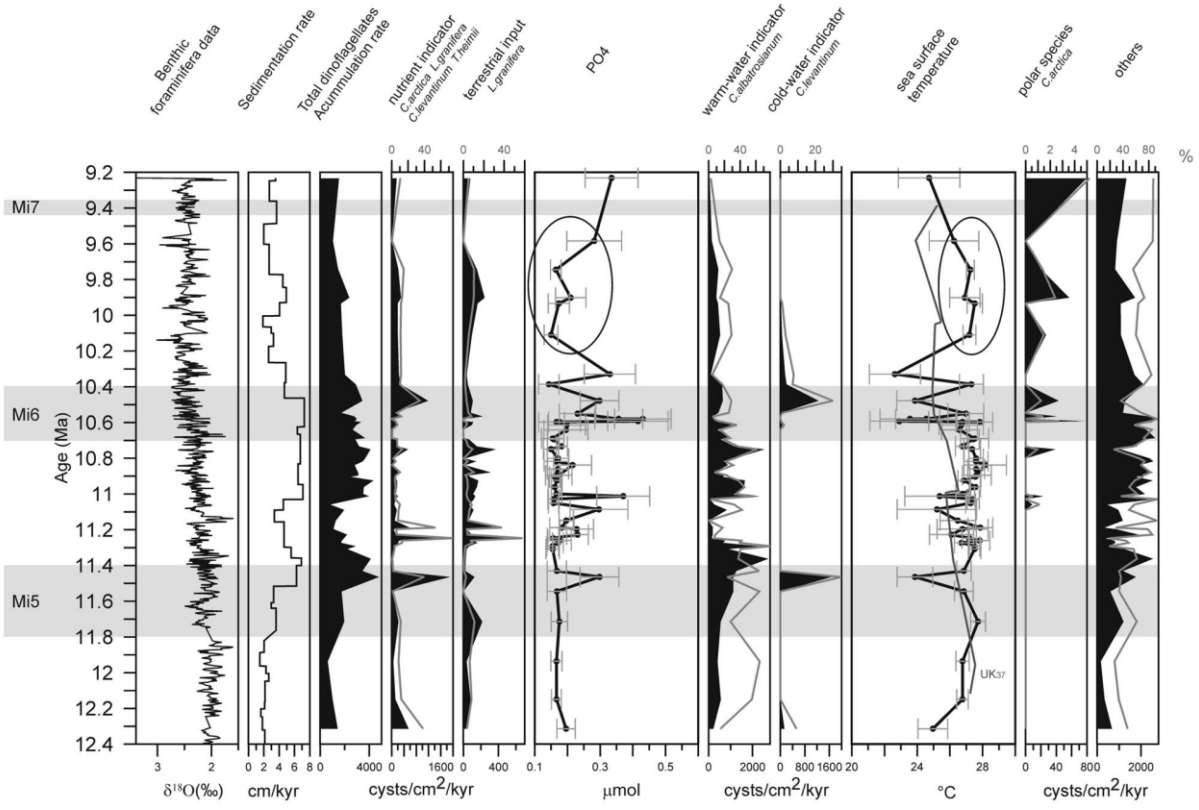

Figure 4.3. Absolute abundances (black shading) and relative abundances (gray lines) of the calcareous dinoflagellate cysts. Phosphate and sea surface temperature (SST) curve of the Modern Analogue Technique. SST from UK37 after Rommerskirchen et al. (2011) (gray curve). Stable oxygen isotope data and sedimentation rates are from Westerhold et al. (2005). Light shaded bars indicate the Miocene cooling events 5 through 7 from Westerhold et al. (2005). Ellipses indicate areas of selective cyst dissolution.

From about 11.9 Ma the sedimentation rate increases to a maximum at about 11.4 Ma. The dinocyst accumulation rates follow the increasing trend with a maximum at about 11.5 Ma.

The dinocyst association is changing contemporaneously with a distinct maximum of the nutrient indicators in both relative abundances and accumulation rates at 11.5 Ma. An increase at that time is also reflected in the phosphate concentration. The accumulation rates of the warm-water indicator increase from about 11.8 Ma onward towards a maximum at 11.4 Ma. However, its relative abundance remains the same as before with two short intervals with lower values at about 11.7 and 11.5 Ma. The cold-water indicator C. levantinum shows with a distinct maximum at 11.5 Ma, when the reconstructed temperatures decrease to a short minimum. *C. arctica* is still absent at that time.

The sedimentation rates as well as the dinocyst AR decrease after 11.4 until about 11.1 Ma. The accumulation rates of the nutrient indicators are low in this time interval but show distinct short maxima at 11.3 and 11.2 Ma. A similar, but more pronounced pattern can be observed for the accumulation rates of the terrestrial input indicator *L. granifera* that shows two short spikes of increased absolute and relative abundances at 11.3 and 11.2 Ma. At 11.2 Ma reflects the phosphate concentrations also a short increase. The warm-water indicator *C. albatrosianum* follows the decreasing trend of the total dinocyst AR until about 11.1 Ma. The sea surface temperature remains at higher values with a short decrease at about 11.1 Ma. The cold-water indicator *C. levantinum* and the polar species *C. arctica* are absent at that time.

From about 11.1 Ma on increases the sedimentation rate to stay at higher values until about 10.5 Ma. The accumulation rate of all dinocysts shows the same pattern except a short minimum at 10.6 Ma. The nutrient indicators have low absolute and relative abundances except one maximum at about 10.5 Ma. *L. granifera*, the terrestrial input indicator, shows an increasing trend towards 10.7 Ma then drops to lower values until 10.4 Ma. The phosphate concentrations show maxima at 11.1 and 11.0 Ma as well as at 10.6 and 10.5 Ma. The warm-water indicator increases from about 11.1 Ma on until a maximum at about 10.8 Ma. Afterwards it decreases towards a minimum at about 10.4 Ma. The cold-water indicator *C. levantinum* occurs in low abundances at 11.6 Ma and with a distinct maximum at 10.5 Ma. A distinct change in the association can be observed by the first occurrence of the polar species *C. arctica* at 11.1 Ma to be present in short

intervals at 11.0, 10.8, 10.6 and 10.5 Ma as well. The temperature curve shows minima contemporaneously to the occurrence of *C. arctica* at 11.1, 11.0, 10.6 and 10.5 Ma.

The sedimentation rate decreases after 10.5 Ma and remains at lower values except one increase at about 9.9 Ma. The total dinocyst AR as well as the nutrient indicator follow this trend, but show a minimum at 9.6 Ma and a slight increase afterwards until 9.2 Ma. *L. granifera* increases from about 10.4 Ma on until a maximum at 9.9 Ma to decrease subsequently until a minimum at 9.6 Ma. Afterwards there is a slight increasing trend of *L. granifera* visible. Phosphate values drop abruptly at about 10.4 Ma to increase afterwards until 10.3 Ma. Then, the phosphate concentration remains at lower values to increase from about 10.7 Ma on until the end of our record. The warm-water indicator *C. albatrosianum* increases from 10.4 Ma on to be present in low values until 9.8 Ma and than decreases again. The cold-water indicator *C. levantinum* decreases after 10.5 Ma and vanishes after 9.9 Ma. *C. arctica* increases in absolute and relative abundances from 10.4 Ma on with two minima at 9.9 and 9.6 Ma. The reconstructed sea surface temperatures show a minimum at 10.3 Ma, then increase again to decrease after about 9.7 Ma towards the end of the dinocyst record.

4.5 Discussion

4.5.1 Possible alteration of the cyst assemblages

By establishing a paleo-environmental reconstruction it is assumed that the calcareous cyst association in sediments reflects upper ocean conditions. However this does not hold if the initial signal has been altered because of dislocation of cysts by ocean currents and/or species-selective dissolution. Sediment trap studies on modern cyst production and deposition revealed that sinking velocities of calcareous dinoflagellate cysts do not allow for a larger lateral displacement of dinocysts (Richter, 2009). So far, detailed surveys of modern calcareous cyst distributions have not reported any indications of pronounced relocation of calcareous cysts. Associations in bottom sediments reflect in detail the

upper water conditions and transitions between upper water masses such as frontal systems (Vink, 2004; Zonneveld et al., 2000). We therefore assume that no selective dislocation has affected the dinocyst association.

Dissolution of calcareous dinocysts can occur during the settling process of the cysts or after settling at the sediment-water interface and thereby affect the primary cyst association. In the upper water column up to 60 % of the carbonate may dissolute by either biological processes within guts of grazers or increased degradation of organic matter within marine snow or aggregates, at which local carbonate-corrosive waters can be formed (Milliman et al., 1999). Jansen and Wolf-Gladrow (2002) suggest that calcite dissolution by grazing does not constitute to the major part of carbonate dissolution in the water column. It has been shown that the size, settling velocity and porosity of aggregates are unfavourable as a carbonate dissolving microenvironment around particles; and as a result dissolution in aggregates or marine snow is assumed to be negligible (Jansen et al., 2002).

In modern sediments calcareous cysts are found to be relatively robust against calcite dissolution and can even be observed in sediments from below the lysocline (Vink et al., 2000). Freshly produced calcareous cysts are covered by a thin organic layer which protects the cysts against calcite dissolution (Karwath, 2000). Site 1085 is taken at depth of 1713 m and lies today well above the lysocline. We therefore assume that dissolution did not alter the cyst association. This is supported by observations on carbonate sedimentation off southwest Africa (Diester-Haass et al., 2004; Kastanja et al., 2006; Krammer et al., 2006). These authors indicate that the drops in carbonate concentrations during the studied time are not caused by dissolution, but by dilution from major increases in clastic input from the Orange River during global sea-level regression and/or changes in the productivity of the calcareous nannoplancton. In contrast to dissolution this will not change the association composition but will have an influence on the total cyst accumulation rates.

4.5.2 Modern ecology of calcareous dinoflagellates

The modern ecology of dinoflagellates forming calcareous walled cysts have been studied in surface sediments, sediment trap studies as well as in culture experiments (e.g. Vink et al. 2002, Vink 2004, Meier and Willems 2003, Richter 2007, 2009, Karwath et al. 2000a/b, Zonneveld et al. 2000). Therefore, several physical factors are known to be important for steering cyst production and germination, such as temperature, salinity, trophic conditions and stratification of the upper water column. It has been shown that individual cyst species have different palaeoenvironmental significance and should therefore used as species specific indicators as it is described in Chapter 4.3.2.

The use of calcareous dinoflagellates as a productivity indicator has been discussed in several studies (Höll et al. 1998, 1999; Meier and Willems, 2003; Richter et al., 2007, 2009; Vink, 2004; Zonneveld et al., 2000). Earlier studies pointed to a negative relationship between productivity of the upper water column and cyst accumulation (Höll et al. 1998, 1999), whereas recently it has been shown that high nutrient availability and primary production in surface waters is leading to increased production of calcareous dinoflagellates (Meier and Willems, 2003, Richter et al., 2007, 2009; Zonneveld et al., 2000). Meier and Willems (2003) investigated the Eastern Mediterranean sapropel S1, which has been deposited under conditions of increased primary production. Most of the investigated dinocyst species increased markedly during S1 (*C. albatrosianum*, *T. heimii*, *L. granifera*, *C. levantinum*) whereas just one species (*L. urania*) decreased in both investigated cores during that interval (Meier and Willems, 2003). Richter et al. (2007) and Richter (2009) demonstrated in surface sediments as well as in sediment traps off NW Africa that nutrient supply stimulated growth of all calcareous dinospecies and subsequent cyst formation. Furthermore they observed increased dinocyst flux during times of enhanced chlorophyll-a concentrations, which are used as a measure of productivity.

In our sediment samples of ODP Site 1085 the dinocyst assemblage consists for the most part of the species *C. albatrosianum*, *T. heimii*, *L. granifera* and *C. levantinum*, which are known to increase during times of enhanced productivity. The only species,

which is so far strongly related to decreased productivity (*L. urania*, Meier and Willems, 2003) has not been found in our samples. We, therefore, use in this study dinocyst concentrations as a signal of productivity.

4.5.3 Benguela upwelling intensity related to productivity changes

Based on the calcareous dinoflagellates cyst assemblages, we observe a first indication for enhancing upper ocean productivity between 11.8-11.4 Ma, reflected by an increase in sedimentation rates and the dinoflagellate accumulation rates as well as a remarkable change in association. In this interval nutrient-and cold-water indicators show a pronounced increase in accumulation rates and dominate since then the cyst association. This indicates that upper waters became colder and more nutrient rich.

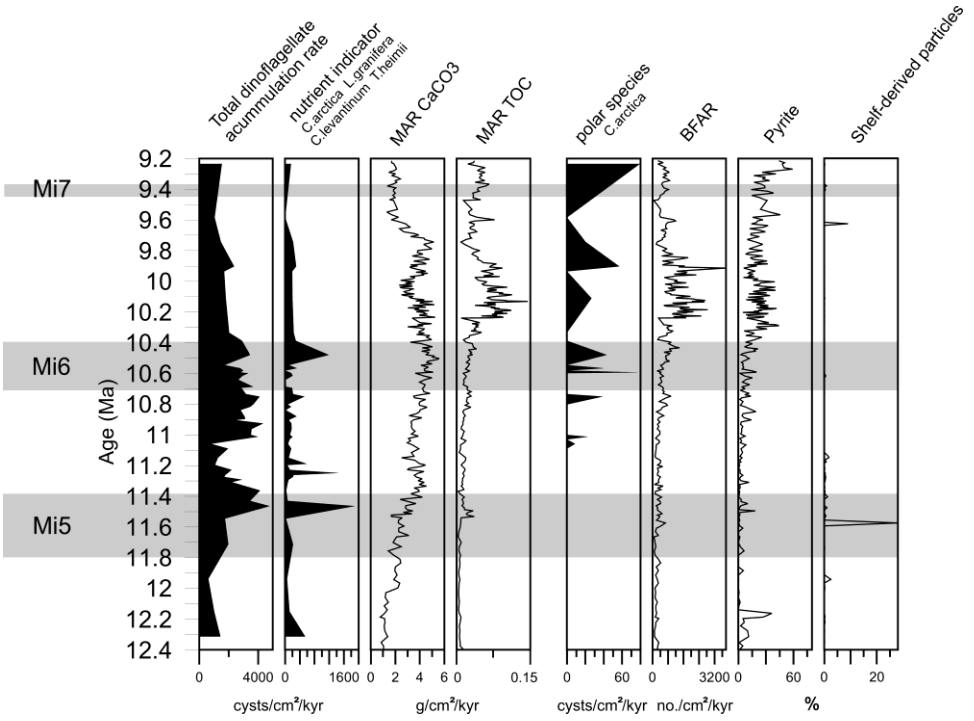

Figure 4.4. Comparison of the dinocyst accumulation rates with sedimentological data from Diester‐Haass et al. (2004). Black shading shows total cysts, nutrient indicators and terrestrial input indicator; black lines show mass accumulation rates of $CaCO_3$ and TOC, concentrations of fish debris, pyrite, and shelf‐derived particles in the sand fraction >63 mm. Light shaded bars indicate the Miocene cooling events 5 through 7 after Westerhold et al. (2005).

Previous to this interval (12.4-11.8 Ma) sedimentation rates, dinocyst accumulation rates and the nutrient indicators are low and the warm-water indicator dominates the cyst association. This implies that relatively warm, oligotrophic conditions prevailed in the surface waters suggesting a low productivity. This is consistent with the study of Krammer et al. (2006) who came to similar conclusions based on the observation of minimal values in the accumulation rate of coccoliths and total calcareous nannofossils during this time interval.The increase in productivity at 11.8 is in agreement with the sedimentological observations from Diester-Haass et al. (2004), which documented an increase in carbonate mass accumulation rates (MAR $CaCO_3$) and in the mass accumulation rates of organic carbon (MAR TOC) at this time. The enhanced organic carbon concentration together with enhanced pyrite concentration at that time suggests the development of a pronounced oxygen minimum zone (*Fig. 4.4*.) (Paulsen, 2005). Further support comes from Twichell et al. (2002), who observed an increase in C_{org}/N_{total} values at this time, which is interpreted to be the result of an increase in the total organic carbon export production of a marine origin.

At 11.5 Ma we observe a maximum in the accumulation rates of all dinocysts as well as in the absolute and relative abundances of the nutrient indicator. The reconstructed phosphate values show an increase as well. This is in agreement with the observed faunal changes and enhanced productivity at that time in the foraminiferal record of Paulsen (2005). We, furthermore, see a pulse of the cold-water indicator *C. levantinum* at 11.5 Ma as well as a decrease of the reconstructed sea surface temperatures, which are located at the end of the cooling event Mi 5. The Mi 5 is observed in this region at about 11.8-11.4 Ma (Westerhold et al., 2005) and is generally associated with a cooling of the world ' s climate and enhanced glaciations on Antarctica (Miller et al., 1991). Based on the dinocyst record, we observe a first maximum of productivity off southwest Africa at the end of this cooling event.

Afterwards the productivity seems to decrease, seen in the decrease of the sedimentation rates and dinocyst accumulation rates. The abrupt drop in the dinocyst accumulation rates is contemporaneous to short spikes of maximal values of the nutrient indicators and that of the terrestrial input indicator *L. granifera*. This suggests that surface waters received

enhanced nutrient availability accompanied with enhanced input of terrestrial material at these times. Our suggestion of enhanced input of terrigenous material at 11.3 and 11.2 Ma is supported by the study of Kastanja et al., (2006), who found high values of terrigenous input at about 11.3 Ma. There is strong evidence that the Namibian Desert was not yet fully developed and that much terrestrial material is transported into the research area via the Orange River (Diekmann et al., 2003; Partridge, 1993; Roters and Henrich, 2008; Siesser, 1980). The increase in nutrient availability in the upper water might therefore be the result of enhanced fluvial nutrient input.

From about 11.1 until 10.4 Ma we see another increase in sedimentation rates and accumulation rates of the dinocysts, which indicates another increase in productivity. Westerhold et al. (2005) observed increasing oxygen isotope values between 10.7-10.4 Ma with a marked increase at 10.4 Ma at Site 1085, implying a decrease in temperature at that time and related this interval to the cooling event Mi 6. Comparable to the succession observed during Mi 5 we see at the end of the Mi 6 another maximum of the nutrient indicators as well as another pulse of the cold-water indicator *C. levantinum*, which suggests another maximum in productivity at that time. Phosphate values are showing two increases, at about 10.6 and 10.5 Ma. Support for the indication of enhanced productivity in the research area at about 10.5 Ma also comes from the coccolith record of Krammer et al., (2006), who report the occurrence of the upwelling indicators *R. minuta* and *R. haquii* in high abundances.

The sedimentation rates as well as the dinocyst accumulation rates decrease after 10.5 Ma, implying a decrease in the dinocyst productivity. This is in contrast to the observation of Diester-Haass et al., (2004). They found suboxic conditions of the pore water based on increasing mass accumulation rates of total organic carbon as well as enhanced pyrite concentrations and an increase in benthic foraminifera accumulation rate (BFAR) for the late Miocene, which indicates a change to a permanent high productivity area during that time and suggested the establishment of the Benguela upwelling (*Fig. 4.4.*). The phosphate values (*Fig. 4.3.*), however, show as well an increase after the Mi6 with an increasing trend from about 9.7 Ma on.

A strong increase in the turbulence of the water column due to upwelling could also be the reason for the decrease in the total dinocyst accumulation rate at that time. It has been shown that strong turbulence is unfavourable for the production of dinoflagellate cysts (Wendler et al., 2002a; 2002b). To date highest production of calcareous cysts are observed at the margin of upwelling cells, rather than within (Vink, 2004; Zonneveld et al., 2000). We therefore assume that from 10.4 Ma on, enhanced upwelling and/or a migration of the upwelling cell caused more unfavourable conditions for most of the dinoflagellates.

4.5.4 Indications for a shift in the source waters of the Benguela upwelling

A first indication for changing conditions in the upwelling regime occurs at 11.1 Ma, about 0.7 Ma after the first upwelling indications, when the polar species *C. arctica* occurs for the first time in our record. From this time on *C. arctica* occurs sporadically in low numbers, but becomes a permanent member of the association after 10.5 Ma. The presence of *C. arctica* implies an influence of subpolar / polar water masses at the studied site.

This appearance of Antarctic calcareous dinoflagellates cyst species coincides with the first occurrence of the polar foraminifera species *Neogloboquadrina pachyderma (s)*. This species is registered to be a permanent member of the plankton in increasing abundances from 11.1 Ma onward (Paulsen, 2005). Other evidence comes from the coccolith record of Krammer et al., (2006) that show a distinct increase in abundance of the cold-water coccolith Coccolithus pelagicus. Today *C. pelagicus* is abundant in the North Atlantic and the subarctic realm whereas a somewhat larger form of *C. pelagicus* is typical for upwelling (Baumann et al., 1999; Samtleben et al., 1995).

As a possible cause for the presence of polar water species in the Benguela region, it can be thought of the scenario that they have been transported by intermediate waters of an Antarctic origin that form the source of the upwelled waters. It has been shown, that today' s subantarctic mode water is the main source for the delivering of nutrients into the

thermocline via upwelling in the Southeast Atlantic (Sarmiento et al., 2004). In this case *C. arctica* would reflect a change in the source of the upwelled water towards the conditions of today. From 10.5 Ma on *C. arctica* establishes which would imply the establishment of modern upwelling conditions. This would be in agreement with the decrease in the dinocyst productivity and the observations of higher surface water turbulence as discussed above. However, *C. arctica* has today never been observed in upwelling regions despite the fact that numerous detailed survey exist for these regions (Esper et al., 2000; Vink, 2004; Zonneveld et al., 2000). Furthermore, so far there is no evidence found that dinoflagellates become laterally transported over long distances via intermediate or deep water currents which are not their living habitat. An explanation for the absence of *C. arctica* in the Benguela region today could be a change in its ecology or in the habitat of the dinoflagellate. It can be thought that *C. arctica* nowadays is not formed in the photic zone of the area, where subantarctic mode water originates as a result of changed conditions in the source region or changed ecological adaptations of the species. As another possible solution for the presence of *C. arctica* it can be thought of a transport via subpolar/polar surface waters. Today *C. arctica* is thriving just south of the polar front and hypothetically a movement of the Polar Frontal Zone northwards could carry *C. arctica* into the research area. A northwards movement of the Polar Frontal Zone at different times in the past has already been suggested by several authors (McIntyre et al., 1989; Pagani et al., 2000; Paulsen, 2005). Pagani et al., (2000) postulated a migration of the Polar Frontal Zone during the middle and upper Miocene (from about 14 Ma on) as result of the development of the Antarctic Circumpolar Current that is thought to have caused the appearance of a relatively strong proto Antarctic Intermediate Water current and therefore a movement of the Polar Frontal Zone towards the North. Paulsen (2005) observed a northwards movement of the Polar Frontal Zone at about 10.3 Ma on the northern slope of Meteor Rise in the sub Antarctic sector of the Southern Ocean. Diekmann et al. (2003) described increases in Linear Sedimentation Rates at the Agulhas Ridge and Meteor Rise from about 11.2 – 9.5 Ma indicating lateral transport via pulses of the Antarctic Circumpolar Current. However, a northward migration of the Polar Frontal Zone up to 29° S has not yet being observed and seems also not to be very realistic since the African continent would act as a barrier for the circulation of the Antarctic Circumpolar Current.

A second possible explanation for the transport of *C. arctica* via polar surface waters into the studied region could be the interaction between the warm - water Agulhas Current and the Antarctic Circumpolar Current. Today, the warm - water Agulhas Current contacts the South Atlantic Current and the Antarctic Circumpolar Current at the retroflection area south of Africa. Within this process large rings develop that migrate into the South Atlantic Ocean (Gordon, 1986). The development and movement of these rings in modern situation has been studied in details by several authors (Ansorge and Lutjeharms, 2003; Boebel et al., 2003a; Boebel et al., 2003b; Gordon, 1985; Hardman - Mountford et al., 2003; Lutjeharms et al., 2001; Lutjeharms et al., 2003; Treguier et al., 2003). The eddies can be further transported in the form of independent features that have the form of large rings into the South Atlantic Ocean by the South Atlantic Current. However, today these rings are drifting slightly south of the studied site and are not reaching it. Changed conditions in terms of a broader Antarctic Circumpolar Current would be necessary to transport the Agulhas eddies farther north.

Despite the fact that we do not find unequivocal evidence from the dinocyst record the most reasonable scenario for the occurrence of Antarctic polar species at 11.1 Ma seem to be a transport via subantarctic mode water. All records, presented so far, reflect polar water influence at 11.1 Ma (Paulsen, 2005). This indicates that a change in nutrient conditions of upper waters, transported by subantarctic mode water, is a likely candidate for explaining the time lag of the establishment of modern upwelling conditions. The mechanism behind the change and the way of subantarctic mode water reached the upwelling site at that time remains a point that requires further study.

4.6 Conclusions

Based on changes in the calcareous dinoflagellates cyst association we come to the following conclusions:

1. The first initiation of productivity off southwest Africa occurred from 11.8-11.4 Ma with a maximum in productivity and a pulse of the cold-water indicator *C. levantinum* at the end of the cooling event Mi 5.

2. During a decrease in productivity from 11.3-11.2 enhanced terrigenous input from the Orange River is observed.

3. At 11.1 Ma productivity increased again. The polar species *C. arctica* occurs for the first time, indicating an influence of subpolar/polar waters on the upwelling region.

4. At the end of the cooling event Mi 6, at 10.5 Ma, another pulse of *C. levantinum* occurs.

5. From 10.4 Ma on the dinocyst productivity decreased caused by the establishment of the Benguela upwelling towards modern conditions. *C. arctica* establishes as well from that time on, implying subantarctic mode water to become the permanent source for the upwelled water.

Acknowledgements

Thanks are given to Petra Witte for her help with the SEM analyzes. We thank Lieselotte Diester-Haass for providing data on the carbon and coarse fraction of the sediments from ODP Site 1085, as well as foraminiferal accumulation rates. Thanks to Thomas Westerhold for providing the age model.

This work was funded through the DFG International Graduate College “Proxies in Earth History”.

Paper II

Chapter 5: Paper II

Western equatorial Atlantic (Ceara Rise) changes in surface and deep ocean circulation related to the middle/late Miocene closure of the Central American Seaway based on calcareous dinoflagellate cysts

Heinrich, S.[1], Zonneveld, K.A.F.[1], Bickert, T.[2], Willems, H.[1]

[1]*Department of Geosciences, University of Bremen, P.O. Box 330 440, D-28334 Bremen, Germany*

[2] *Marum-Center for Marine Environmental Sciences, P.O. Box 330 440, D-28334 Bremen, Germany*

(To be submitted to Palaeogeography, Palaeoclimatology, Palaeoecology)

Abstract

Sediment samples from ODP 154 Site 926A (Ceara Rise, western equatorial Atlantic Ocean) spanning the Neogene time interval of about 12.8 to 9.2 Ma were investigated in order to get a better understanding of the oceanographic changes during the middle and upper Miocene in relation to tectonic events, such as the closure of the Central American Seaway and the uplift of the Andes with the development of the Amazon River. Based on an increase in the accumulation rate of calcareous dinoflagellate cysts we reconstruct better calcite preservation from about 12.4-11.8 Ma, as well as at 11.5, 10.1 and 9.7 Ma and suggest this to be due to the influence of North Atlantic Deep Water, which was forced to flow into the South Atlantic after a first rapid uplift of the Panama Sill.

The dinoflagellate cyst association changes at about 11.2 from an almost mono specific assemblage to a higher cyst diversity. At this time the appearance and increased abundances of the species *Leonella granifera* indicate an influence of river discharge waters which can be linked to the developing Amazon River which waters reached the study site as result of a reversed southward flowing North Brazil Current. After 10.5 Ma the dinoflagellate cyst association reflects that the terrestrial Amazon input decreases at Site 926A, probably as result of a reduced inflow of Pacific waters through the Central American Seaway and a reverse of the North Brazil Current to its modern flow pattern.

5.1 Introduction

The middle- and upper Miocene represent a time-interval of major changes in palaeoceanography that favoured the cooling of the climate and culminated in the Northern Hemisphere Glaciation. During this time interval, the basis for the development of the modern deepwater circulation pattern, e.g. thermohaline circulation, was established. Tectonic events are thought to have played a key role in the progressing Miocene climate and oceanography, such as the narrowing of the Central American Seaway between North and South America (e.g. Duque-Caro, 1990) and the uplift of the Andes associated with development of the Amazon River, which influences the western tropical Atlantic surface water by delivering a huge amount of freshwater and nutrients (Gibbs, 1970; Milliman and Meade, 1983).

The closure of the Central American Seaway is thought to have started around 17 Ma with a gradually narrowing of the deepwater passage, and ending around 2.7 Ma with its final closure (Coates et al., 2003; Duque-Caro, 1990; Steph et al., 2006). The closure is discussed to be linked to changes in North Atlantic Deep Water formation and its pathway (Butzin et al., 2011; Lear et al., 2003, Nisancioglu et al., 2003). It has been shown that with an open Central American Seaway less saline Pacific upper ocean water was flowing into the Atlantic, leading to a reverse flow of the North Brazil Current towards the SE compared to opposite direction of today (*Fig. 5.1.B*; Butzin et al., 2011; Maier-Reimer et al., 1990; Newkirk and Martin, 2009; Nisancioglu et al., 2003; Prange and Schulz, 2004). Furthermore, a lower salinity contrast between the Pacific and the Atlantic is thought to have led to a weaker northern heat transport and to reduced northern deep water formation (Butzin et al. 2011; Prange and Schulz, 2004). However, several authors suggested the presence of a northern deep water mass already prior to the final closure of the Central American Seaway and suggested the initiation of such a water mass from about 12.5 to 12 Ma on (Lear et al., 2003; Miller and Fairbanks, 1985; Nisancioglu et al., 2003; Wright et al. 1993; Wright and Miller, 1996). It is thought that this early deep water mass was probably exported into the Pacific through the open Central American Seaway (Nisancioglu et al., 2003). Nisancioglu et al. (2003) showed that the uplift of the Panama Sill to about 1000 m water depth at 12.9-11.8 Ma (as reconstructed by Duque-Caro, 1990) prevented the passage of North Atlantic Deep Water and

forced it to flow into the South Atlantic. The decreased inflow of upper Pacific waters into the Atlantic from about 10.7 Ma on (Kameo and Sato, 2000) might have reversed the North Brazil Current to its current flow pattern towards the NE. The consecutively enhanced northward heat transport would, in turn, have increased North Atlantic Deep Water to be produced and have led to the development of the modern thermohaline circulation system (Kameo and Sato, 2000; Newkirk and Martin, 2009).

Despite the increase in information about the palaeoceanographic succession in this time interval, the complex interaction between the gradual closing of the Central American Seaway, the flow pattern of the North Brazil Current as well as the development of the North Atlantic Deep Water, and thus the oceanographic progression towards our present day circulation is still under debate (e.g. Molnar, 2008). It is for instance yet not well understood how North Atlantic Deep Water production is possible with an open Central American Seaway. Maier-Reimer et al. (1990) suggested that North Atlantic Deep Water production is reduced to near zero when the Central American Seaway is open. Butzin et al. (2011) found as well North Atlantic Deep Water to be absent or weak with a depth range of the Central American Seaway of 1-3 km. Nisancioglu et al. (2003), however, showed a significant amount of North Atlantic Deep Water production prior to the closure of the Central American Seaway.

Furthermore, most of the existing studies about the North Brazil Current during the middle/late Miocene concentrate on its role for the cross-equatorial transport of heat and salinity surface waters (Butzin et al., 2011; Nisancioglu et al., 2003; Prange and Schulz, 2004) and so far little is known about the influence of the reverse of the North Brazil Current for regional features such as the pathway of the Amazon outflow and sedimentary load.

Here, we contribute to this discussion by presenting a reconstruction of middle to late Miocene western Atlantic deep and surface water conditions based on the abundance and association of calcareous dinoflagellate cysts. For this purpose we analysed sediments from a core at the Ceara Rise, an aseismic ridge at current depths of 2600-3200 m below sea level (Curry et al., 1995). Ceara Rise is located in the western equatorial Atlantic and lies today within the mixing zone between North Atlantic Deep Water and Antarctic Bottom Water (*Fig.*

5.1.A). It is therefore ideally situated to trace changes in the presence and pathway of North Atlantic Deep Water in the past. Furthermore, the Ceara Rise, about 800 km east of the Amazon River mouth, is surrounded on the north, west and southwest by distal Amazon Fan deposits (Curry et al., 1995).

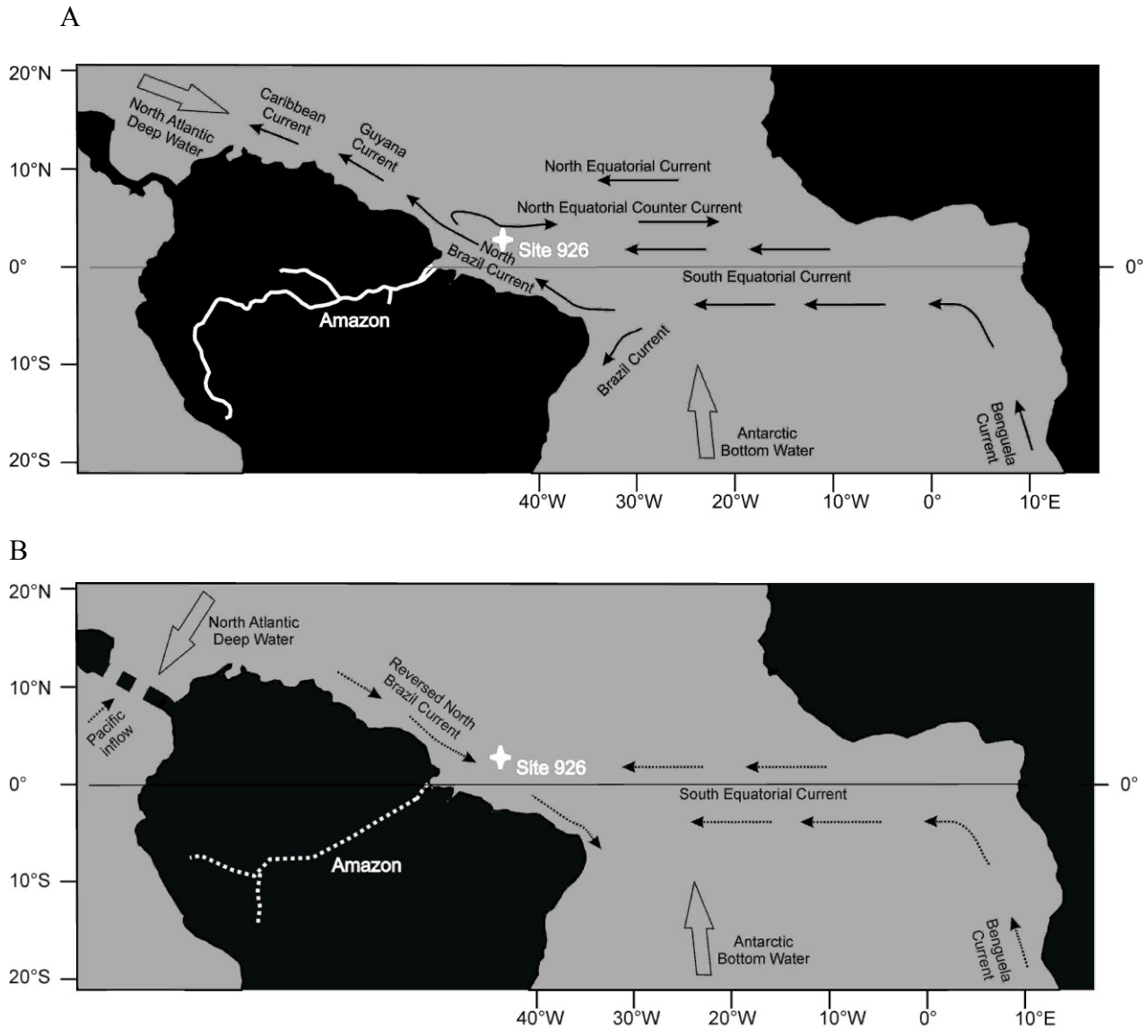

Fig.5.1. Map of the research area depicticg the core site ODP 926. A: major sea surface and deep water currents of the recent equatorial Atlantic. Adapted from Peterson and Stramma (1991) and Philander (2001). B: major sea surface and deep water currents of the reconstructed Miocene equatorial Atlantic (e.g. Newkirk and Martin, 2009; Nisancioglu et al., 2003). Amazon River during the late Miocene after Hoorn et al. (2010).

Calcareous cyst forming dinoflagellates belong to the group of phytoplankton and can be found in all oceanic environments (Dale and Dale, 1992; Marret and Zonneveld, 2003). They are phototrophic/mixotrophic and live in the photic zone. The dinoflagellate cysts are species-specific and the fossilized assemblage reflects the environmental conditions of the surface water masses at the time of their production (Vink, 2004; Zonneveld et al., 2000). Calcareous cysts can additionally be vulnerable for dissolution in a carbonate dissolving environment (Wendler et al., 2002b, Vink et al., 2002).

Here we use the changes in cyst accumulation rates to reconstruct phases of differential dissolution whereas the cyst association is used to reconstruct upper water conditions that can be related to varying upper water circulation patterns and the development of the Amazon River.

5.2 Sedimentation at Ceara Rise

The sediments of the Ceara Rise mainly consist of calcareous microfossils and terrigenous material. The terrigenous sediments have origin from the Amazon River. The organic carbon content is low due to the distance of the River mouth and to areas of strong primary productivity and upwelling (Curry et al., 1995). The surface waters at Ceara Rise show small seasonal variability and the input of the terrigenous material generates a higher sedimentation rate than usually observed under such low nutrient surface waters (Curry et al., 1995).

The variations in the biogenic sedimentation on the Ceara Rise are during the Miocene mainly influenced by regional productivity. The calcium carbonate content is additionally influenced by carbonate preservation related to changes in deepwater chemistry and circulation patterns (Curry et al., 1995). Differences in lithology between different sites on a depth transect on the Ceara Rise primarily reflect these changes. By comparing the lateral change in thickness of lithostratigraphic units along the depth transect, Curry et al. (1995)

observed a thinner exposure of the middle to late Miocene unit II at Site 926 compared to the same unit of the shallower Site 925 and suggest this to be the result of dissolution.

Recent studies on carbonate preservation at the Ceara Rise revealed an early increase in carbonate preservation at about 11.5 Ma and an overall increasing trend from about 10.1 Ma on (Preiß-Daimler, 2011). Between 9.5 and 9.2 Ma the carbonate content is reconstructed to decrease whereas calcite preservation is good. It is thought that during this time interval the carbonate pattern is driven by a productivity decrease of carbonate producing organisms (Preiß-Daimler, 2011).

The terrigenous input during the Miocene is thought to be generally controlled by the uplift of the Andes, with the growth of the Amazon fan. It has been shown that the accumulation of terrigenous (non carbonate) material on Ceara Rise was low between 20-10 Ma and increased markedly from about 10 Ma on (Curry et al., 1995; Dobson et al., 2001).

5.3 Material and Methods

5.3.1 Site description

The Ceara Rise is a bathymetric high in the western equatorial Atlantic which was formed at the Mid Atlantic Ridge about 80 Ma ago. Since that time the Ceara Rise drifts westwards and slightly northwards (Curry et al., 1995). The Ceara Rise is surrounded by a seafloor of an average depth of about 4500 m. It is located approximately 800 km east of the Amazon River mouth and is bounded on the north, west and southwest by the Amazon Fan. The Fan deposits lap onto the base of the western side at about 4200 m water depth (Curry et al., 1995).

ODP Site 926 (3°43.146`N, 42°54.489`W) is the southernmost of five sites, drilled in 1994 during Leg 154 as part of a depth transect. It is located at the SW flank of the Ceara

Rise, which today is slightly outside of the direct influence of the Amazon deposition. At Site 926 three holes were drilled (926A, 926B, 926C). 43 samples of core 926A have been analysed on their dinoflagellates content. 30 samples are derived at depths of 225-233 mbsf with a sample spacing between 10 and 55 cm from cores 24H to 25H. 13 samples have additionally been collected to develop a low resolution trend line covering an enlarged time span with 7 samples collected between 253 and 235 mbsf (core 25H) and 5 samples collected between 224 and 208 mbsf (cores 23H to 24H). Sample spacing ranges hereby between 100 and 700 cm (*Fig.5.2.*). Site 926A consists of clayey nannofossil chalk and nannofossil chalk with clay and foraminifers (Curry et al., 1995).

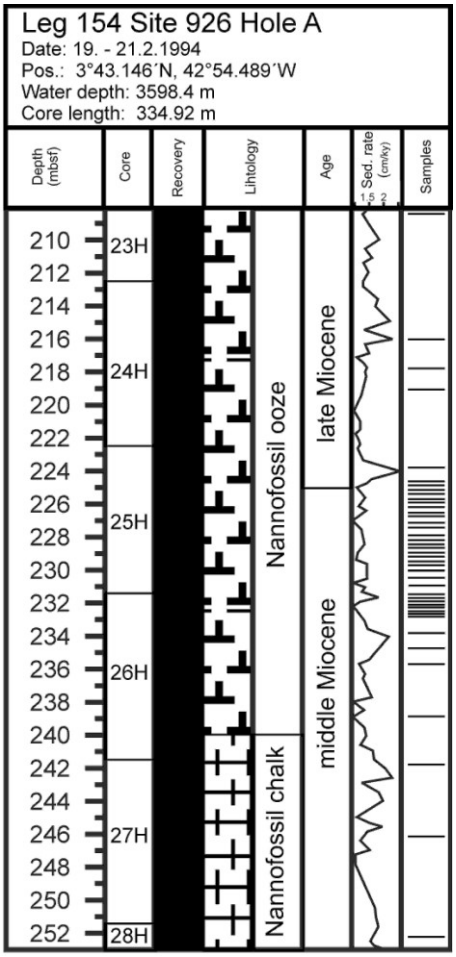

Fig.5.2. Lithologic column of the ODP core 926 after Curry, Shackleton and Richter et al. (1995) with the sample positions of the calcareous dinoflagellates cyst analyzes. Sedimentation rates based on the time scale by Shackleton and Crowhurst (1997).

5.3.2 Stratigraphic framework

The stratigraphic framework is based on the orbitally tuned time-scale of Shackleton and Crowhurst (1997), generated by correlating lithologic cyclicity to the astronomically determined variations in northern hemisphere summer insolation. The sedimentation rates vary between 0.5 and 2.6 cm/ky (Shackleton and Crowhurst, 1997). The 30 samples span the time interval of the upper Miocene (11.5-10.5 Ma) with sample spacing ranging from 12-100 kyrs. The additional 13 samples cover the time intervals from 12.8-11.6 Ma and 10.4-9.2 Ma with sample spacing between 100 and 500 kyrs.

5.3.3 Sample procedure

From each sample 1 cm^3 sediment was dried at 60° C. About 0.25 g of the dried material was dispersed in tap water and sieved through 63 µ and 20 µ sieves. The fractions coarser 63 µm and smaller 20 µm contained no dinocysts and have not been analysed. The fractions 20-63 µm were transferred to a test tube and centrifuged at 3200 rpm for 6 min. The overlaying water was removed using a pipette and the material was transferred to an Eppendorf cup where the volume was standardized to 1 ml. A fixed amount of material was placed upon a microscopic slide, mounted in glycerine jelly and sealed air tight using paraffin wax. Calcareous-walled dinoflagellate cysts were counted using a light microscope with polarised light (Janofske, 1996). At least one slide per sample was counted. If a slide contained less than 150 specimens, additional slides were analysed. We calculated relative cyst abundances as well as cyst accumulation rates (cysts cm^{-2} ky^{-1}) for all samples.

We distinguish four different environmental indicators which are based on the ecological characteristics of the dinoflagellate species in modern environments:

Warm water indicators

Calciodinellum albatrosianum and *Calciodinellum operosum* are in modern sediments adapted to temperate to tropical regions. They form an increasing part of the association with

increasing surface water temperatures (Esper et al., 2000; Vink, 2004; Wendler et al., 2002a). Vink (2004) suggested that these two species might be genetically linked to each other.

Terrestrial input indicator

Leonella granifera has high abundances in areas characterized by enhanced nutrient availability in the upper water column and is exclusively found in areas characterized by terrestrial input (Richter et al., 2007; Vink, 2004; Wendler et al., 2002a).

Cosmopolitan species

Thoracosphaera heimii is today the most abundant calcareous dinoflagellate species and often dominates the cyst associations due to its short reproduction cycle (Zonneveld et al. 2000; Vink 2004; Wendler et al. 2002 a,b,c; Dale and Dale 1992; Richter et al 2007). Highest percent abundances of *T. heimii* are found in the somewhat cooler regions of the South Atlantic (i.e. in the South Atlantic Gyre and the Benguela upwelling regions; Vink, 2004). However, Kohn and Zonneveld (2010) found no significant correlation between cyst concentration and temperature, salinity and chlorophyll-a concentration. They concluded that turbulence of the upper water masses is a major factor controlling cyst production with a decrease in production by increasing turbulence of the water column.

Indicator for the influence of central gyre waters

Pernambugia tuberosa is mainly confined to oligotrophic and relatively saline (36-37 p.s.u) water conditions (Vink, 2004; Meier et al., 2004b). *P. tuberosa* shows today a clear restricted distribution pattern to nutrient poor regions, such as the South Atlantic Gyre (Vink, 2004). In culture experiments cyst production occurred at relatively high temperatures (Meier et al., 2004b), whereas statistical analyses of a sediment trap study revealed no correlation between cyst concentration and temperature (Richter et al., 2009).

Pirumella parva and Scrippsiella regalis

Pirumella parva is a Cenozoic species which appeared in the early Danian and continued at least into the early Pleistocene (Fütterer, 1984). Little information on its ecology is known.

This species is therefore not used as an indicator in this study. *Scrippsiella regalis* occurs just in very small numbers and is therefore grouped together with *P. parva* as "*others*".

5.4 Results

*Fig. 5.3.*A shows the trendline of the calcareous dinoflagellates covering the time interval from about 12.8-9.2 Ma. North Atlantic Deep Water/Northern Component Water percentages are given after Wright and Miller (1996) from about 12.5-9.2 Ma. In the interval from about 10.2 to 9.4 are additionally Carbonate mass accumulation rates (MAR $CaCO_3$) shown after Preiß-Daimler (2011).

The total dinoflagellate accumulation rate shows increasing trends together with higher percentages of North Atlantic Deep Water production (Wright and Miller, 1996) around 12, 11.5, 10.1 and 9.7 Ma. The increase of the dinoflagellate accumulation rate at about 10.7 Ma is, however not reflected as an increase in North Atlantic Deep Water percentage.

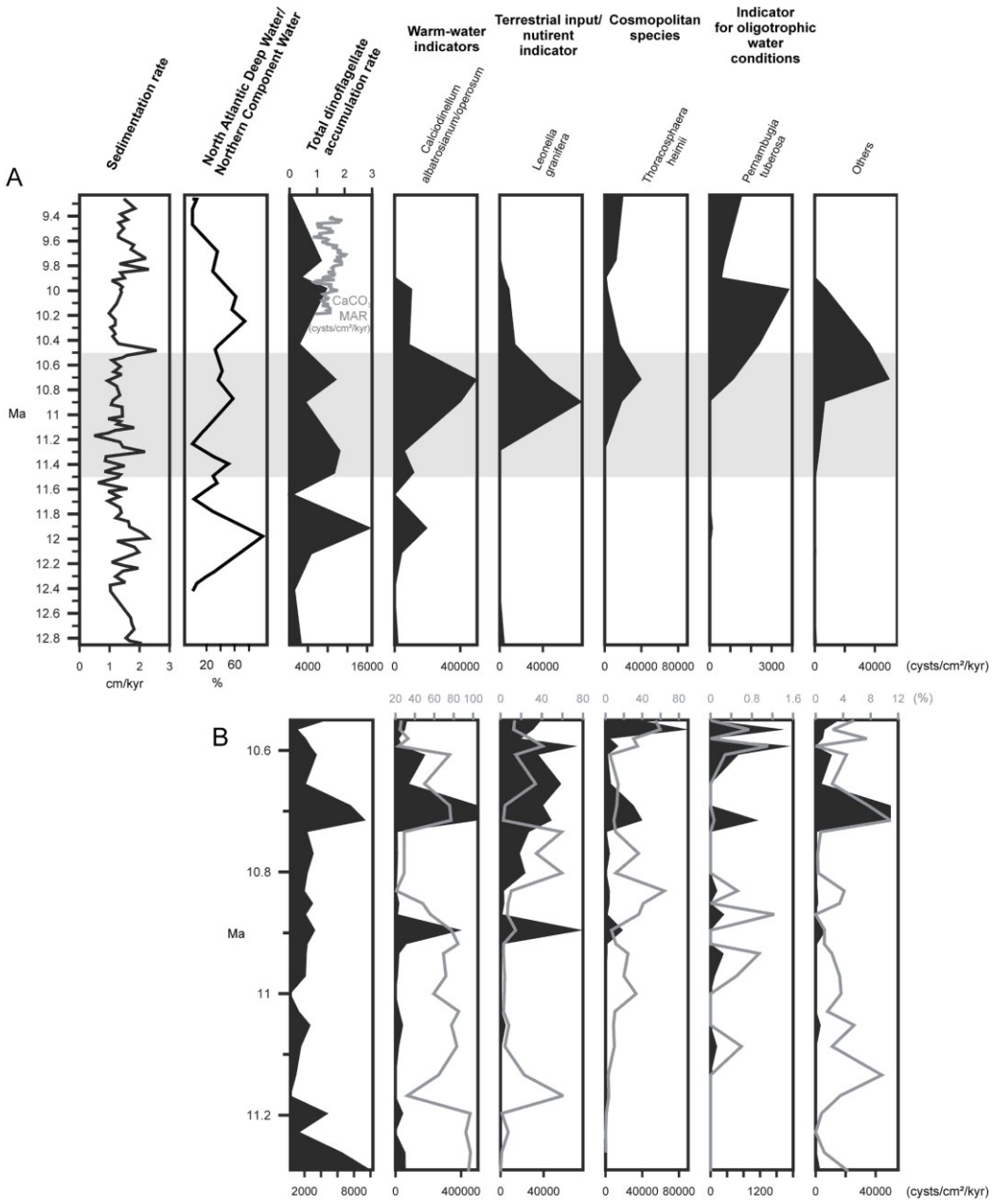

Fig. 5. 3. Calcareous dinoflagelate cyst data. A: trendline of the calcareous dinoflagellate cyst accumulation rates. Sedimentation rates are after Shackleton and Crowhurst (1997). North Atlantic Deep Water/Northern Component Water percentages are after Wright and Miller (1996). Carbonate mass accumulation rates (MAR $CaCO_3$) are after Preiß-Daimler (2011). Light grey shaded bar indicates the section of higher resolution in the dinoflagellate data presented in B. Calcareous dinoflagellate cyst absolute abundances (black areas) and relative abundances (grey lines).

The oldest part of the record from about 12.9 Ma to about 12.4 Ma is characterized by low dinoflagellate cyst diversity. The warm water indicators *C. albatrosianum* and *C. operosum* dominate the association. In the time interval from about 11.2 to about 10.4 the warm water indicators (*C. albatrosianum*/*C. operosum*), the terrestrial input indicator (*Leonella granifera*) and the cosmopolitan species (*Thoracosphaera heimii*) show an increasing trend. The indicator for more oligotrophic upper water conditions (*Pernambugia tuberosa*) increases from about 10.8 Ma. In the youngest part of the record from about 9.7 to 9.2 Ma only the cosmopolitan species as well as the species which indicate more oligotrophic conditions are present. The warm water indicators disappear at about 9.9 Ma and the terrestrial input indicator at about 9.7 Ma. The carbonate mass accumulation rates (MAR $CaCO_3$; Preiß-Daimler, 2011), show similar trends in comparison to the dinoflagellate accumulation rates, with increases at about 10 and 9.7 Ma. However, at about 9.6 Ma increases the carbonate mass accumulation rate while the dinoflagellate cyst accumulation rate decreases (*Fig.5.3.*A).

The greys shaded bar in *Fig. 5.3.*A presents the time interval that has been sampled with a higher resolution (11.3-11.5 Ma). The total dinoflagellate accumulation rate shows throughout this time interval two distinct minima, at about 11.1 and 11 Ma and two distinct maximum at about 11.3 and 10.7 Ma (*Fig. 5.3.*B).

In the interval from 11.3 to 10.9 Ma the warm water indicators (*C. albatrosianum*/*C. operosum*) dominate the association except for a single decrease between 11.2 and 11.1 Ma, where the terrestrial input indicator (*Leonella granifera*) shortly dominates. The cosmopolitan species (*Thoracosphaera heimii*) is present during this time interval from about 11.1 Ma on. *Pernambuggia tuberosa*, the indicator for oligotrophic conditions occurs sporadically at about 11.1 Ma and between 11 and 10.9 Ma. At about 10.9 Ma the warm water indicators, the terrestrial input indicator and the cosmopolitan species have an increase in their absolute abundance. The indicator for more oligotrophic waters is absent at that time, but appears in the record at about 10.8 Ma. At about 10.7 Ma all species show an increase in their absolute abundances. The warm water indicators remain at higher relative and absolute abundances until about 10.6 Ma except for a short decrease in between. After this date decrease the warm water indicators to lower values. The terrestrial input indicator increases in absolute numbers

in the time interval from about 10.8 until 10.6 and decreases slightly afterwards. *Thoracosphaera heimii*, the cosmopolitan species, shows after the increase at around 10.7 Ma another increase in absolute abundances around 10.5 Ma. The indicator for more oligotrophic conditions has in this time interval (ca. 10.6-10.5) an increase in absolute accumulation rates as well.

5.5 Discussion

5.5.1 Possible alteration of calcareous dinoflagellate cysts caused by transport

In paleoenvironmental reconstructions it is assumed that the calcareous cyst association in sediments reflect upper ocean conditions. However this is not true if the original signal has been changed because of species-selective preservation and/or displacement of cysts by oceanic currents. Sediment trap studies on modern cyst production and deposition have shown that sinking velocities of calcareous dinoflagellate cysts are high minimizing the risk of lateral displacement of cysts in the water column during the settling process (Richter, 2009). So far, detailed surveys of modern calcareous cyst distributions have revealed that cyst associations in bottom sediment reflect in detail upper water current systems including the exact position and movement of features like for instance front systems (Vink, 2004; Zonneveld et al., 2000). Also in the Miocene, calcareous dinoflagellate cysts are known to reflect changes in upper water conditions in detail (Heinrich et al., 2011). So far never indications of species selective relocation of calcareous cysts in the water column or after settling have been observed in modern sediments. We therefore assume that no selective dislocation has affected the dinoflagellate cyst association in this study either.

5.5.2 Signals of dissolution in relation to deep water changes

Calcareous dinoflagellate cysts can be dissolved during the settling process or after settling at the sediment-water interface (Wendler et al., 2002a,b). Species selective dissolution can thereby effect the primary signal (Wendler et al., 2002a,b).

In modern situations calcareous cysts are found to be relatively robust against calcite dissolution and calcareous cyst dissolution in the water column has, so far, never been shown (Vink et al., 2000; Richter 2009). Freshly produced calcareous cysts are covered by a thin organic layer which protects the cysts against calcite dissolution (Karwath, 2000). However, Vink et al. (1999) showed dissolution of calcareous dinoflagellate cysts over a depth transect at the Ceara Rise because of under saturation of seawater with respect to carbon ions at greater water depths.

Site 926 is recovered at a depth of 3598 m and is today bathed in North Atlantic Deep Water, in which carbonate preservation is known to be very good. During the Miocene, however, North Atlantic Deep Water production as well as its flow pattern was reconstructed to be different from today and it is reconstructed that at about 12.5 Ma the study site was under the influence of a more corrosive southern water mass (Southern Component Water analogue to Antarctic Bottom Water; King et al., 1997). An indication for dissolution at the site between about 12.6-12.4 Ma was, moreover, shown by Shackleton and Crowhurst (1997), who observed a reduced flux of the coarse fraction (> 63µm) at that time. We observe low dinoflagellate cyst accumulation rates and enhanced fragmentation of the cysts during this time interval and therefore assume this to be the result of carbonate dissolution at Site 926 throughout this time.

After 12.4 Ma increases the total dinoflagellate accumulation rates, which suggest a change in bottom waters with a less corrosive character. This is conform with observations of Wright and Miller (1996) who reconstructed percentage of North Atlantic Deep Water production based on changes in Neogene mantle plume activities in this time interval (*Fig. 5.3.*A).

Also other recordings confirm our suggestions. Based on reconstructions of carbonate fluxes King et al. (1997) suggested that influence of less corrosive Northern Component

Water (analogue to North Atlantic Deep Water) results in a shoaling of the lysocline and in enhanced preservation of calcite. However, it is reconstructed that early North Atlantic Deep Water was probably flowing into the Pacific, due to an open Panama Seaway and, therefore, did not reach Site 926 (Nisancioglu et al., 2003). From about 13-12 Ma, however, a rapid uplift of the Panama Seaway to about 1000 m water depth is reconstructed which might have reduced or even prevented the passage of the northern deep water into the Pacific and forced it to flow as a western boundary current into the South Atlantic (Duque-Caro, 1990; Nisancioglu et al., 2003). We, therefore, suggest that the better preservation at Site 926A after 12.4 Ma reflects this pulse of North Atlantic Deep water, which reached the studied site related to an uplift of the Panama sill.

Further increases in the total dinoflagellate accumulation rates around 11.5, 10.1 and 9.7 Ma suggest additional pulses of North Atlantic Deep Water at Site 926. This is in line with increases in North Atlantic Deep Water production (Wright and Miller, 1996) and increase in carbonate mass accumulation rates at the Ceara Rise ($CaCO_3$ MAR; Preiß-Daimler, 2011). We, therefore, assume that these increases in cyst accumulation rate reflect better carbonate preservation due to pulses of North Atlantic Deep Water.

However, at about 11.2 until about 10.5 Ma a decrease in total dinoflagellate accumulation rate with the exception of a short increase at about 10.7 Ma is observed, suggesting decreased preservation. This is in contrast to reconstructions of North Atlantic Deep Water productions that indicate another production increase during that time interval (Wright and Miller, 1996). At the same time, (from ca. 11.2 Ma on), increases the cyst diversity and therewith the abundances of the species *Thoracosphaera heimii*. Shells of *T. heimii* are relatively small and porous and it has been shown that *T. heimii* is most prone to calcite dissolution (Wendler et al., 2002 b). The increase of *T. heimii* shells as well as the fact that the cysts showed no signals of enhanced fragmentation during this time interval leads to the assumption that calcite preservation during this time interval is good which is in contrast to what initially can be inferred from the total accumulation rate. We, therefore, assume that a change in cyst production and composition resulted in the changed accumulation rates, rather than dissolution. This is also supported by an increase in carbonate mass accumulation rates ($CaCO_3$ MAR) observed from about 11.5 Ma on (Preiß-Daimler, 2011). Another reason for a

decreased cyst accumulation rate from about 11.2-10.4 Ma could be that enhanced terrigenous input had led to dilution (see also section 5.5.3). At about 9.9 Ma we find a short decrease in the accumulation rates of all species suggesting more corrosive conditions occurring at the sampling site. The carbonate mass accumulation rate also shows a decrease at about that time (Preiß-Daimler, 2011). This short decrease could possibly be tied to the lowest stand of sea level during the Miocene at around 10 Ma (Haq et al., 1987; Woodruff and Savin, 1989). The cyst accumulation rate increases afterwards again until a maximum at about 9.8 and then decreases until the end of this record. This coincides with an interruption in North Atlantic Deep Water production around 9 Ma (Wright et al., 1991, 1992; Wright and Miller, 1996). However during this time interval the sample resolution is low and our suggestions are just based on single points. Therefore, they have to be considered with care.

5.5.3 Terrigenous input on Ceara Rise in conjunction with the development of the Amazon River

On top of the variations in cyst accumulation rates which we mainly ascribe to changes in deep water advection we observe a distinct change in the dinoflagellate cyst association from about 11.2 Ma on. Here, the cyst diversity significantly increases by the arrival of the species *Thoracosphaera heimii* and *Pernambugia tuberosa*. Furthermore, we observe an increase the terrestrial input indicator, *Leonella granifera*, in relative abundance and accumulation rates (*Fig. 5.3*.B). To date *L. granifera* can only be observed in regions where terrestrial derived nutrient and trace elements enter the marine system by river discharge (Meier et al., 2004a; Vink 2004; Wendler et al., 2002c). *T. heimii* occurs today in many different environments. Highest production rates, however, are observed in regions and at times when upper waters are relatively well stratified (e.g. at times of upwelling relaxation; Kohn and Zonneveld 2010; Richter, 2009; Wendler et al., 2002a). *Pernambugia tuberosa* is today predominantly present in the central Atlantic gyres where oligotrophic conditions prevail (Vink 2004).

The occurrence of *L. granifera* at about 11.2 Ma suggests an input of nutrient/trace elements from a riverine source (Richter et al., 2007; Vink 2004, Wendler et al., 2002a).

Today the Amazon discharge waters flow northwards as a result of the present day circulation system with strong northward directed North Brazil, Guyana and Caribbean Currents. During the late middle Miocene (ca. 12 Ma) however, it is thought that the Amazon River was in its developing phase as a result of the uplift of the Eastern Cordillera in the Colombian Andes (Hoorn et al., 1995, 2010). A connection to the Atlantic Ocean was thought to be still absent at that time (Hoorn et al., 1995, 2010). However, observations based on a combination of biostratigraphic, isotopic and well log data show that the development of the Amazon as a transcontinental river occurred probably more early and a connection to the Atlantic Ocean might have been present already from 11.8-11.3 Ma (Figueiredo et al., 2009). Our results support this theory as we observe the first occurrence of low concentrations *L. granifera* already from about 11.6 Ma on with a further increase in abundance at about 11.3 Ma.

Our results suggest an earlier date for the development of an Atlantic Ocean connection as was reconstructed based on grain-size and elemental analyses of Sites 925 and 929 on the Ceara Rise (Dobson et al., 2001). Here a distinct increase of terrigenous material derived from the Andes was not observed until about 10 Ma (Dobson et al., 2001). Sites 925 and 929 are drilled on more northerly positions on the Ceara Rise compared to Site 926 which is studied here.

Today our site is less influenced by the Amazon compared to the other sites, as the northward flowing North Brazil Current transports the terrigenous Amazon load away from the southern part of the Ceara Rise (Curry et al., 1995). During Miocene times, however, the North Brazil Current was reversed compared to today as a result of the inflow of Pacific waters into the Atlantic through the open Panama Seaway (see also section 5.2.; Butzin et al., 2011; Prange and Schulz, 2004). The southward flowing North Brazil Current would have transported the Amazon load away from the more northern sites (925, 929) towards the southernmost Site 926. We therefore assume that at Site 926 changes in Amazon development and discharge would be registered more early compared to the sites that have a more northward position as observed by Dobson et al. (2001).

From about 10.5 Ma the terrestrial input indicator decreases and is absent from about 9.8 Ma on. The opposite trend is observed for the indicator for central gyre waters,

Pernambugia tuberosa. This correspond with the results of Harris and Mix (2002), who observed low terrigenous mass accumulation rates on Ceara Rise from about 10.5 until 8 Ma on and King et al. (1997), who found distinct changes in the terrigenous flux at 10.7 Ma and from 9.7-9.5 Ma based on synthetic records of terrigenous mass accumulation rates. A shift in the surface currents might form an explanation for these changed conditions to reduced nutrient availability in the upper water column at Site 926.

From about 10.7 Ma on, a decreased inflow of Pacific waters into the Atlantic through the Central American Seaway is reconstructed based on increasing carbonate mass accumulation rates in the Caribbean, changes in the foraminiferal assemblage as well as changes in the calcareous nannofossils, where the assemblages in the equatorial Pacific and the assemblages in the Caribbean became completely different (Chaisson and Hondt, 2000; Kameo and Sato, 2000; Newkirk and Martin, 2009). Such a decrease would lead to a northward flow of the North Brazil Current and, thereby, transport the terrigenous material away from the study site like it does today and bringing the sampling site under influence of the South Atlantic Gyre water masses. Our results suggest therefore that from 10.5 Ma onward the inflow of Pacific waters was reduced so much that South Atlantic Gyre waters permanently influenced Site 926.

5.6 Conclusions

The analysis of calcareous dinoflagellate cysts in sediment samples from ODP 154, Site 926A (Ceara Rise, western equatorial Atlantic Ocean), revealed the following conclusions:

1. From about 12.4-11.8 Ma we find the influence of North Atlantic Deep Water which is reflected in an increase in the dinoflagellate cyst accumulation rate due to a better carbonate preservation. The uplift of the Panama Sill during that time interval diverted the North Atlantic Deep Water to flow southwards and thereby reaching the Ceara Rise.

2. Further pulses of North Atlantic Deep Water production are reflected in the dinoflagellate cyst accumulation rate around 11.5, 10.1 and 9.7 Ma.

3. We found a distinct shift in the cyst association at about 11.2 Ma until about 10.4 Ma, where it changes from an almost mono specific assemblage to increased diversity. The occurrence of the terrestrial/nutrients indicator *L. granifera* reflects the first influence of the Amazon River. The Amazon load reached the study site due to a reversed North Brazil Current, which transported the terrigenous material southwards.

4. The decreased occurrence of the terrigenous/nutrients input indicator from about 10.4 Ma on reflects the reverse of the North Brazil Current to a northwards flow like in modern conditions, due to a decrease in Pacific inflow through the Central American Seaway.

Acknowledgements

We thank Inga Preiß-Daimler for making the carbonate mass accumulation rates available. Thanks are also given to the members of the working group of Historical Geology and Paleontology for their general assistance and helpful discussions.

This research was carried out within the framework of the International Graduate College: Proxies in Earth History (EUROPROX).

Paper III

Chapter 6: Paper III

Late Miocene stable oxygen isotopes of *Thoracosphaera heimii* from the western equatorial Atlantic Ocean (Ceara Rise)

Sonja Heinrich[1] and Karin A. F. Zonneveld[1]

[1]*Department of Geosciences, University of Bremen, P.O. Box 330 440, D-28334 Bremen, Germany*

(To be submitted to Micropalaeontology)

Abstract

Late Miocene stable oxygen isotopes have been measured on the shells of the calcareous dinoflagellate cyst species *Thoracosphaera heimii*, retrieved from sediments of the western equatorial Atlantic (Ceara Rise, ODP Site 926). Isotope values of *T. heimii* have been compared to stable oxygen isotopes of the foraminifer species *Globogerinoides sacculifer*. This comparison shows an offset that is probably a result of the symbiont photosynthetic activity of *G. sacculifer*. Late Miocene temperatures have been reconstructed by using the equation for inorganic calcite (Kim and O´Neill, 1997) and a new equation specifically derived from *T. heimii* (Dekeyzer et al., subm.). In comparison to today, the reconstructed temperatures indicate generally lower mean tropical temperatures for the western Atlantic.

The isotope and temperature trends suggest an effect of freshwater input from the developing Amazon River at about 10.9 Ma, which is transported towards Site 926 by a southwards flowing North Brazil Current during that time interval. At about 9.9 Ma, the isotopes exhibit a strong shift to lower values that can be related to a change in the seawater isotopic composition related to a major sea level drop. Around 9.8 Ma, increasing isotopic values reflect a decrease in the Amazon freshwater influence. Amazon waters were likely transported away from Site 926 at this time because of a reversal of the North Brazil Current into its modern flow path. Within the studied Miocene time interval where isotopic data of *G. sacculifer* was available (from about 10 Ma on), the isotopic curves of *G. sacculifer* are similar but exhibit less pronounced trends in comparison to the curve of *T. heimii*.

This study shows the first reconstruction of Miocene sea surface temperatures using stable oxygene isotopes of the calcareous dinoflagellate cyst T. heimii.

6.1 Introduction

In order to gain a thorough understanding of the development of modern sea surface circulation patterns, detailed and accurate reconstructions of the changing upper water properties over time are essential. For example, temperature reconstructions from the low latitudes can be useful in this respect, as they can act as a tracer for heat passage over the equator (Curry et al., 1995; Wright, 2001). Oceanic heat transport out of the equatorial regions is an important factor for thermohaline circulation. It has been suggested that modern thermohaline circulation patterns originated during the middle and upper Miocene (Billups, 2002; Wright et al., 1991). Thus, late Miocene temperature reconstructions from equatorial regions, which play an important role in the oceanic heat transport, are important components for our understanding of the development of modern sea surface circulation patterns. However, such reconstructions are virtually non-existent. In this paper we provide this information by reconstructing temperatures of the Ceara Rise Site 926 during the late Miocene based on isotopes of *Thoracosphaera heimii*.

The Ceara Rise, a bathymetric high in water depths of about 3000 – 5000 m, is located in the western equatorial Atlantic which today is the region where the main pathway exist when warm surface water south of the equator flow northwards into the North Atlantic (Philander and Pacanowski, 1986). The Ceara Rise is located beneath the warm surface waters of the western tropical Atlantic, which makes it ideally situated to obtain sediment archives that reflect the history of tropical sea surface temperatures (Curry et al., 1995) and, thereby, heat passage over the equator.

A common tool for reconstructing sea surface temperatures is based on the stable oxygen isotopic compositions of different marine organisms (e.g. corals, planktic foraminifera, coccolithophorids, bivalves; Felis et al., 2000; Goodwin et al., 2003; Guilderson et al., 2001; Margolis et al., 1975; Peeters et al., 2000). However, all of these different organisms have restrictions as to the usability of their stable oxygen isotopes, such as i) the photosynthetic activities of symbionts, which can influence the isotopic signal, ii) limitations of their geographic and/or stratigraphic distribution, and iii) migration through the water

column, which hamper the isolated signal from discrete water masses (Lohmann, 1995; Wefer and Berger, 1991). It is a relatively new approach to use calcareous dinoflagellate cysts for isotope investigations (Friedrich and Meier, 2003, 2006; Dekeyzer et al., subm.; Kohn et al., 2011; Zonneveld, 2004). One cyst species, *Thoracosphaera heimii*, has particularly attracted special interest, as it seems to exclude some of the aforementioned restrictions (Kohn et al., 2011; Kohn and Zonneveld, 2010; Zonneveld, 2004).

T. heimii is a photosynthetic species that contains no symbionts and is, in comparison to other calcite producing organisms, relatively resistant against calcite dissolution (Baumann et al., 2003; Vink et al., 2002; Zonneveld et al., 2000). Geographically, *T. heimii* occurs in a broad band between sub-polar and tropical environments with the highest diversity and abundance in subtropical areas (e.g. Esper et al., 2000; Meier and Willems, 2003; Vink, 2004; Wendler et al., 2002a; Zonneveld et al., 1999; Zonneveld et al., 2000). Stratigraphically, *T. heimii* is found in sediments since the Late Cretaceous (e.g. Hildebrand-Habel and Willems, 2000; Streng et al., 2004). The highest concentrations of living *T. heimii* are found in or just above the deep chlorophyll maximum (DCM), indicating its calcification depth is positioned within these layers (Kohn and Zonneveld 2010). Culture experiments (e.g. Inoyer and Pienar, 1982), as well as sediment trap studies (e.g. Wendler et al. 2002), showed that *T. heimii* reproduces throughout the year and thus is not biased by seasonality. The isotopic composition of *T. heimii*, therefore, reflects mean annual seawater conditions. It has additionally been shown that, due to the characteristically small size of *T. heimii* (9-27 μm; Fütterer 1977; Kamptner 1967), it is relatively easy to separate the cysts from other sedimentary components in order to achieve monospecific samples for analysis (Kohn et al., 2011; Zonneveld, 2004).

However, this new tool has only been used for palaeoceanographic reconstructions of Late Quaternary (since 45,000 years) sequences (Kohn et al., 2011). In this study, we measure, for the first time, the isotopic composition of *T. heimii* shells from late Miocene sediment samples and compare our findings to isotopic measurements of the planktic foraminifera *Globogerinoides sacculifer* (Shackleton and Hall, 1997). Additionally, we calculated paleotemperatures by using a new equation based on the correlation between recent sea surface temperatures and the $\delta^{18}O_{calcite} - \delta^{18}O_{water}$ composition of *T. heimii* from a

combined Atlantic and Indian Oceans dataset (Dekeyzer et al., subm.), and with the commonly used equation for inorganic calcite of Kim and O´Neil (1997).

6.2 Study area

6.2.1 Oceanic circulation of the recent western equatorial Atlantic

Today, three main factors influence the oceanic surface currents of the equatorial Atlantic: the strength of the trade winds, the Coriolis Effect (curling from wind stress), and the position of the Intertropical Convergence Zone (ITCZ). The ITCZ is a zone where the winds, circulating in the North and South, converge (e.g. Grodsky and Carton, 2002; Höflich, 1974). The latitudinal position of the ITCZ varies from 15 °N in the boreal summer, due to the prevailing strong southeast trade winds, and 1 °N in the winter, when the northeast trade winds are at their minimal strength.

In boreal summer and autumn (i.e. May-October) when the southeast trade winds are at their maximal strength, the South Equatorial Current, which is mainly fed by the colder Benguela Current and flows westwards towards eastern South America, is also at its strongest (Figure 1a). The South Equatorial Current then bifurcates into the stronger North Brazil Current, which continues into the northern hemisphere, and the relatively weaker southwards-flowing Brazil Current (Peterson and Stramma, 1991). The strong trade winds (in boreal summer and autumn) shift the ITCZ, northward, which in turn lead to a strong positive curl of the wind stress at about 8 °N and 51 °W. The northwest-flowing North Brazil Current generates, hereby, a series of unstable anticyclonic eddies, which contribute to the development of the eastwards-flowing North Equatorial Counter Current (*Fig. 6.1*.a) (Muller-Karger et al., 1988; Philander and Pacanowski, 1986a; Philander 2001; Richardsen and Mc Kee, 1984). On the northern flanks of these eddies, upwelling and, thus, nutrient enrichment, can occur (Longhurst, 1993). The portion of the North Brazil Current that does not generate these eddies continues northwest to form the Guyana Current, the Caribbean Current and the Gulf Stream. The North Brazil Current is, therefore, an important water mass for the

interhemispheric transport of heat within the Atlantic meridional overturning cell (Goni and John, 2001).

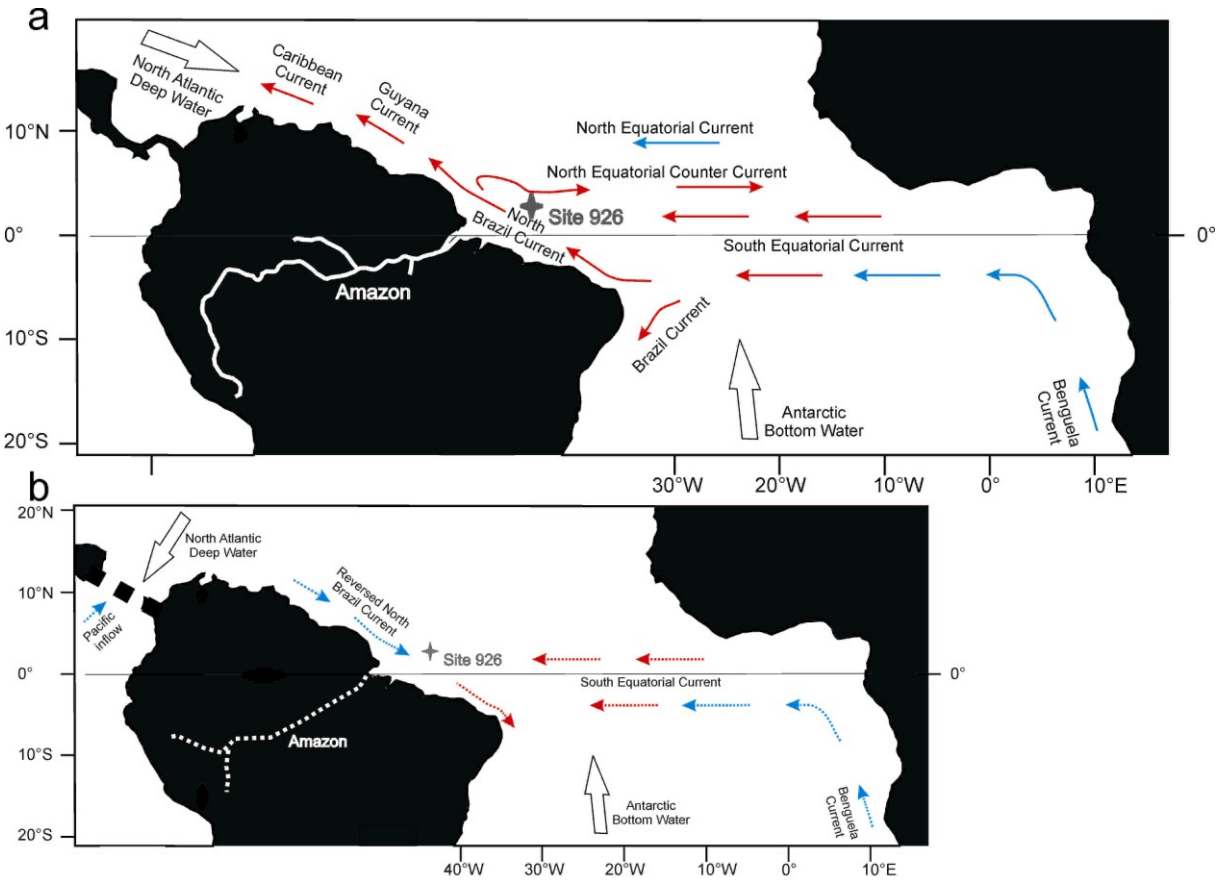

Figure 6.1. Map of the research area: a: main currents of the recent equatorial Atlantic adapted from Peterson and Stramma (1991) and Philander (2001), b: reconstructed main currents of the Miocene equatorial Atlantic (e.g. Butzin et al., 2011; Prange and Schulz, 2004). Late Miocene Amazon River after Hoorn et al. (2010).

When the southeast trades are not as strong, as during boreal winter and spring, the North Equatorial Counter Current and the North Brazil Current retroflection area weakens considerably or vanishes entirely. The North Brazil Current and associated retroflection area is also important for the freshwater input from the Amazon River into the tropical Atlantic. About 70% of the Amazon discharge waters flow around the retroflection area into the North Equatorial Counter Current (Muller-Karger et al., 1995), which translates into a freshwater contribution to the tropical Atlantic of about 6 x 1012 m3 (Gibbs, 1970). North of the retroflection area and the North Equatorial Counter Current, at about 15° N, the North

Equatorial Current flows westwards and transports colder saline waters from the Canary Current into the tropics.

The intermediate depth water masses consist of the northward-flowing Antarctic Intermediate Water and the southward-flowing North Atlantic Deep Water. The bottom water masses are formed either by North Atlantic Deep Water, which flows at a depth of about 1000-4200 m, or Antarctic Bottom Water, which flows below 4200 m (Peterson and Stramma, 1991).

6.2.2 Oceanic circulation of the Miocene western equatorial Atlantic

Numerous studies suggest that during the middle to late Miocene oceanic circulation of the western equatorial Atlantic was strongly influenced by the closure of the Central American Seaway (e.g. Billups 2002; Butzin et al., 2011; Nisancioglu et al., 2009). Before about 13 Ma, an open seaway allowed the unrestricted exchange of water masses between the Pacific and the Atlantic and an inflow of cool Pacific surface waters into the Atlantic throughout that time has been suggested by several studies (*Fig 6.1*.b) (Butzin et al. 2011; Chiasson and D'Hondt, 2000; Kameo and Sato, 2000; Maier-Reimer et al., 1990; Newkirk and Martin, 2009; Nisancioglu et al. 2003; Prange and Schulz, 2004).

The volume flux from the Pacific into the Atlantic was consequently balanced by the southward transport of warm waters (Prange and Schulz, 2004), which is thought to have caused a reversal in the flow direction of the North Brazil Current (in comparison to its direction today) with a resultant transport of heat into the South Atlantic (Butzin et al., 2011; Prange and Schulz, 2004). It was previously shown that the heat transport into the North Atlantic, also called meridional overturning circulation, was clearly weaker during the Miocene than today (e.g. Micheels et al., 2011; Mikolejvicz and Crowley, 1997; You et al., 2009). This decreased northern heat transport, together with relatively low salinity thermocline waters, are thought to have suppressed deep water formation in the North Atlantic (Butzin et al., 2011; Prange and Schulz, 2004). Initially, North Atlantic deep water probably flowed through the open Central American Seaway into the Pacific (Nisancioglu et al., 2003). However, a rapid uplift of the Panama Sill at about 12.9 - 11.8 Ma (Duque-Caro,

1990) prevented the passage of deep water from the North Atlantic into the Pacific and, instead, forced it to flow as a western boundary current into the South Atlantic (Nisancioglu et al., 2003). This then led to a deeper carbonate dissolution depth and an overall better carbonate preservation at depth (e.g. King et al., 1997). A decrease in the influx of Pacific waters, probably related to another Panama Sill uplift, can be observed in the Caribbean Basin, where carbonate mass accumulation rates (MARs) increase and calcareous nannofossil assemblages subsequently became completely distinct from the assemblages found in the Pacific (Kameo and Sato 2000; Newkirk and Martin, 2009).

6.3 Material and Methods

6.3.1 Site description and stratigraphic framework

ODP Site 926 (3°43.146`N, 42°54.489`W) was investigated during Leg 154 on the Ceara Rise. The Ceara Rise is a bathymetric high in the western equatorial Atlantic approximately 800 km east of the Amazon River mouth (Curry et al., 1995) and is situated in an area with an average water depth of about 4500 m. At Site 926, three cores were retrieved (926A, 926B, 926C). The sedimentary succession of 926A, the core investigated in this study, consists of clayey nannofossil chalk and nannofossil chalk with clay and abundant foraminifera (Curry et al., 1995). 78 samples were initially taken from 23H to 28H (at depths ranging between 208-253 mbsf), but 57 samples (*Fig.6.3*) (23H- 25H at depths of 208-232 mbsf) would appropriate for stable oxygen and carbonate isotope investigations (see Section 6.3.2.).

The stratigraphic framework is based on the orbitally tuned time-scale of Shackleton and Crowhurst (1997), generated by correlating lithological cyclicity to the astronomically determined variations in northern hemisphere summer insolation. Sedimentation rates vary between 0.5 and 2.6 cm/ky (Shackleton and Crowhurst, 1997) so that the 57 samples span the time interval of the late Miocene (11.1- 9.2 Ma).

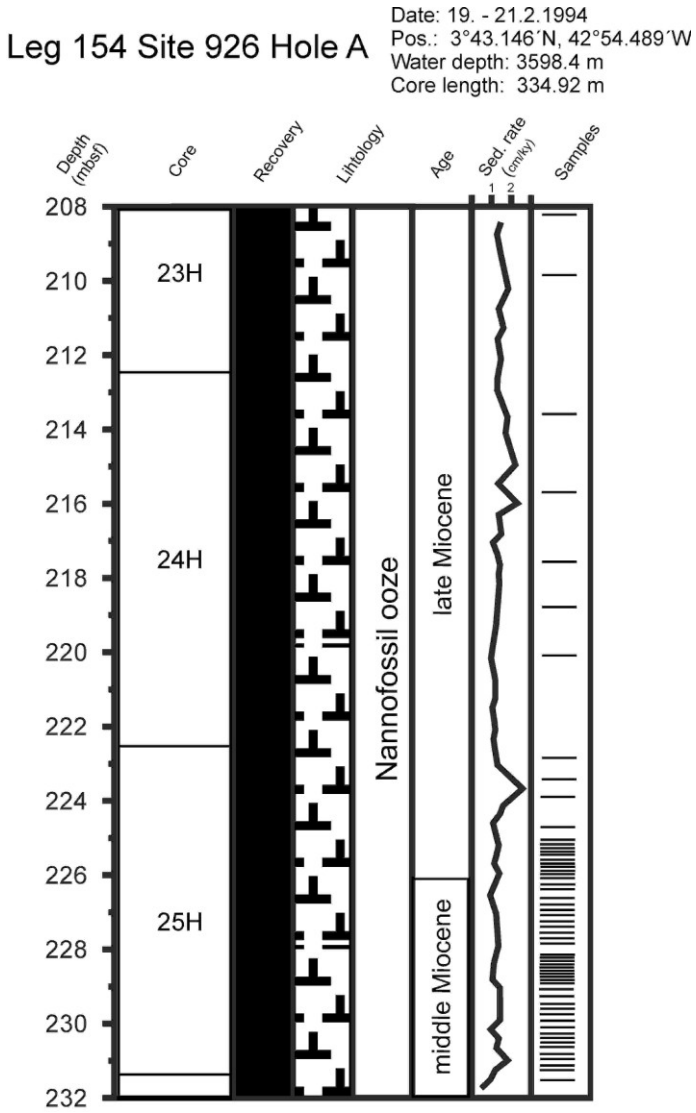

Figure 6.2. Lithologic column of the ODP core 926 (after Curry et al., 1995) including the sample positions of the isotope investigations. Sedimentation rates are based on the time scale by Shackleton and Crowhurst (1997).

6.3.2 Sample preparation

The separation of the calcareous dinoflagellate cyst species *Thorscosphaera heimii* was accomplished using the density/size separation method described by Zonneveld (2004). The method is a combination of sieving, settling and decanting steps to remove calcareous material other than *T. heimii* from the sediment. These steps are repeated until ≥ 85% of the calcareous particles remaining are *T. heimii*. This is done because samples with more than

15% of other calcareous material will distort the isotopic signal. From the 78 samples treated with the density/size separation method, 57 samples were used for further isotopic measurements. In 15 samples no or too few cysts of *T. heimii* were found and the 85% purity was not reached by 6 samples (*Table 1*).

Stable isotope measurements were performed at the Center for Marine Environmental Sciences (MARUM), University of Bremen, Bremen, Germany. A Finnigan MAT 251 mass spectrometer was used with an automatic preparation line (KIEL II carbonate device). Analytical precision of the N18O analysis was 0.07‰. Stable isotope values are given in δ-notation versus Vienna Pee Dee Belemnite (VDPD). The trendline of the isotope curve of *T. heimii* shows a moving average, established by the mean isotope value of every 100 kyrs.

6.3.3 Temperature Calculations

Temperatures were calculated from the stable oxygen isotopic compositions of *T. heimii* and *Globigerinoides sacculifer* (*Table 2*) (isotopes from Shackleton and Hall, 1997) by using the paleotemperature equation for inorganic calcite by Kim and O´Neill (1997) (eq. 1), and by the calculated correlation between recent sea surface temperatures and the $\delta^{18}O_{calcite} - \delta^{18}O_{water}$ composition of *T. heimii* determined through the use of a combined dataset of Atlantic and Indian Ocean data (eq. 2; Dekeyzer et al. subm.):

$$T\ (°C) = 16.1 - 4.64\ (\delta^{18}O_c - \delta^{18}O_{sw}) + 0.09\ (\delta^{18}O_c - \delta^{18}O_{sw})^2 \quad \text{(eq. 1)}$$

$$T\ (°C) = -3.1489\ (\delta^{18}O_c - \delta^{18}O_{sw}) + 19.028 \quad \text{(eq. 2)}$$

In eq. 1 and 2, $\delta^{18}O_c$ is defined as the oxygen isotopic composition of the calcite of *T. heimii* and $\delta^{18}O_{sw}$ as the oxygen isotopic composition of the seawater at the time of calcification.

To calculate the oxygen isotopic composition of the seawater, we used the equations of Fairbanks and Wright (1992) (eq. 3) and Zachos et al. (1994) (eq. 4). Salinity values (S) for equation 3 were taken from Schmidt, G. A., G. R. Bigg and E. J. Rohling. 1999. "Global Seawater Oxygen-18 Database - v1.21" (http://data.giss.nasa.gov/o18data/). In equation 4 is y the absolute latitude in the range 0-70 °C. For conversion from $\delta^{18}O_{sw}$ referencing to Vienna Standard Mean Ocean Water (VSMOW) to the reference of Vienna Pee Dee Belemnite (VDPD), equation (5) after Hut (1987) was used.

$$\delta^{18}O_{sw}\ (\text{VSMOW}) = 0.19 * S - 5.97 \qquad \text{(eq. 3)}$$

$$\delta^{18}O_{sw}\ (\text{VSMOW}) = 0.576 + 0.041y - 0.0017y^2 + 1.35*10\text{-}5y^3 \qquad \text{(eq. 4)}$$

$$\text{VPDB} = \text{VSMOW} - 0.27‰ \qquad \text{(eq. 5)}$$

The trendline for the calculated temperatures of *T. heimii* (eq. 1) also shows a moving average as described for the isotope values.

Table 1. Stable carbon and oxygen isotope data of Thoracosphaera heimii. Temperature data based on the stable oxygen isotopes. Purification rate of the samples based on the % of T. heimii of the total calcareous particles.

Leg-Site-Hole-Section	Top (cm)	Bottom (cm)	$\delta^{13}C$ (‰) vs VPDB	$\delta^{18}O$ (‰) vs VPDB	Temperature (°C) Kim and O´Neil, 1997	Temperature (°C) Dekeyzer et al., 2012	Purification (% *T. heimii* of total calcareous particles)
154-926A-23H-4	3	4	0.20	-0.68	22.21	23.07	> 85
154-926A-23H-5	31	32	0.18	-0.28	20.24	21.79	> 85
154-926A-24H-1	5	6	0.56	-0.32	20.47	21.94	> 85
154-926A-24H-3	90	91	0.56	-0.08	19.27	21.15	> 85
154-926A-24H-4	4	5	0.46	-1.01	23.82	24.11	> 85
154-926A-24H-5	110	111	0.42	-0.61	21.85	22.84	> 85
154-926A-24H-6	112	113	1.37	-0.70	22.28	23.12	> 85
154-926A-25H-1	30	31	0.40	-0.68	22.17	23.05	> 85
154-926A-25H-1	127	128	0.17	-0.61	21.86	22.85	> 85
154-926A-25H-2	4	5	0.44	-0.87	23.11	23.66	> 85
154-926A-25H-2	90	91	0.29	-0.79	22.73	23.41	> 85
154-926A-25H-3	105	106	0.17	-0.49	21.27	22.46	> 85
154-926A-25H-3	112	113	-0.29	-0.50	21.31	22.49	> 85
154-926A-25H-3	120	121	0.44	-0.61	21.86	22.85	> 85
154-926A-25H-3	127	128	0.38	-0.75	22.54	23.29	> 85
154-926A-25H-3	130	131	0.22	-0.51	21.37	22.53	> 85
154-926A-25H-3	135	136	-0.12	-0.76	22.57	23.30	> 85
154-926A-25H-3	140	141	-0.30	-0.72	22.40	23.19	> 85
154-926A-25H-3	8	9	-0.36	-0.64	21.99	22.93	> 85
154-926A-25H-3	14	15	0.27	-0.75	22.52	23.27	> 85
154-926A-25H-3	18	19	-0.06	-0.73	22.42	23.21	> 85
154-926A-25H-3	54	55	-0.08	-0.82	22.86	23.49	> 85
154-926A-25H-3	78	79	0.23	-0.63	21.93	22.90	> 85
154-926A-25H-3	97	98	0.42	-0.49	21.26	22.46	> 85
154-926A-25H-3	104	105	0.09	-0.73	22.44	23.22	> 85
154-926A-25H-3	108	109	0.46	-0.95	23.49	23.90	> 85
154-926A-25H-3	145	146	-0.10	-0.84	22.97	23.56	> 85
154-926A-25H-3	6	7	0.06	-0.73	22.45	23.23	> 85
154-926A-25H-4	12	13	0.11	-0.82	22.89	23.51	> 85
154-926A-25H-4	34	35	0.52	-0.83	22.92	23.53	> 85
154-926A-25H-4	56	57	0.73	-0.89	23.21	23.72	> 85
154-926A-25H-4	64	65	0.34	-0.87	23.13	23.67	> 85
154-926A-25H-4	89	90	0.34	-0.78	22.69	23.38	> 85
154-926A-25H-4	108	109	0.59	-0.82	22.85	23.49	> 85
154-926A-25H-4	115	116	-0.36	-1.50	26.24	25.64	> 85
154-926A-25H-4	124	125	0.60	-0.69	22.23	23.09	> 85
154-926A-25H-4	131	132	0.55	-0.69	22.24	23.09	> 85
154-926A-25H-4	6	7	0.51	-1.36	25.52	25.19	> 85

154-926A-25H-5	13	14	0.70	-0.88	23.18	23.70	> 85
154-926A-25H-5	34	35	0.45	-0.69	22.24	23.09	> 85
154-926A-25H-5	46	47	1.04	-0.69	22.22	23.08	> 85
154-926A-25H-5	58	59	1.10	-0.74	22.48	23.25	> 85
154-926A-25H-5	66	67	0.76	-0.73	22.42	23.21	> 85
154-926A-25H-5	72	73	0.49	-0.83	22.92	23.53	> 85
154-926A-25H-5	83	84	0.81	-0.75	22.51	23.27	> 85
154-926A-25H-5	121	122	1.16	-0.50	21.33	22.50	> 85
154-926A-25H-5	133	134	0.99	-0.14	19.58	21.36	> 85
154-926A-25H-5	8	9	1.38	-0.91	23.31	23.78	> 85
154-926A-25H-6	17	18	1.09	-0.93	23.41	23.85	> 85
154-926A-25H-6	28	29	0.88	-0.46	21.12	22.36	> 85
154-926A-25H-6	47	48	0.94	-0.56	21.59	22.67	> 85
154-926A-25H-6	58	59	0.49	-0.97	23.63	23.98	> 85
154-926A-25H-6	61	62	0.49	-0.48	21.21	22.43	> 85
154-926A-25H-6	75	76	0.68	-0.88	23.15	23.68	> 85
154-926A-25H-6	105	106	0.85	-0.74	22.48	23.25	> 85
154-926A-25H-6	116	117	1.14	-0.03	19.04	21.00	> 85
154-926A-25H-6	3	4	0.50	-0.85	23.03	23.60	> 85
154-926A-25H-7	9	10	-	-	-	-	< 85
154-926A-26H-1	6	7	-	-	-	-	< 85
154-926A-26H-1	28	29	-	-	-	-	< 85
154-926A-26H-1	37	38	-	-	-	-	< 85
154-926A-26H-1	43	44	-	-	-	-	< 85
154-926A-26H-1	48	49	-	-	-	-	< 85
154-926A-26H-1	55	56	-	-	-	-	*T. heimii* absent
154-926A-26H-1	61	62	-	-	-	-	*T. heimii* absent
154-926A-26H-1	69	70	-	-	-	-	*T. heimii* absent
154-926A-26H-1	74	75	-	-	-	-	*T. heimii* absent
154-926A-26H-1	85	86	-	-	-	-	*T. heimii* absent
154-926A-26H-1	105	106	-	-	-	-	*T. heimii* absent
154-926A-26H-1	134	135	-	-	-	-	*T. heimii* absent
154-926A-26H-2	8	9	-	-	-	-	*T. heimii* absent
154-926A-26H-2	118	119	-	-	-	-	*T. heimii* absent
154-926A-26H-3	75	76	-	-	-	-	*T. heimii* absent
154-926A-26H-5	119	120	-	-	-	-	*T. heimii* absent
154-926A-27H-1	24	25	-	-	-	-	*T. heimii* absent
154-926A-27H-3	117	118	-	-	-	-	*T. heimii* absent
154-926A-27H-4	4	5	-	-	-	-	*T. heimii* absent
154-926A-28H-2	8	9	-	-	-	-	*T. heimii* absent

Table 2. Stable carbon and oxygen isotope data of Globogerinoides sacculifer (Shackleton and Hall, 1997). Temperature data based on the stable oxygen isotopes.

Leg-Site-Hole-Section	Top (cm)	Bottom (cm)	δ18O (‰) vs VPDB	Temperature (°C) Kim and O´Neil, 1997	Temperature (°C) Dekeyzer et al., subm.
154-926A-23H-4	8	10	-1.11	24.30	24.41

154-926A-23H-4	18	20	-0.87	23.12	23.66
154-926A-23H-4	31	33	-0.74	22.48	23.25
154-926A-23H-4	38	40	-0.82	22.87	23.50
154-926A-23H-4	48	50	-0.78	22.67	23.37
154-926A-23H-4	58	60	-0.93	23.41	23.85
154-926A-23H-4	68	70	-0.94	23.46	23.88
154-926A-23H-4	78	80	-0.97	23.61	23.97
154-926A-23H-4	88	90	-0.84	22.97	23.56
154-926A-23H-4	98	100	-0.82	22.87	23.50
154-926A-23H-4	108	110	-0.74	22.48	23.25
154-926A-23H-4	118	120	-0.96	23.56	23.94
154-926A-23H-4	128	130	-0.84	22.97	23.56
154-926A-23H-4	138	140	-0.94	23.46	23.88
154-926A-23H-4	148	150	-0.83	22.92	23.53
154-926A-23H-5	8	10	-0.99	23.71	24.03
154-926A-23H-5	18	20	-0.98	23.66	24.00
154-926A-23H-5	28	30	-0.99	23.71	24.03
154-926A-23H-5	38	40	-0.81	22.82	23.47
154-926A-23H-5	48	50	-0.87	23.12	23.66
154-926A-23H-5	58	60	-0.92	23.36	23.81
154-926A-23H-5	68	70	-1.13	24.40	24.48
154-926A-23H-5	78	80	-0.72	22.38	23.18
154-926A-23H-5	88	90	-1.04	23.95	24.19
154-926A-23H-5	98	100	-1.01	23.80	24.10
154-926A-23H-5	108	110	-1.01	23.80	24.10
154-926A-23H-5	118	120	-0.72	22.38	23.18
154-926A-23H-5	128	130	-0.81	22.82	23.47
154-926A-23H-5	138	140	-0.88	23.16	23.69
154-926A-23H-5	148	150	-0.95	23.51	23.91
154-926A-24H-2	44	46	-0.82	22.87	23.50
154-926A-24H-2	54	56	-0.90	23.26	23.75
154-926A-24H-2	64	66	-0.96	23.56	23.94
154-926A-24H-2	74	76	-0.85	23.02	23.59
154-926A-24H-2	84	86	-0.91	23.31	23.78
154-926A-24H-2	94	96	-0.95	23.51	23.91
154-926A-24H-2	104	106	-0.89	23.21	23.72
154-926A-24H-2	114	116	-0.99	23.71	24.03
154-926A-24H-2	124	126	-1.13	24.40	24.48
154-926A-24H-2	134	136	-1.23	24.89	24.79
154-926A-24H-2	144	146	-1.02	23.85	24.13
154-926A-24H-3	4	6	-1.02	23.85	24.13
154-926A-24H-3	14	16	-0.94	23.46	23.88
154-926A-24H-3	24	26	-0.90	23.26	23.75
154-926A-24H-3	34	36	-0.84	22.97	23.56
154-926A-24H-3	44	46	-1.31	25.29	25.04
154-926A-24H-3	54	56	-0.89	23.21	23.72
154-926A-24H-3	64	66	-1.00	23.75	24.07
154-926A-24H-3	74	76	-1.04	23.95	24.19
154-926A-24H-3	84	86	-0.99	23.71	24.03
154-926A-24H-3	94	96	-1.14	24.45	24.51
154-926A-24H-3	104	106	-1.19	24.69	24.66
154-926A-24H-3	114	116	-0.87	23.12	23.66
154-926A-24H-3	124	126	-1.09	24.20	24.35
154-926A-24H-3	134	136	-1.27	25.09	24.92

154-926A-24H-3	142	144	-1.19	24.69	24.66
154-926A-24H-4	14	16	-1.15	24.50	24.54
154-926A-24H-4	24	26	-1.19	24.69	24.66
154-926A-24H-4	34	36	-1.18	24.64	24.63
154-926A-24H-4	44	46	-1.02	23.85	24.13
154-926A-24H-4	54	56	-1.11	24.30	24.41
154-926A-24H-4	74	76	-1.12	24.35	24.44
154-926A-24H-4	84	86	-1.04	23.95	24.19
154-926A-24H-4	94	96	-1.27	25.09	24.92
154-926A-24H-4	104	106	-1.18	24.64	24.63
154-926A-24H-4	110	112	-1.20	24.74	24.70
154-926A-24H-4	134	136	-1.14	24.45	24.51

6.4 Results

6.4.1 Stable oxygen isotope composition and calculated temperatures of *Thoracosphaera heimii* and *Globogerinoides sacculifer*

The isotope curve of *T. heimii* covers the time interval from about 11.1 Ma until 9.2 Ma (*Fig. 6.3*.a). During the time interval ca. 10-9.2 Ma additional isotope data of *G. sacculifer* (Shackleton and Hall, 1997) was available for comparison to *T. heimii* (*Fig. 6.3*.b).

The temperatures calculated from the oxygen isotope signal of *T. heimii* (black curves) and *G. sacculifer* (grey curves) are displayed in *Fig. 6.4*. The left black and grey curves show the calculated temperatures using the equation (eq.1) after Kim and O´Neil (1997). The right black and grey curves show the temperatures calculated by using the equation (eq. 2) from Dekeyzer et al. (subm.).

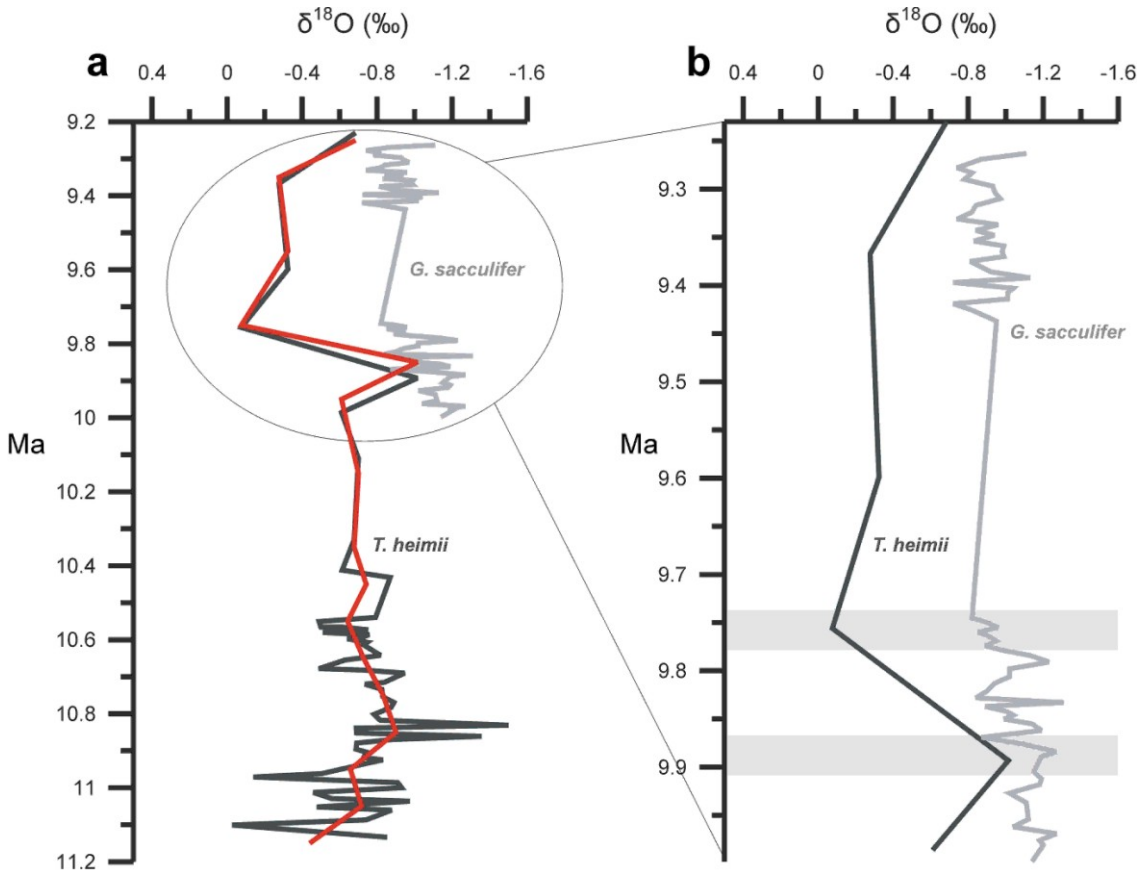

Figure 6.3. Oxygen isotopic composition of Thoracosphaera heimii and Globigerinoides sacculifer (Shackleton and Hall 1997), a: red trendline shows a moving average of the T. heimii isotopes, b: zoom into the interval, which is marked by the ellipse. Light shaded bars indicate similarities in the curve progression.

Values of the isotopic composition and calculated temperatures of *T. heimii* cysts and *G. sacculifer* (Shackleton and Hall, 1997) are given in *Table 1*. The range of the isotopic composition for *T. heimii* is -1.5‰ to 0.026‰ resulting in a temperature range of 19-26.2 °C (after eq.1) and 21-25.6 °C (after eq.2). For *G. sacculifer* is the range of the isotopic composition within -1.013‰ to -0.075‰ with temperatures between 22.4 and 25.3 °C (after eq.1) and 23.1 and 25 °C (after eq.2). The two isotope curves show an average offset of about 0.28‰. The overall temperature offset is about 1.35 °C for eq.1 and about 0.87 °C for eq.2.

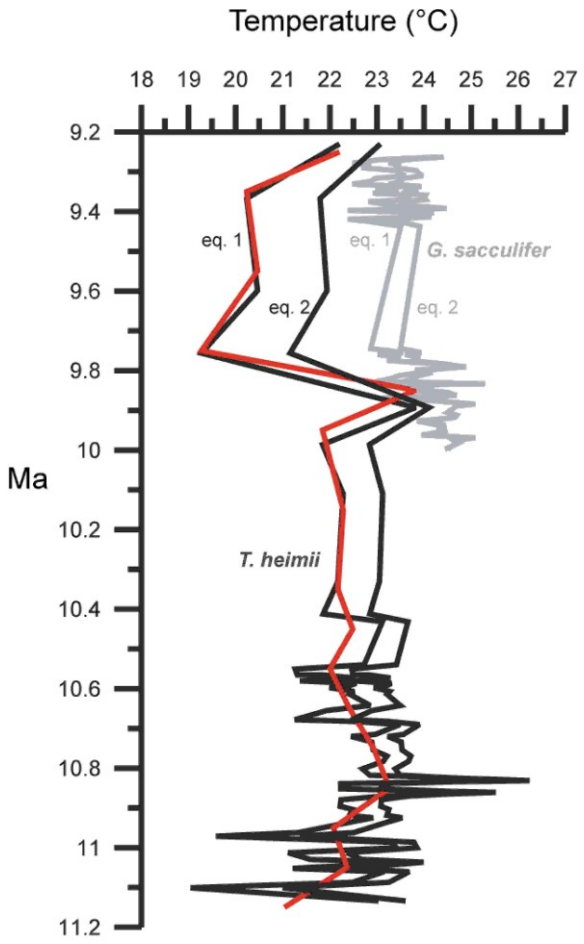

Figure 6.4. Temperature calculations based on the oxygen isotopic composition of Thoracosphaera heimii and Globigerinoides sacculifer (Shackleton and Hall, 1997). Eq.1: calculations after the equation of Kim and O'Neil (1997), eq.2: calculations after the equation of Dekeyzer et al. (subm.).

The *T. heimii* isotopes drop to more negative values, resulting in more positive temperatures from 11.2 Ma until about 11.1 Ma. Afterwards, the slightly more positive values/negative temperatures until about 10.9 Ma are observed. After this date isotope values became more negative values again and temperatures increase until about 10.8 Ma. The final trend is a shift to more positive values/negative temperatures until about 10.5 Ma, where it remains relatively stable around an isotope value of ca. -0.68‰ and a temperature of ca. 22.2 °C until about 10 Ma. After ca. 10 Ma, the isotope and temperature curve shifts to more negative values/positive temperatures until about 9.9 Ma, than the isotope values increase to

almost 0 at 9.7 Ma. After this time, the isotopes reverse towards more negative values and the temperatures towards enhanced values until the end of the record at ca. 9.2 Ma.

Fig. 6.3.b shows the similar trend of *T. heimii* and *G. sacculifer*. The two isotope curves converge around 9.9 Ma and 9.3 Ma. At about 9.9 Ma and 9.75 Ma, both show curves with similar shifts to more negative and more positive values, respectively. Afterwards, the isotopes of *T. heimii* and *G. sacculifer* shift to slightly more negative values.

6.5 Discussion

6.5.1 Usability of *Thoracosphaera heimii* in stable oxygen isotope investigations during the late Miocene

In order to perform isotopic investigations on the shells of *T. heimii*, two prerequisites have to be fulfilled: cysts of *T. heimii* have to be sufficiently separated from the sediment to get a monospecific isotopic signal, and a specific amount of separated shells are necessary to obtain reliable stable isotopic results (about 5x106 individual shells; Zonneveld 2004). For both requirements it is essential that the original sediments contain enough shells of *T. heimii*, which implies that *T. heimii* has been abundant in the water column in order to be deposited in such concentrations. Today, *T. heimii* is the most abundant calcareous dinoflagellate species, where it often dominates the cyst associations due to its short reproduction cycle (Dale and Dale, 1992; Richter et al., 2007; Vink 2004; Wendler et al., 2002 a,b,c; Zonneveld et al. 2000), and can be found in the sedimentary record since the early Cenozoic (Fütterer, 1977; Hildebrand-Habel and Willems 2000).

In the sediments comprising Site 926A, *T. heimii* occurred in the sediments frequently between 11.2-11.1 Ma and was constantly found until the end of our record at about 9.2 Ma. However, no *T. heimii* cysts were found between 12.8-11.2 Ma and there are a few different reasons for the absence of *T. heimii* in these sediments. One reason could be that calcite

dissolution severely affected the cyst preservation. In comparison to other calcareous organisms, calcareous dinoflagellate cysts are generally thought to be more resistant against calcite dissolution (Baumann, 2003; Vink et al., 2002; Zonneveld et al., 2000). However, like all calcareous particles, dissolution of the cysts can occur in a carbonate dissolving environment (Wendler et al., 2002b; Zonneveld et al., 2005). An investigation of total calcareous dinoflagellate cyst accumulation rates as well as changes in the cyst association within the same sediments, however, showed no signs of dissolution during the critical time interval (section 5.5.2.). It is also possible that the absence of *T. heimii* can be due to unfavourable conditions in the local environment, such as turbulence in the water column, which can hamper *T. heimii* cyst production (Kohn and Zonneveld, 2010). In this stage of the investigation, we cannot definitively determine the cause of the absence of *T. heimii* during this specific time slice.

6.5.2 Effects on the isotopic composition

In order to obtain information about the characteristics of seawater (e.g., temperatures) from oxygen isotopes of calcareous organisms, it is required that the organism calcifies in equilibrium with respect to seawater. However, three potential effects are currently known to affect the isotopic composition in relation to the calcification process, namely i) kinetic effects ii) metabolic effects, and iii) pH effects.

i) Kinetic effects occur during the hydration and hydroxylation processes of CO2 (McConnaughey, 1989, 2003). During the rapid growth of organisms, carbon precipitates faster than the combined processes of CO^2 hydration and hydroxylation. The resultant faster hydration of ^{12}C and ^{16}O out of CO^2 leads to a depletion in ^{13}C and ^{18}O of the carbonate relative to isotopic equilibrium. A linear correlation between $\delta^{13}C$ and $\delta^{18}O$ would thus be a consequence of incomplete isotopic equilibrium (McConnaughey, 1989, 2003). However, such a correlation has so far never been observed for *T. heimii* in natural environments or in culture experiments (*Fig.6.5*.) (Zonneveld, 2004; Zonneveld et al., 2007).

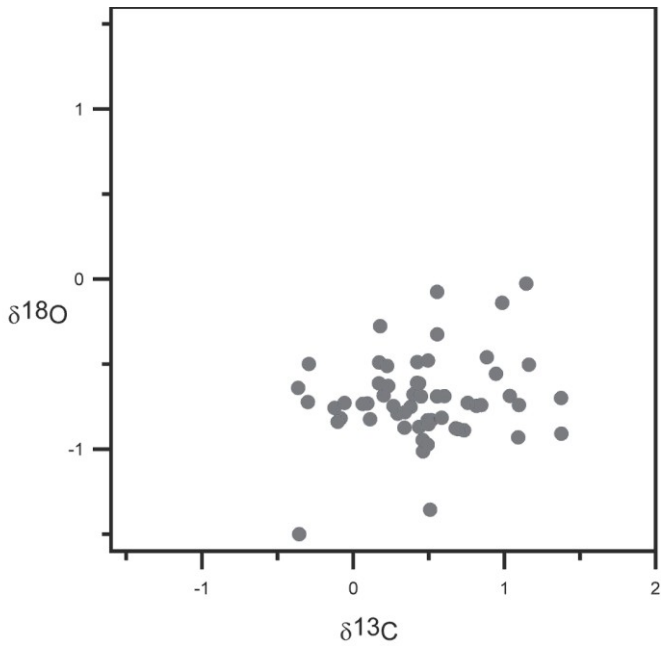

Figure 6.5. Comparison of the carbon and oxygen isotopic composition of Thoracosphaera heimii.

ii) Metabolic effects are mainly caused by photosynthesis and respiration and describe changes in the $\delta^{13}C$ of the dissolved inorganic carbon pool, which can have a secondary influence the ^{18}O composition (McConaughey, 1989). It has been shown that *T. heimii* partly uses respired carbon for calcite precipitation, as has been shown in the relatively negative carbon isotope values in relation to equilibrium (Kohn 2010; Zonneveld et al., 2007). However, in this data the carbon isotope values appear to be much higher than in the studies of Kohn (2010) and Zonneveld et al. (2007), which implies little or no metabolic influence on the isotopic composition (*Table 1*).

iii) An effect of pH on the stable oxygen isotope fractionation with increasing $\delta^{18}O$ values at decreasing pH values has been found in culture experiments on other species, such as corals and planktonic foraminifera (Spero et al., 1997; Zeebe et al., 1999; Zeebe, 2001). For *T. heimii*, a negative pH effect with decreasing $\delta^{18}O$ at increasing pH has been described in the culture experiment of Kohn (2010). Since there are no values of the isotopic composition of Miocene seawater available, we cannot exclude the possibility of a pH effect on the isotopic composition of *T. heimii* in this paper.

Another factor that can influence the isotopic signal is the migration of some calcareous organisms between seawater masses, which have different isotopic compositions. Kohn and Zonneveld (2011) showed that *T. heimii* is produced at a stable position in the water column, at and just above the deep chlorophyll maximum, and therefore, the isotopic signal of *T. heimii* would not reflect an isotopic signal of different water masses. However, the influence of different water masses as a result of migration through the water column on the isotopic composition of calcareous is visible in our comparison of *T. heimi* and the foraminifer *G. sacculifer*. The two isotope curves display an offset on the average of -0.28‰, with the more negative values belonging to *G. sacculifer* (*Fig. 6.3*.a, b). The influence of different water masses and different calcification processes of dinoflagellates and foraminifera on the isotopic composition may explain the offset. It has, for instance, been shown that a significant part of the population of *G. sacculifer* adds a secondary calcite crust and reproduces at water depths well below the mixed layer, thus calcifying in different water depths in comparison to *T. heimii* (Kohn and Zonneveld, 2010; Rosenthal et al., 2000). However, Spero and Lea (1993) determined that ontogenic processes do not affect the $\delta^{18}O$ signal. They showed instead that photosynthetic activity of foraminifer symbionts causes the main effect, where $\delta^{18}O$ values decrease with increasing light i.e. with increasing symbiont photosynthetic activity. *T. heimii*, in contrast to *G. sacculifer*, is a non-symbiont bearing species and, therefore, not influenced by symbiont photosynthetic activity. This difference between the two organisms is the most likely explanation for the offset of *G. sacculifer* in comparison to *T. heimii*.

6.5.3 Effects on the temperature reconstruction

Palaeotemperature calculations from oxygen isotopes can contain some systematic errors. Seawater properties of the past are scarcely known and, so far, no information regarding the pH of Miocene seawater is available. For highly accurate temperature reconstructions, the oxygen isotopic composition of the seawater at the times when organisms undertake calcification ($\delta^{18}O_{sw}$) is essential. The global mean oxygen isotopic composition of seawater ($\delta^{18}O_{sw}$) is primarily dependent on the volume of continental ice-sheets (Bice et al., 2000), whereas the regional $\delta^{18}O_{sw}$ is a function of the global mean composition as well as geographical variations such as changes in evaporation/precipitation patterns, oceanic circulations and possible riverine influences (Schmidt, 1998; Zachos et al., 1994). Several

approaches have already been attempted to reconstruct local palaeo $\delta^{18}O_{sw}$ (Fairbanks and Wright, 1992; Williams et al 2005; Zachos et al., 1994). Fairbanks and Wright (1992) described a linear relationship between salinity and the isotopic composition of seawater, and generated an equation to estimate seawater $\delta^{18}O$ using regional salinities. Another approach was used by Zachos et al. (1994), which related the $\delta^{18}O_{sw}$ to the palaeolatitude within a latitudinal range of 0-70°. Additionally, Williams et al. (2005) used two more methods to calculate seawater $\delta^{18}O$. They reconstructed the present day global distribution of $\delta^{18}O$ using GEOSECS data and other data by Schmidt (1999), and developed a continuous surface model with a spatial interpolation routine based on grid averaging. To include changes in precipitation and evaporation for the Miocene, Williams et al. (2005) generated another interpretation of seawater $\delta^{18}O$ based on a climate modelling study for the Messinian.

Table 3. Different approaches for the reconstruction of the recent and past stable oxygen isotopic composition of seawater.

Isotopic composition of seawater (western equatorial Atlantic Ocean)					
Fairbanks and Wright (1992)	Zachos et al. 1994	Williams et al. 2005		Delaygue et al. 2000	
linear relation between the $\delta^{18}O_{sw}$ and salinity	relation of the $\delta^{18}O_{sw}$ to the palaeo latitude	Data from GEOSECS/ Schmidt et al. (1999)	Messinian model	Box model	General Circulation Model (GCM)
palaeo	palaeo	recent	palaeo	recent	recent
0.87‰ (SMOW)	0.7‰ (SMOW)	0.98‰ (SMOW)	0.65‰ (SMOW)	1.0-1.2‰ (SMOW)	

In this study, we reconstructed local $\delta^{18}O_{sw}$ after Fairbanks and Wright (eq. 3; 1992) and after Zachos et al. (eq. 4; 1994). Equation 3 is based on modern salinity concentrations (from Schmidt, G. A., G. R. Bigg and E. J. Rohling. 1999. "Global Seawater Oxygen-18 Database - v1.21" (http://data.giss.nasa.gov/o18data/) as no Miocene salinity values are available. The resulting $\delta^{18}O_{sw}$ values for this study, as well as the reconstructions from Williams et al. (2005) along with a reconstruction of seawater $\delta^{18}O$ based on the oceanic general circulation model (Delaygue et al., 2000), are shown in *Table 3*. The different methods produce different seawater $\delta^{18}O$. The largest difference is seen in the two methods used by Williams et al. (2005), which exhibit an offset of 0.33‰, whereas our reconstructions after Zachos et al. (1994) and Fairbanks and Wright (1992) display a difference of 0.16‰. The modelling study of Delaygue et al. (2000) shows intermediate values in modern $\delta^{18}O_{sw}$ of the western equatorial Atlantic Ocean. Two reconstructions fall within the modern range (our

reconstructions after Fairbanks and Wright, 1992; reconstructions with modern data from Schmidt, 1999 made by Williams et al., 2005). The other two reconstructions (ours after Zachos et al., 1994; Messinian model after Williams et al., 2005) show lower values.

The differences in reconstructed seawater $\delta^{18}O$ correspondingly lead to differences in the calculation of water temperatures. For instance, the offset between the $\delta^{18}O_{sw}$ we calculated after Fairbanks and Wright (1992) and Zachos et al. (1994), is 0.16‰, which leads to an average temperature difference of 0.64 °C from equation 1 after Kim and O´Neil (1997) and 0.5 °C with the use of equation 2 after Dekeyzer et al. (subm). For the temperature calculations in this paper, we used an isotopic composition of seawater of 0.87‰ VSMOW (after Fairbanks and Wright 1992) and the conversion to VPDB standard after Hut (eq. 5, 1987) resulted in a $\delta^{18}O_{sw}$ of 0.6‰ VPDB.

The observed differences indicate that there is still a need to improve the existing methods for reconstructing seawater $\delta^{18}O$. However, beside the uncertainties in the exact temperature values are the trends in temperature well reflected. Therefore, although we acknowledge that our reconstructed temperatures are certainly not absolute and only semi-quantitative, the purpose of this study was an initial assessment of the overall temperatures trends from an understudied time interval (late Miocene) using a new paleotemperature proxy (*T. heimii*) in comparison with a well-established one (stable oxygen isotopes of foraminifera).

6.5.4 Late Miocene upper water temperatures

Mean temperature values

Reconstructed temperatures for the middle to late Miocene based on the isotopic composition of *T. heimii* show an average value of 22.32 °C after the equation of Kim and O´Neil and 23.14 °C after Dekeyzer et al. (subm.), which are slightly higher (*Table 1*, *Fig. 6.4.*). Equatorial Atlantic surface waters show temperatures today that are about 5 °C warmer in comparison to our calculated Miocene temperatures (ca. 27° C, World Ocean Atlas 2009).

According to the model study (based on an atmospheric general circulation model coupled to a mixed-layer ocean model) of Micheels et al. (2007), the climate during this period (11-8 Ma) was warmer than today. However, model results of Steppuhn et al. (2006), as well as a data set of published planktic foraminifera oxygen isotopes (Williams et al., 2005), show cooler upper water temperatures in the tropics in comparison to today. Williams et al. (2005) found the reconstructed tropical Atlantic Ocean to be 3-7 °C cooler than today, which is in agreement with our temperature calculations.

An early temperature study based on oxygen isotopes of the foraminifera species *Globigerinoides sacculifer* (core 234, 5°45N, 21°43W), revealed middle/late Miocene surface temperatures for the tropical Atlantic Ocean of about 22.8 °C (Emiliani, 1956). Emiliani (1956) suggested that a weakened Florida Current due to an open Panama Seaway was the cause for the decreased temperatures. Another reason for cooler tropical temperatures in comparison to today could be the inflow of colder Pacific waters through an open Central American Seaway. It has been shown that cooler waters influenced the Caribbean during the Miocene, seen in the abundance of temperate foraminiferal assemblages dominated by Globoconellids (Chaisson and Hondt, 2000). These colder upper waters transported farther south by the reversed North Brazil Current (see Section 2.3) would result in western equatorial Atlantic cooler temperatures. This suggestion for cooler tropics also coincides with latitudinal reductions in coral reef belts and lower taxonomic diversity of corals during the latest Miocene (Perrin, 2002). Whether the late Miocene tropics were cooler than today or the original temperature signal is masked by environmental and/or technical influences, we cannot unequivocally say. However, there is some supporting evidence for our finding that temperatures may have been cooler in the equatorial western Atlantic in the late Miocene. Therefore, for the remainder of our discussion, we chose to concentrate on the temperature trends rather than on the exact values.

Late Miocene stable oxygen isotope and temperature trends

Figures 6.3.a, b and *6.4*. display the stable oxygen isotopic curves and corresponding temperature records of *T. heimii* and *G. sacculifer* (Shackleton and Hall, 1997). There is a trend to more negative isotope values of *T. heimii* and subsequently increased temperatures from about 11.2 to 10.9 Ma with a short interruption around 11 Ma. A decrease in stable

oxygen isotope values can have different causes. It can be caused by warmer sea surface temperatures, a decrease in the stable oxygen isotopic composition of seawater ($\delta^{18}O_{sw}$) due to continental ice reduction, or a decrease in the local $\delta^{18}O_{sw}$ due to enhanced freshwater input, or reduced precipitation (Miller et al., 1987, 1991). This particular trend of decreasing isotope values and increasing temperature in our data probably reflects a change in the local $\delta^{18}O_{sw}$ due to increased freshwater input via the Amazon River. A river connection to the Atlantic Ocean is thought to have already existed from about 11.8-11.3 Ma (Figueiredo et al., 2009). A study on the changes in the calcareous dinoflagellate cyst assemblage on Ceara Rise showed the first influence of the Amazon River from about 11.3 Ma, demonstrated by the occurrence of a cyst species (*Leonella granifera*) that is strongly related to riverine influence (Chapter 5). It is thought that Amazon waters were transported to the studied site due to the North Brazil Current, which flowed in the opposite direction compared to today because of the ability of Pacific waters to flow through an open Central American Seaway (see Section 6.2.3.). Thus, the freshwater of the Amazon River could have influenced the overall isotopic composition of the seawater. After 10.9 Ma, the isotope values increased slightly until ca. 10.6 Ma where they remained relatively stable until about 10 Ma. Afterwards, at about 9.9 Ma, our data indicate a further shift to lower isotope values in *T. heimii*, which is less pronounced though also present in the isotopes of *G. sacculifer*. Miller et al. (1987) compared stable oxygen isotope changes based on benthic and planktic foraminifera and found that a decrease in the isotope values was related to a change ice sheet growth accompanied with a sea level fall of about 30-50 m, which altered the isotopic composition of seawater (Haq et al., 1987).

Around 9.8 Ma, our data demonstrate a different trend towards more positive isotope values and decreasing temperatures (*Fig. 6.3., 6.4.*). Again, the reason for this trend might be a change in the isotopic composition of seawater; however, this would result from a decrease in Amazon freshwater input. The uplift of the Panama isthmus reduced the influx of Pacific waters (Kameo and Sato, 2000) and is thought to have caused the reversal of the North Brazil Current into a flow path similar to modern conditions (Chapter 5). In Chapter 5 the authors suggested that a northward flowing North Brazil Current would have transported the Amazon freshwater away from the studied site at about 9.8 Ma, which is corroborated by the absence of the calcareous dinoflagellate *L. granifera*, known to be a strong indicator for riverine input (e.g. Richter et al., 2009; Vink, 2004). However, in the time interval from about 10-9.2 Ma, the sampling resolution is low and therefore, all predictions have to be handled with care.

6.6 Conclusions

1. This study represents the first measurements of stable oxygen isotopes on the shells of *Thoracosphaera heimii* from Miocene age sediments. Despite the fact that *T. heimii* cysts were not present in sufficient quantities in some middle Miocene samples due to unfavourable environmental conditions or calcite dissolution of the cysts, our results reveal that *T. heimii* has a high potential as a proxy for the temperature reconstructions in the late Miocene.

2. The stable oxygen isotopes of *T. heimii* demonstrate little to no kinetic effects as well as little or no metabolic effects. However, due to missing data regarding the stable oxygen isotope composition of Miocene seawater, we cannot fully exclude the influence of a pH effect on the isotopic signal. Additionally, we were able to compare a part of the *T. heimii* isotope curve to stable oxygen isotope measurements of the foraminifer *Globigerinoides sacculifer*. The two isotope curves display an offset with overall more negative isotope values for *G. sacculifer*. Symbiont photosynthetic activity of *G. sacculifer*, in comparison to *T. heimii*, which is a non-symbiont bearing species, is the likely cause of this offset.

3. Using the stable oxygen isotopes of *T. heimii*, we reconstructed sea surface temperatures for our studied time interval. According to the calculated temperatures, the mean temperatures for the late Miocene were cooler in comparison to the modern western Atlantic tropics. While we cannot be sure if the original temperature signal is masked by environmental and/or technical influences, or if the tropical temperatures were as cold as calculated during the late Miocene, it is possible that the temperature trends we observed are linked to the closing of the Central American Seaway and the influence of freshwater input from the Amazon River.

Acknowledgements

We would like to thank Monika Segl for carrying out the isotope measurements. Stefanie Dekeyzer is gratefully acknowledged for providing the temperature equation. Thanks are also given to Kara Bogus for improving the language of this manuscript. The working group of Historical Geology and Palaeontology is warmly acknowledged for their general support.

This study was funded through the Deutsche Forschungs Gemeinschaft International Graduate College “Proxies in Earth History” program, EUROPROX.

Chapter 7: Conclusions and Perspectives

7.1 Main Conclusions

This thesis effectively showed that calcareous dinoflagellate cyst assemblages react sensitively to paleoenvironmental change occurring in the equatorial and southern Atlantic Ocean during the middle and late Miocene. Specifically, they are able to record the initiation of increased productivity off the coast of Namibia (ODP Site 1085) in relation to establishment of the Benguela upwelling regime due to the influence of Antarctic waters. This is reflected primarily by the occurrence and increasing abundance of the polar species *Caracomia arctica*. Between pulses of productivity, the dinoflagellate cyst *Leonella granifera* showed an increase in terrigenous input via the Orange River.

Furthermore, in the western equatorial Atlantic (ODP Site 926), the calcareous dinoflagellate cysts record pulses of early North Atlantic Deep Water production, shown by a better calcite preservation of the cysts during these intervals. *L. granifera* also indicates an increase in terrigenous load here, which was delivered by the developing Amazon River. The Amazon influence is also reflected in the stable oxygen isotopic signal of the calcareous cyst *Thoracosphaera heimii*. Reconstructed temperatures based on the isotopic composition of *T. heimii* in general display colder mean tropical temperatures in comparison to today.

A concluding question of this thesis was whether there exists a teleconnection between the different reconstructed processes, i.e. the development of the Benguela upwelling and the closing of the Central American Seaway. It is a striking coincidence that the first reconstructed influence of Antarctic waters on the Benguela upwelling occurred around 11.1 Ma, which is relatively consistently with the timing of the first Amazon influence at the Ceara Rise around 11.2 Ma. Andean tectonism, which led to the development of the Amazon River and the Antarctic cooling with glaciations and the development of the Antarctic Circumpolar

Current, which was the provider of the subantarctic mode water for the Benguela upwelling, seemed hereby to be linked to each other. Moreover, the reconstructed establishment of the Benguela upwelling around 10.4 Ma again is fairly coincident with the reversal of the North Brazil Current as a consequence of reduced Pacific inflow into the Atlantic through the Central American Seaway around 10.5 Ma. These timely occurrences seem to suggest that there exists a linkage between all these processes, and shows that calcareous dinoflagellate cysts are sensitive enough proxies to record this. However, further studies are required to confirm and deepen this concluding remark.

7.2 Future perspectives

The following research topics are recommended to improve the use of calcareous dinoflagellate cysts as paleoenvironmental indicators and to confirm the initial findings of this study.

A geographic extension of the Miocene calcareous dinoflagellate cyst record would be highly valuable in both locations, the Benguela upwelling regime and the Ceara Rise.

For more information about the influence of Antarctic waters on the Benguela upwelling in relation to glaciations on Antarctica and the development of the Antarctic Circumpolar Current, it would be interesting to investigate samples from Sites 1086/ 1087, which are located further south of the studied Site 1085. Furthermore, so far no study exists on the recent distribution of *Caracomica arctica* (the indicator for subantarctic waters in this study) in upwelling areas. To test if *C. arctica* is also transported by subantarctic waters today, it would be useful to investigate sediment trap samples (CBi-4/5), taken off Cape Blanc (Mauritania) during the RV Merian cruise 04b. During this cruise, the influence of Antarctic waters on the sediment traps were occasionally detected, which would provide the opportunity to investigate the occurrence of *C. arctica* today.

During Leg 154, a transect was drilled on Ceara Rise, which makes it possible to get more information about the development of the Amazon River together with the changing pathway of the North Brazil Current during the late Miocene. Site 927 is located closest to the Amazon River, but has also the lowest carbonate content, whereas Sites 925 and 929 are known to have good carbonate content and a complete sediment record (Curry et al., 1995) and would therefore be suitable for dinoflagellates cyst investigations.

To prove the usability of calcareous cyst species *Thoracosphaera heimii* for isotopic measurements during the Miocene it is required to get records with a higher resolution and within a larger time interval. Additional would it be interesting to compare the isotopes of *T. heimii* with an established isotope proxy e.g. *Globogerinoides ruber* (pink), which was already successful done for the late Quaternary (Kohn et al., 2011).

Finally, another useful confirmation for the dinoflagellate cyst data and to prove the oceanographic reconstructions of this study would be to generate a modelling study in the given time slice and areas. The main subject hereby could be to combine the findings of this study from the eastern South Atlantic Ocean and the western equatorial Ocean and prove the coincidences of the different climatic processes.

References

Anderson, D.M. and K.D. Stolzenbach, (1985), Selective retention of two dinoflagellates in a well-mixed estuarine embayment: The importance of diel vertical migration and surface avoidance. Marine Ecology. Progress Series 25, 39-50.

Ansorge, I., and J. Lutjeharms (2003), Eddies Originating at the South-West Indian Ridge, Journal of Marine Systems, 39(1-2), 1-18.

Arndt, H. and J. Mathes, (1991) Large heterotrophic flagellates form a significant part of protozooplankton biomass in lakes and rivers. Ophelia 33, 225-234.

Barker, P. F., G. M. Filippelli, F. Florindo, E. E. Martin, H. D. Scher, (2007), Onset and role of the Antarctic Circumpolar Current, Deep Sea Research Part II: Topical Studies in Oceanography, 54(21-22), 2388-2398.

Baumann, K.-H., M. Cepek, H. Kinkel (1999), Coccolithophores as indicators of ocean water masses, surface-water temperature, and paleoproductivity-examples from the South Atlantic, in: The South Atlantic Ocean, Present and Past Circulation. Springer-Verlag, Berlin, 117–144.

Baumann, K.-H., B. Boeckel, B. Donner, S. Gerhardt, R. Henrich, A. Vink, A. Volbers, H. Willems, K.A.F. Zonneveld (2003), Contributions of calcareous plankton groups to the carbonate budget of South Atlantic surface sediments, in: The South Atlantic in the Late Quaternary, G. Wefer et al. (eds.), reconstruction of material budgets and Current Systems. Springer Verlag, Berlin.

Bemis, B.E., H.J. Spero, J. Bijma, D.W. Lea, (1998), Reevaluation of the oxygen isotopic composition of planktonic foraminifera: experimental results and revised palaotemperature equations. Paleoceanography 13, 150–160.

Berger, W. H., and G. Wefer (2002), On the reconstruction of upwelling history: Namibia upwelling in context, Marine Geology, 180(1-4), 3-28.

Bice, K. L., L. C. Sloan, and E. J. Barron (2000), Comparison of early Eocene isotopic paleotemperatures and the three-dimensional OGCM temperature field: The potential for use of model-derived surface water d18O, in Warm Climates in Earth History, B. T. Huber et al. (eds), 79– 131, Cambridge Univ. Press, New York.

Bickert, T. (2000) Influence of geochemical processes on stable isotope distribution in marine sediments, in: Marine Geochemistry, H. D. Schulz and M. Zabel (eds.). Springer Verlag, Berlin, 309-334.

Billups, K., and D. Schrag (2002), Paleotemperatures and ice volume of the past 27 Myr revisited with paired Mg/Ca and 18O/16O measurements on benthic foraminifera, Paleoceanography, 17(1), 1003.

Bison, K., G. J. M. Versteegh, F. Orszag-Sperber, J. M., Rouchy, H. Willems (2009), Palaeoenvironmental changes of the early Pliocene (Zanclean) in the eastern Mediterranean Pissouri Basin (Cyprus) evidenced from calcareous dinoflagellate cyst assemblages, Marine Micropaleontology, 73(1-2), 49-56.

Boebel, O., J. Lutjeharms, C. Schmid, W. Zenk, T. Rossby, C. Barron (2003a), The Cape Cauldron: a regime of turbulent inter-ocean exchange, Deep-Sea Research Part II, 50(1), 57-86.

Boebel, O., T. Rossby, J. Lutjeharms, W. Zenk, C. Barron (2003b), Path and variability of the Agulhas Return Current, Deep-Sea Research Part II 50(1), 35-56.

Broecker, W. S. (1997), Thermohaline Circulation, the Achilles Heel of Our Climate System: Will Man-Made CO2 Upset the Current Balance? Science, 278(5343), 1582-1588.

Butzin, M., G. Lohmann, T. Bickert (2011), Miocene ocean circulation inferred from marine carbon cycle modeling combined with benthic isotope records, Paleoceanography Vol. 26(1), 1-19, PA1203.

Chaisson, W.P., and S.L. D'Hondt, (2000), Neogene planktonic foraminifer biostratigraphy at Site 999, western Carribean Sea, Proceedings of the Ocean Drilling Program, Scientific Results, 165, 19-56.

Clark, P.U., N. G. Pisias, T. F. Stocker and A. J. Weaver (2002), The role of the thermohaline circulation in abrupt climate change, Nature, Vol. 415, 863-869.

Coates, A.G., M.-P. Aubry, W.A. Berggren, L.S. Collins, M. Kunk (2003), Early Neogene history of the Central American arc from Bocas del Toro, western Panamá. Geological Society of America Bulletin, 115, 271–287.

Curry WB, N.J. Shackleton, C. Richter, (1995), Leg 154 synthesis, Proceedings of the Ocean Drilling Program, Initial results, College Station, Texas, Ocean Drilling Program 154, 421-442.

Dale, B., (1992b), Thoracosphaerids: Pelagic fluxes, in: Dinoflagellate contribution to the Deep Sea, S. Honjo (ed.), Woods Hole Oceanographic Institution, Woods Hole.

Dale, B., and A. Dale (1992), Dinoflagellate contributions to the deep sea, Ocean Biocoenosis Series 5, 45-73, Woods Hole Oceanographic Institution, Woods Hole.

DeConto, R., and D. Pollard (2000), Rapid Cenozoic glaciation of Antarctica induced by declining atmospheric CO 2, Physical Status Solidi A178, 701-708.

Dekeyzer, S.P.M. and K.A.F. Zonneveld , S. (subm.), Correlation between temperature and the δ18O composition of Thoracosphaera heimii shells in core top sediments from the Indian and Atlantic Ocean, Micropalaeontology.

Dekeyzer, S.P.M. (2011), Minor element composition and stable oxygen isotopes of calcareous shells of the dinoflagellate Thoracosphaera heimii, Ph.D thesis, Staats-und Universitätsbibliothek Bremen, Bremen, Germany.

Delaygue, G., J. Jouzel, J.-C. Dutay (2000), Oxygen 18-salinity relationship simulated by an oceanic general circulation model, Earth and Planetary Science Letters, 178(1-2), 113-123.

Diekmann, B., M. Falker, G. Kuhn (2003), Environmental history of the south-eastern South Atlantic since the Middle Miocene: evidence from the sedimentological records of ODP Sites 1088 and 1092, Sedimentology 50(3), 511-529.

Diester-Haass, L., P. A. Meyers, P. Rothe (1990), Miocene history of the Benguela Current and Antarctic ice volumes: evidence from rhythmic sedimentation and current growth across the Walvis Ridge (Deep Sea Drilling Project Sites 362 and 532), Paleoceanography Vol. 5(5), 685-707.

Diester-Haass, L., P. A. Meyers, P. Rothe (1992), The Benguela Current and associated upwelling on the southwest African Margin: a synthesis of the Neogene-Quaternary sedimentary record at DSDP sites 362 and 532, Geological Society London Special Publications, 64(1), 331.

Diester-Haass, L., P. A. Meyers, T. Bickert (2004), Carbonate crash and biogenic bloom in the late Miocene: Evidence from ODP Sites 1085, 1086, and 1087 in the Cape Basin, southeast Atlantic Ocean, Paleoceanography Vol. 19(1), 1–19.

Dingle, R., and Q. Hendey (1984), Late Mesozoic and Tertiary sediment supply to the eastern Cape Basin (SE Atlantic) and palaeo-drainage systems in southwestern Africa, Marine Geology 56(1-4), 13-26.

Dobson, D.M., G.R. Dickens, D.K. Rea (2001), Terrigenous sediment on Ceara Rise: a Cenozoic record of South American orogeny and erosion, Palaeogeography, Palaeoclimatology, Palaeoecology 165, 215–229.

Duque‐Caro, H. (1990), Neogene stratigraphy, paleoceanography and paleobiogeography in northwest South America and the evolution of the Panama Seaway, Palaeogeography, Palaeoclimatology, Palaeoecology, 77, 203–234.

Emiliani, C. (1956), Oligocene and Pleistocene Temperatures of the Equatorial and Subtropical Atlantic Ocean. The Journal of Geology, Vol. 64, No. 3, 281-288.

Esper, O., K. A. F. Zonneveld, C. Höll, B. Karwath, H. Kuhlmann, R. Schneider, A. Vink, I. Weise-Ihlo, H. Willems (2000), Reconstruction of palaeoceanographic conditions in the South Atlantic Ocean at the last two Terminations based on calcareous dinoflagellate cysts, International Journal of Earth Sciences, 88(4), 680-693.

Esper, O., G. J. M. Versteegh, K.A.F. Zonneveld, H. Willems (2004), A palynological reconstruction of the Agulhas Retroflection (South Atlantic Ocean) during the Late Quaternary, Global and Planetary Change, 41(1), 31-62.

Fairbanks RG, C.D. Charles, J.D. Wright (1992), Origin of global meltwater pulses, in: Radiocarbon after Four Decades, R.E. Taylor (ed.), Springer Verlag, New York, 473–500.

Felis, T., J. Pätzold, Y.Loya (2003), Mean oxygen-isotope signatures in corals: inter-colony variability and correction for extension-rate effects, Coral Reefs, 22(4), 328-336.

Fensome, R.A., F.J.R. Taylor, G. Norris, W.A.S. Sarjeant, D.I. Wharton, G.L. Williams, (1993), A Classification of Modern and Fossil Dinoflagellates. Micropaleontology Special Publication 7, Sheridan Press, Hanover, NH, 351.

Figueiredo , J. , C. Hoorn , P. van der Ven , E. Soares (2009), Late Miocene onset of the Amazon River and the Amazon deep-sea fan: Evidence from the Foz do Amazonas Basin, Geology 37, 619 – 622.

Flower, B., and J. Kennett (1994), The middle Miocene climatic transition: East Antarctic ice sheet development, deep ocean circulation and global carbon cycling, Palaeogeography, Palaeoclimatology, Palaeoecology, 108(3-4), 537-555.

Friedrich, O., and K. J. S. Meier (2003), Stable isotopic indication for the cyst formation depth of Campanian/Maastrichtian calcareous dinoflagellates, Micropaleontology 49(4), 375-380.

Friedrich, O., and K. J. S. Meier (2006), Suitability of stable oxygen and carbon isotopes of calcareous dinoflagellate cysts for paleoclimatic studies: Evidence from the Campanian/Maastrichtian cooling phase, Palaeogeography, Palaeoclimatology, Palaeoecology, 239(3-4), 456-469.

Füterer, D. (1977), Distribution of calcareous dinoflagellates in Cenozoic sediments of Site 366, Eastern North Atlantic, Deep Sea Drilling Projekt, Initial Reports 61, 709-737, Washington.

Füterer, D. (1984), Pithonelloid calcareous dinoflagellates from the upper Cretaceous and Cenocoic of the southeastern Atlantic Ocean, Deep Sea Drilling Projekt, Initial Reports 74, T.C. Moore et al. (eds), Washington, U.S.Govt. Printing Office.

Gasse, F. (2000), Hydrological changes in the African tropics since the Last Glacial Maximum, Quaternary Science Reviews, 19(1-5), 189-211.

Gibbs, R.J., (1970), Circulation in the Amazon River Estuary and adjacent Atlantic Ocean, Journal of Marine Research 28, 113–123.

Gingele, F. X. (1996), Holocene climatic optimum in Southwest Africa: evidence from the marine clay mineral record. Palaeogeography, Palaeoclimatology, Palaeoecology 122, 77–87.

Godhe, A., F. Norén, M. Kuylenstierna, C. Ekberg, B. Karlson (2001), Relationship between planktonic dinoflagellate abundance, cysts recovered in sediment traps and environmental factors in the Gullmar Fjord, Sweden, Journal of Plankton Research, 23(9), 923-938.

Goodwin, D.H., B.R. Schöne, D.L. Dettmann (2003), Resolution and Fidelity of Oxygen Isotopes as Paleotemperature Proxies in Bivalve Mollusk Shells: Models and Observations PALAIOS, vol. 18, 110-125.

Gordon, A. (1985), Indian-Atlantic transfer of thermocline water at the Agulhas Retroflection, Science 227(4690), 1030-1033.

Gordon, A. (1986), Interocean exchange of thermocline water, Journal of Geophysical Research, 91(C4), 5037-5046.

Graham, J. M., A.D. Kent, G.H. Lauster, A.C. Yannarell, L.E. Graham, E.W. Triplett (2004), Seasonal Dynamics of Phytoplankton and Planktonic Protozoan Communities in a Northern Temperate Humic Lake: Diversity in a Dinoflagellate Dominated System, Microbial Ecology, 48(4), 528-540.

Grodsky, S. A., and J. A. Carton (2001) Coupled land/atmosphere interactions in the West African Monsoon, Geophysical Research Letters, 28, 1503– 1506.

Guilderson, T. P., R.G. Fairbanks, J.L. Rubenstone (2001), Tropical Atlantic coral oxygen isotopes: glacial/interglacial sea surface temperatures and climate change, Marine Geology, 172(1-2), 75-89.

Haq, B. U., J. Hardenbol, P. R. Vail (1987), Chronology of Fluctuating Sea Levels Since the Triassic, Science 235(4793), 1156-1167.

Hardman - Mountford, N., A.J. Richardson, J. J. Agenbach, E. Hagen, L. Nykjaer, , F.A. Shillington, C. Villacastin (2003), Ocean climate of the South East Atlantic observed from satellite data and wind models, Progress In Oceanography, 59(2-3), 181-221.

Harris, S.E. and A.C. Mix (2010), Climate and tectonic influences on continental erosion of tropical South America, 0-13 Ma, Geology, 30,447-450.

Heinrich, S., K.A.F. Zonneveld, T. Bickert, H. Willems (2011), The Benguela upwelling related to the Miocene cooling events and the development of the Antarctic Circumpolar Current: Evidence from calcareous dinoflagellate cysts, Paleoceanography Vol. 26, PA3209

Hildebrand-Habel, T., H. Willems (2000), Distribution of calcareous dinoflagellates from the Maastrichtian to early Miocene of DSDP Site 357 (Rio Grande Rise, western South Atlantic Ocean), International Journal of Earth Sciences 88, 694-707.

Höflich, O. (1974), The seasonal and secular variation of the Organic-walled dinoflagellate cysts from meteorological parameters on both sides of the ITCZ in the surface sediments of Nagasaki Bay and Senzaki Bay, West Atlantic Ocean. Global Atmospheric Research Program's Japan. Bull. Fac. Liberal Arts Nagasaki Univ. Nat. Sci. 25 Atlantic Tropical Experiment (GATE) Rep. 2 (6), 1–36.

Holbourn, A., W. Kuhnt, M. Schulz, H. Erlenkeuser (2005), Impacts of orbital forcing and atmospheric carbon dioxide on Miocene ice-sheet expansion, Nature, 438(7067), 483-487.

Holbourn, A., W. Kuhnt, M. Schulz, J.A: Flores, N. Anderson (2007), Orbitally-paced climate evolution during the middle Miocene "Monterey" carbon-isotope excursion, Earth and Planetary Science Letters, 261(3-4), 534-550.

Hoorn, C., J.G. Gustavo, A. Sarmiento, M.A. Lorente (1995), Andean tectonics as a cause for changing drainage patterns in Miocene northern south America, Geology 23,237-240.

Hoorn, C., F. P. Wesselingh, H. Steege, M. A. Bermudez, A. Mora, J. Sevink, I. Sanmartín, A. Sanchez-Meseguer, C. L. Anderson, J. P. Figueiredo, C. Jaramillo, D. Riff, F. R. Negri,1 H. Hooghiemstra, J. Lundberg, T. Stadler, T. Särkinen, A. Antonelli (2010), Amazonia Through Time: Andean Uplift, Climate Change, Landscape Evolution, and Biodiversity, Science Vol. 330, 927-931.

Huber, M., L.C. Sloan, C. Shellito (2003), Early Paleogene oceans and climate: A fully coupled modelling approach using NCAR CCSM, Geological Society of America, Special Paper 369.

Hut, G. (1987), Consultants group meeting on stable isotope reference samples for geochemical and hydrological investigations. Report to the Director General of the International Atomic Energy Agency, Vienna, 1-42.

Inouye, I. and R.N. Pienaar (1983), Observations on the life cycle and microanatomy of Thoracosphaera heimii (Dinophyceae) with special reference to its systematic position. S. Afr. J. Bot., 2, 63–75.

IPCC, (2007), Summary for Policymakers. In: Climate Change 2007: Impacts, Adaptation and Vulnerability. Contribution of Working Group II to the Fourth Assessment Report of the Intergovernmental Panel on Climate Change, M.L. Parry et al. (eds), Cambridge University Press, Cambridge, UK, 7-22.

Janofske, D., 1992. Kalkiges Nannoplankton, insbesondere kalkige Dinoflagellate-Zysten der alpinen Ober-Trias: Taxonomie, Biostratigraphie und Bedeutung für die Phylogenie der Peridinales. Berliner Geowiss. Abh. E (4), 1-93.

Janofske, D. (1996), Ultrastructure types in recent calcispheres, Bulletin de l'Institut océanographique(Monaco), 295-303.

Janofske, D. And B. Karwarth (2000), Oceanic calcareous dinoflagellates of the equatorial Atlantic Ocean: cyst-theca relationship, taxonomy and aspects on ecology, in: Ecological Studies on Living and Fossil Calcareous Dinoflagellates of the Equatorial and Tropical Atlantic Ocean, B. Karwath (ed), 93–136, Universität Bremen, Bremen, Germany.

Jansen, H., D. A. Wolf-Gladrow (2002). Carbonate dissolution in copepod guts: a numerical model. Marine Ecology Progress Series 221, 199-207.

Jansen, H., R.E. Zeebe, D. A. Wolf-Gladrow (2002), Modeling the dissolution of settling CaCO3 in the ocean, Global Biogeochemical Cycles, 16(2), 11.

Juggins, S. (2007), C2 Version 1.5 User guide, Software for ecological and palaeoecological data analysis and visualisation, Newcastle University, Newcastle upon Tyne, UK, 73.

Kameo, K., and T. Sato (2000), Biogeography of Neogene calcareous nannofossils in the Caribbean and the eastern equatorial Pacific: floral response to the emergence of the Isthmus of Panama, Marine Micropaleontology, 39(1-4), 201-218.

Kamykowski, D., A.J. Milligan, R.E. Reed (1998), Relationships between geotaxis/phototaxis and dial vertical migration in autotrophic dinoflagellates, Journal of Plankton Research 20, 1781–1796.

Karwath, B. (2000), Ecological studies on living and fossil calcareous dinoflagellates of the equatorial and tropical Atlantic Ocean, Berichte, Fachbereich Geowissenschaften, Universität Bremen, 152, 175.

Kastanja, M. M., B. Diekmann, R. Henrich (2006), Controls on carbonate and terrigenous deposition in the incipient Benguela upwelling system during the middle to the late Miocene (ODP Sites 1085 and 1087), Palaeogeography, Palaeoclimatology, Palaeoecology, 241(3-4), 515-530.

Kim, S.-T. and J.R. O´Neil (1997), Equilibrium and nonequilibrium oxygen isotope effects in synthetic carbonates. Geochimica et Cosmochimica Acta, 61(16), 3461-3475.

King, T.A., W.G. Ellis, D.W. Murray, N.J. Shackleton, S. Harris (1997), Miocene evolution of carbonate sedimentation at the Ceara Rise: A multivariate data/proxy approach, Proceeding of the Ocean Drilling Program, Scientific Results 154, 349-365.

Kohn, M. and K.A.F. Zonneveld (2010), Calcification depth and spatial distribution of Thoracosphaera heimii cysts: Implications for palaeoceanographic reconstructions, Deep-Sea Research 1 57, 1543-1565.

Kohn, M. (2010), The stable oxygen isotope signal of the calcareous-walled dinoflagellate *Thoracosphaera heimii* as a new proxy for sea surface temperature, Ph.D thesis, Staats- und Universitätsbibliothek Bremen, Bremen, Germany.

Kohn, M., S. Steinke, K.-H. Baumann, B. Donner, H. Meggers, K. A.F. Zonneveld (2011) Stable oxygen isotopes from the calcareous-walled dinoflagellate Thoracosphaera heimii as a proxy for changes in mixed layer temperatures off NW Africa during the last 45,000 yr, Palaeogeography, Palaeoclimatology, Palaeoecology, 302(3-4), 311-322.

Krammer, R., K. H. Baumann, R. Henrich (2006), Middle to late Miocene fluctuations in the incipient Benguela Upwelling System revealed by calcareous nannofossil assemblages (ODP Site 1085A), Palaeogeography, Palaeoclimatology, Palaeoecology, 230(3-4), 319-334.

Kremp, A., Anderson, D.M., 2000. Factors regulating germination of resting cysts of the spring bloom dinoflagellate Scrippsiella hangoei from the northern Baltic Sea. Journal of Plankton Research 22 (7), 1311-1327.

Lear, C. H., Y. Rosenthal, J. D. Wright (2003), The closing of a seaway: Ocean water masses and global climate change, Earth Planet Science Letters 210, 425–437.

Lewis, J. (1991), Cyst-theca relationships in Scrippsiella (Dinophyceae) and related orthoperidinoid genera, Botanica Marina, 34, 91–106.

Lohmann, G.P., (1995), A model for variation in the chemistry of planktonic foraminifera due to secondary calcification and selective dissolution. Palaeoceanography Vol. 10 (3), 445–457.

Longhurst, A., (1993), Seasonal cooling and blooming in tropical oceans, Deep-Sea Research 40, 2145–2165.

Lutjeharms, J. R. E (2001), Agulhas Current, in: Encyclopedia of Ocean Sciences, J. H. Steele et al. (eds.), Academic Press, Oxford, 104-113.

Lutjeharms, J., and J. Meeuwis (1987), The extent and variability of south-east Atlantic upwelling, South African Journal of Marine Science 5(1), 51-62.

Lutjeharms, J., and J. Cooper (1996), Interbasin leakage through Agulhas Current filaments, Deep-Sea Research Part I 43(2), 213-238.

Lutjeharms, J. R. E., and W. P. M. de Ruijter (1996), The influence of the Agulhas Current on the adjacent coastal ocean: possible impacts of climate change, Journal of Marine Systems 7(2-4), 321-336.

Lutjeharms, J. R. E., O. Boebel, H. T. Rossby (2003), Agulhas cyclones, Deep Sea Research Part II: Topical Studies in Oceanography 50(1), 13-34.

Margolis, S. V., P. M. Kroopnick, D. E. Goodney, W. C. Dudley, M. E. Mahoney. (1975), Oxygen and Carbon Isotopes from Calcareous Nannofossils as Paleoceanographic Indicators, Science 189(4202), 555-557.

Marotzke, J. (2000), Abrupt climate change and thermohaline circulation: Mechanisms and predictability, Proceedings of the National Academy of Sciences 97(4), 1347-1350.

Marret, F., and K. Zonneveld (2003), Atlas of modern organic-walled dinoflagellate cyst distribution, Review of Palaeobotany and Palynology 125(1-2), 1-200.

McConnaughey, T. (1989), 13C and 18O isotopic disequilibrium in biological carbonates: II. In vitro silmutations, I. patterns. Geochim. Cosmochim. Acta 53, 151-162.

McConnaughey, T. A. (2003), Sub-equilibrium oxygen-18 and carbon-13 levels in biological carbonates: carbonate and kinetic models, Coral Reefs, 22(4), 316-327.

McIntyre, A., W. F. Ruddiman, K. Karlin, A. C. Mix (1989), Surface water response of the equatorial Atlantic Ocean to orbital forcing, Paleoceanography, 4(1).

McKinney, C.R., J.M. McCrea, S. Epstein, H.A. Ellen, H.C. Urey, (1950), Improvements in mass spectrometers for the measurements of small differences in isotope abundance ratios, Review of Scientific Instruments, Vol. 21(8), 724-730.

Meeuwis, J., and J. Lutjeharms (1990), Surface thermal characteristics of the Angola-Benguela Front, South African Journal of Marine Science, 9(1), 261-279.

Meier, K., and H. Willems (2003), Calcareous dinoflagellate cysts in surface sediments from the Mediterranean Sea: distribution patterns and influence of main environmental gradients, Marine Micropaleontology, 48(3), 321-354.

Meier, K.J.S., C. Höll, H. Willems (2004a), Effect of Temperature on Culture Growth and Cyst Production in the Calcareous Dinoflagellates Calciodinellum albatrosianum, Leonella granifera and Pernambugia tuberosa, Micropaleontology Vol. 50, Supplement 1: Advances in the biology, ecology and taphonomy of extant calcareous nannoplankton , 93-106.

Meier, K.J.S., K.A.F. Zonneveld, S. Kasten, H. Willems (2004b), Different nutrient sources forcing increased productivity during eastern Mediterranean S1 sapropel formation as reflected by calcareous dinoflagellate cysts, Paleoceanography Vol. 19, 1-12, PA000895.

Meier, K.J.S., J.R. Young, M. Kirsch, S. Feist-Burkhardt (2007). Evolution of different life-cycle strategies in oceanic calcareous dinoflagellates. European Journal of Phycology 42 (1), 81-89.

Maier‐Reimer, E., U. Mikolajewicz, T. J. Crowley (1990), Ocean general circulation

model sensitivity experiment with an open central American isthmus, Paleoceanography,5, 349–366.

Metcalf, W.G. and M.C. Stalcup (1967). Origin of the Atlantic Equatorial Undercurrent. Journal of Geophysical Research, 72, 4959–4975.

Micheels, A., A. A. Bruch, D. Uhl, T. Utescher, V. Mosbrugger (2007) A Late Miocene climate model simulation with ECHAM4/ML and its quantitative validation with terrestrial proxy data. Palaeogeography, Palaeoclimatology, Palaeoecology 253, 251–270.

Mikolajewicz, U. and T.J. Crowley (1997), Response of a coupled ocean/energy balance model to restricted flow through the central American isthmus. Palaeoceanography Vol. 12 (3), 429–441.

Miller, K. G., R. G. Fairbanks, and G. S. Mountain (1987), Tertiary oxygen isotope synthesis, sea level history, and continental margin erosion, Paleoceanography Vol. 2, 1-19.

Miller, K., J. D. Wright, R. G. Fairbanks (1991), Unlocking the ice house: Oligocene-Miocene oxygen isotopes, eustasy, and margin erosion, Journal of Geophysical Research, 96(B4), 6829-6848.

Milliman, J.D. and R.H. Meade (1983), World-wide delivery of river sediment to the oceans, Journal of Geology 91, 1–21.

Milliman, J., P. J. Troy, W. M. Balch, A. K. Adams, Y. H. Li, F. T. Mackenzie (1999), Biologically mediated dissolution of calcium carbonate above the chemical lysocline?, Deep-Sea Research Part I 46(10), 1653-1669.

Molnar, P. (2008), Closing of the Central American Seaway and the Ice Age: A critical review, Paleoceanography Vol. 23, PA2201.

Montresor, M., A. Zingone, D. Sarno (1998), Dinoflagellate cyst production at a coastal Mediterranean site, Journal of Plankton Research 20, 2291–2312.

Mulitza, S., D. Boltovskoy, B. Donner, H. Meggers, A. Paul, G. Wefer (2003), Temperature: d18O relationship of planktonic foraminifera collected from surface waters. Palaeogeography, Palaeoclimatology, Palaeoecology 202, 143–152.

Muller-Karger, F.E., C.R. McClain, P.L. Richardson (1988), The dispersal of the Amazon's water, Nature 333, 56–59.

Nelson, G., and L. Hutchings (1983), The Benguela upwelling area, Progress In Oceanography 12(3), 333-356.

Newkirk, D.R., and E.E. Martin (2009), Circulation through the Central American Seaway during the Miocene carbonate crash, Geology Vol. 37, 87-90.

Nisancioglu, K., M. E. Raymo, and P. H. Stone (2003), Reorganization of Miocene deep water circulation in response to the shoaling of the Central American Seaway, Paleoceanography Vol. 18(1), 1006.

Nuzzo, L. and M. Montresor (1999), Different excystment patterns in two calcareous cyst-producing species of the dinoflagellate genus. Scrippsiella, Journal of Plankton Research 21, 2009–2018.

Olli, K. and D.M. Anderson (2002), High encystment success of the dinoflagellate Scrippsiella lachrymosa in culture experiments Journal of Phycology 38 (1), 145-156.

Pagani, M., M. A. Arthur, K. H. Freeman (2000), Variations in Miocene phytoplankton growth rates in the southwest Atlantic: Evidence for changes in ocean circulation, Paleoceanography Vol. 15(5).

Pagani, M., J. C. Zachos, K. H. Freeman, B. Tipple, S. Bohaty (2005), Marked Decline in Atmospheric Carbon Dioxide Concentrations during the Paleogene, Science 309(5734), 600 – 603.

Paul, A., S. Mulitza, J. Pätzold, T. Wolff (1999), Simulation of oxygen isotopes in a global ocean model, in: Use of proxies in Paleoceanography: Examples from the South Atlantic, G. Fischer and G. Wefer (eds.), Springer, Berlin Heidelberg, 655-686.

Partridge, T. (1993), The evidence for Cainozoic aridification in southern Africa, Quaternary International 17, 105-110.

Paulsen, H. (2005), Miocene changes in the vertical structure of the Southeast Atlantic near-surface water column: Influence on the paleoproductivity, Ph.D thesis, Staats-und Universitätsbibliothek Bremen, Bremen, Germany.

Peeters, F.J.C. (2000), The distribution and stable isotope composition of living planktic foraminifera in relation to seasonal changes in the Arabian Sea. Ph.D. Thesis, Free University, Amsterdam, The Netherlands, 184 pp.

Perrin, C. (2002), Tertiary: The emergence of modern reef ecosystems, in: Phanerozoic reef patterns. Spec. Publ., W. Kiessling and E. Flügel (eds.), Vol. 72. SEPM, Tulsa, 587–621.

Peterson, R. G., and L. Stramma (1991), Upper-level circulation in the South Atlantic Ocean, Progress In Oceanography 26(1), 1-73.

Pfiester, L.A. and D.A. Anderson (1987), Dinoflagellate reproduction, in: The Biology of Dinoflagellates, F.J.R. Taylor (ed.), Blackwell Scientific Publications, Oxford, UK, 611–648.

Philander, S.G.H. and R.C. Pacanowski (1986a), A model of the seasonal cycle in the tropical Atlantic Ocean. Journal of Geophysical Research 91, 14,192–14,206.

Philander, S.G. (2001), Atlantic Ocean Equatorial Currents, Princeten University, Princeton, NJ, USA.

Prange, M., and M. Schulz (2004), A coastal upwelling seesaw in the Atlantic Ocean as a result of the closure of the Central American Seaway, Geophysical Research Letters, 31(17), L17207.

Preiß-Daimler, I. (2011), The Miocene Carbonate crash: Shifts in carbonate preservation and contribution of calcareous plankton, Ph.D thesis, Staats-und Universitätsbibliothek Bremen, Bremen, Germany.

Rahmstorf, S., (2002), Ocean circulation and climate during the past 120,000 years, Nature Vol. 419, 207-214.

Richardson, P.L., T.K. McKee (1984), Average seasonal variation of the Atlantic equatorial currents from historical ship drifts, Journal of Physical Oceanography 14, 633–652.

Richter, D., A. Vink, K.A.F. Zonneveld, H. Kuhlmann, H. Willems (2007), Calcareous dinoflagellate cyst distributions in surface sediments from upwelling areas off NW Africa, and their relationships with environmental parameters of the upper water column, Marine Micropaleontology 63(3-4), 201-228.

Richter, D. (2009), Characteristics of calcareous dinoflagellate cyst assemblages in a major upwelling region (NW Africa) Spatial distribution, fluxes and ecology, Ph.D thesis, Staats-und Universitätsbibliothek Bremen, Bremen, Germany.

Rintoul, S. R. (2009), Antarctic Circumpolar Current, Encyclopedia of Ocean Sciences, J. H. Steele, K. K. Turekian, S. A. Thorpe (Eds.), (2009), Academic Press, Oxford, 2nd Edition, 3445-3458.

Rosenthal, Y., G. P. Lohmann, K. C Lohmann, R. M. Sherrell (2000), Incorporation and Preservation of Mg in Globigerinoides sacculifer: Implications for Reconstructing the Temperature and 18O/16O of Seawater, PaleoceanographyVol. 15(1), 135-145.

Roters, B., and R. Henrich (2008), The middle to late Miocene climatic development of Southwest Africa derived from the sedimentological record of ODP Site 1085A, International Journal of Earth Sciences 99(2), 459-471.

Ruddiman, W. F. (2001), Earth's Climate: past and future, W. H. Freeman and Company, 2nd Edition, New York, 154-161.

Samtleben, C., P. Schäfer, H. Andruleit, A. Baumann, K. H. Baumann, A. Kohly, J. Matthiessen, A. Schröder-Ritzrau, A (1995), Plankton in the Norwegian-Greenland Sea: from living communities to sediment assemblages-an actualistic approach, Geologische Rundschau 84(1), 108-136.

Sarmiento, J., N. Gruber, M. A. Brzezinski, J. P. Dunne (2004), High-latitude controls of thermocline nutrients and low latitude biological productivity, Nature Vol. 427(69), 56–60.

Schmidt, G. A., G. R. Bigg and E. J. Rohling (1999), Global Seawater Oxygen-18 Database - v1.21, (http://data.giss.nasa.gov/o18data/).

Schmidt, G.A. (1998), Oxygen-18 variations in a global ocean model. Geophysical Research Letters 25, 1201–1204.

Schmidt, G.A., (1999), Forward modeling of carbonate proxy data from planktonic foraminifera using oxygen isotope tracers in a global model, Paleoceanography Vol. 14, 482–497.

Sgrosso, S., F. Esposito, M. Montresor (2001), Temperature and daylength regulate encystment in calcareous cyst-forming dinoflagellates. Marine Ecology Progress Series 211, 77–87.

Shackleton, N.J. and S. Crowhurst (1997), Sediment fluxes based on an orbitally tuned time scale 5 Ma to 14 Ma, Site 926, in: Proceedings of the Ocean Drilling Program, Scientific Results, W.B. Curry et al. (eds.), College Station, TX, 154, 69–82.

Shackleton, N.J. and M.A. Hall (1997), The Late Miocene stable isotope record, Site 926, Proceedings of the Ocean Drilling Program, Scientific Results, vol. 154, 1997, 367–373.

Shannon, L. (1985), The Benguela ecosystem. I: Evolution of the Benguela physical features and processes, Oceanography and Marine Biology, 23, 105-182.

Shannon, L., and G. Nelson (1996), The Benguela: large scale features and processes and system variability, The South Atlantic: present and past circulation, 163–210.

Shannon, L. V., et al. (2001), Benguela Current, in: Encyclopedia of Ocean Sciences, J. H. Steele et al. (eds.), Academic Press, Oxford, 255-267.

Shevenell, A., J. P. Kennett, D. W. Lea (2004), Middle Miocene southern ocean cooling and Antarctic cryosphere expansion, Science Vol. 305(5691), 1766 – 1770.

Siesser, W. (1980), Late Miocene Origin of the Benguela Upwelling System off Northern Namibia, Science Vol. 208(4441), 283-285.

Spero, H.J. and D.W. Lea (1993), Intraspecific stable isotope variability in the planktic foraminifera Globigerinoides sacculifer: Results from laboratory experiments. Marine Micropaleontology 22, 221-234.

Spero, H.J. and D.W. Lea (1996), Experimental determination of stable isotope variability in Globigerina bulloides: implications for paleoceanographic reconstructions, Marine Micropaleontology 28, (3-4), 231-246.

Steph, S., R. Tiedemann, M. Prange, J. Groeneveld, D. Nürnberg, L. Reuning, M. Schulz, G.H. Haug (2006), Changes in Caribbean surface hydrography during the Pliocene shoaling of the Central American Seaway. Paleoceanography Vol. 21, PA4221.

Steppuhn, A., A. Micheels, G. Geiger, V. Mosbrugger (2006), Reconstructing the Late Miocene climate and oceanic heat flux using the AGCM ECHAM4 coupled to a mixed-layer ocean model with adjusted flux corrections. Palaeogeography, Palaeoclimatology, Palaeoecology 238, 399–423.

Stover, L.E., H. Brinkhuis, S.P. Damassa, L. Verteuil, R.J. Helby, E. Monteil, A. Partridge, A.J. Powell, J.B. Riding, M. Smelror, G.L. Williams (1996), Mesozoic-Tertiary dinoflagellates, acritarchs and prasinophytes, in: Palynology: principles and

applications, J. Jansonius and D.C. McGregor (eds.), American Association of Stratigraphic Palynologists Foundation, Dallas, 641-750.

Stramma, L., and M. England (1999), On the water masses and mean circulation of the South Atlantic Ocean, Journal of Geophysical Research 104.

Streng, M., T. Hildebrand-Habel, H. Willems (2002), Revision of the genera Sphaerodinella Keupp and Versteegh, 1989 and Orthopithonella Keupp in Keupp and Mutterlose, 1984 (Calciodinelloideae, calcareous dinoflagellate cysts), Journal of Paleontology 76(3), 397.

Streng, M., T. Hildebrand-Habel, H. Willems (2004), A proposed classification of archeopyle types in calcareous dinoflagellate cysts, Journal of Paleontology 78 (3), 456-483.

Tangen, K., L.E. Brand, P.L. Blackwelder, R.R.L. Guillard (1982), Thoracosphaera heimii (Lohmann) Kamptner is a dinophyte: observations on its morphology and life cycle, Marine Micropaleontology 7, 193-212.

Taylor, F.J.R. and U. Pollingher (1987), The ecology of dinoflagellates, in: The biology of dinoflagellates, F.J.R. Taylor (ed.), Blackwell Scientific Publications, Oxford, 398-529.

Treguier, A., O. Boebel, B. Barnier, G. Madec (2003), Agulhas eddy fluxes in a 1/6 Atlantic model, Deep-Sea Research Part II 50(1), 251-280.

Twichell, S. C., P.A. Meyers, L. Diester-Haass (2002), Significance of high C/N ratios in organic-carbon-rich Neogene sediments under the Benguela Current upwelling system, Organic Geochemistry 33(7), 715-722.

Van Zinderen Bakker, E. (1984), Aridity along the Namibian coast, Palaeoecol. Afr, 16, 421-428.

Van Zinderen Bakker, E. M., and J. H. Mercer (1986), Major late cainozoic climatic events and palaeoenvironmental changes in Africa viewed in a world wide context, Palaeogeography, Palaeoclimatology, Palaeoecology 56(3-4), 217-235.

Vincent, E., and W. Berger (1985), Carbon dioxide and polar cooling in the Miocene- The Monterey hypothesis, in: The carbon cycle and atmospheric CO 2: Natural variations archean to present, Proceedings of the Chapman Conference on Natural Variations in Carbon Dioxide and the Carbon Cycle, Washington, DC, 455-468.

Vink, A., K. A. F. Zonneveld, H. Willems (2000), Distributions of calcareous dinoflagellate cysts in surface sediments of the western equatorial Atlantic Ocean, and their potential use in palaeoceanography, Marine Micropaleontology 38(2), 149-180.

Vink, A. (2004), Calcareous dinoflagellate cysts in South and equatorial Atlantic surface sediments: diversity, distribution, ecology and potential for palaeoenvironmental reconstruction, Marine Micropaleontology 50(1-2), 43-88.

Wefer, G., and W. H. Berger (1991), Isotope paleontology: growth and composition of extant calcareous species, Marine Geology 100(1-4), 207-248.

Wefer, G., W. Berger, C. Richter (1998), Proceedings of the Ocean Drilling Program, Initial Reports, Vol. 175, College Station, TX, 385-428.

Wendler, I., K. A. F. Zonneveld, H. Willems (2002a), Calcareous cyst-producing dinoflagellates: ecology and aspects of cyst preservation in a highly productive oceanic region, in: Clift, P.D., The Tectonic and Climatic Evolution of the Arabian Sea Region, D. Kroon et al. (eds.), Geological Society, London, Special Publications 195, 317-340.

Wendler, I., K.A.F. Zonneveld, H. Willems (2002b). Production of calcareous dinoflagellate cysts in response to monsoon forcing off Somalia: a sediment trap study, Marine Micropaleontology, 46,1-1 I.

Wendler, I., K. A. F. Zonneveld, H. Willems (2002c), Oxygen availability effects on early diagenetic calcite dissolution in the Arabian Sea as inferred from calcareous dinoflagellate cysts, Global and Planetary Change 34(3-4), 219-239.

Westerhold, T. (2003), The middle Miocene carbonate crash: relationship to neogene changes in ocean circulation and global climate, Ph.D thesis, Staats-und Universitätsbibliothek Bremen, Bremen, Germany.

Westerhold, T., T. Bickert, U. Röhl (2005), Middle to late Miocene oxygen isotope stratigraphy of ODP site 1085 (SE Atlantic): new constrains on Miocene climate variability and sea-level fluctuations, Palaeogeography, Palaeoclimatology, Palaeoecology 217(3-4), 205-222.

Williams, M., A.M. Haywood, S.P. Taylor, P.J. Valdes, B.W. Sellwood, C.-D. Hillenbrand (2005), Evaluating the efficacy of planktonic foraminifer calcite δ18O data for sea surface temperature reconstruction for the Late Miocene, Geobios 38(6), 843-863.

Woodruff F. and S.M. Savin (1989), Miocene Deepwater Oceanography, Paleoceanography Vol. 4, NO. 1, 87-140.

Wright, J.D., K.G. Miller, R.G. Fairbanks (1991), Evolution of modern deep water circulation: evidence from the late Miocene Southern Ocean, Paleoceanography Vol. 6, 275-290.

Wright, J.D., K.G. Miller, R.G. Fairbanks (1992), Early and middle Miocene Stable Isotopes: Implications for Deepwater Circulations and Climate, Paleoceanography Vol. 7, NO. 3, 357-389.

Wright, J.D. and K.G. Miller (1996), Control of North Atlantic Deepwater Circulation by the Greenland-Scotland Ridge, Paleoceanography Vol. 11, No. 2, 157-170.

Wright, J. D. (2001), Cenozoic Climate - Oxygen Isotope Evidence, in: Encyclopedia of Ocean Sciences, 415-426, Academic Press, Oxford.

You, Y., M. Huber, R.D. Muller, C.J. Poulsen, J. Ribbe (2009), Simulation of the middle Miocene climate optimum, Geophysical Research Letters 36 (4), L04702.

Zachos, J.C., L.D. Stott, K.C. Lohmann (1994), Evolution of early Cenozoic marine temperatures, Paleoceanography Vol. 9, 353–387.

Zachos, J., M. Pagani, L. Sloan, E. Thomas and K. Billups (2001a), Trends, Rhythms, and Aberrations in Global Climate 65 Ma to Present, Science Vol. 292, 686-693.

Zachos, J. C., G. R. Dickens, R. E. Zeebe (2008), An early Cenozoic perspective on greenhouse warming and carbon-cycle dynamics, Nature 451(7176), 279-283.

Zeebe, R.E. (1999), An explanation of the effect of seawater carbonate concentration on foraminiferal oxygen isotopes, Geochim. Cosmochim. Acta 63, 2001-2007.

Zeebe, R. E. (2001), Seawater pH and isotopic paleotemperatures of Cretaceous oceans, Palaeogeography, Palaeoclimatology, Palaeoecology 170(1-2), 49-57.

Zonneveld, K.A.F., C. Höll, D. Janofske, B. Karwarth, B. Kerntopf, C. Rühlemann, H. Willems (1999), Calcareous Dinoflagellate Cysts as Paleo-Environmental Tools, in: Use of Proxies in Paleoceanography: Examples from the South Atlantic, G. Fischer and G. Wefer (eds.), Springer Verlag, Berlin Heidelberg, 145-164.

Zonneveld, K. A. F., A. Brune, H. Willems (2000), Spatial distribution of calcareous dinoflagellate cysts in surface sediments of the Atlantic Ocean between 13°N and 36°S, Review of Palaeobotany and Palynology 111(3-4), 197-223.

Zonneveld, K.A.F. (2004), Potential use of stable isotope composition of Thoracosphaera heimii (Dinophyceae) for upper water column (thermocline) temperature reconstruction, Marine Micropaleontology 50(3–4), 307–317.

Zonneveld, K. A. F., S. K. J. Meier, O. Esper, D. Siggelkow, I. Wendler, H. Willems (2005), The (palaeo) environmental significance of modern calcareous dinoflagellate cysts: a review, Paläontologische Zeitschrift 79(1), 61-77.

Zonneveld, K.A.F., A. Mackensen, K.-H. Baumann (2007), Stable oxygen isotopes of Thoracosphaera heimii (Dinophyceae) in relationship to temperature; a culture experiment, Marine Micropalaeontology 64 (1–2), 80–90.